Bio-fuel Composition Sensing

Multi domain spectroscopy to determine the composition of bio-fuel mixtures

L. M. Middelburg

Electronic Instrumentation Laboratory

TU Delft Delft University of Technology

Ford

Electronic Instrumentation Laboratory

Challenge the future

BIO-FUEL COMPOSITION SENSING

MULTI DOMAIN SPECTROSCOPY TO DETERMINE THE COMPOSITION OF BIO-FUEL MIXTURES

by

L. M. Middelburg

in partial fulfillment of the requirements for the degree of

Master of Science
in Microelectronics

at the Electronic Instrumentation Laboratory,
Department of Electrical Engineering,
Delft University of Technology,
to be defended publicly on Wednesday September 28, 2016 at 2:00 PM.

Supervisor:	dr. ir. A. Bossche
Thesis committee:	dr. G. de Graaf
	dr. ir. G. J. M. Janssen
	dr. ir. R. F. Wolffenbuttel
	ing. J. Bastemeijer

An electronic version of this thesis is available at http://repository.tudelft.nl/.

TU Delft Delft University of Technology

PREFACE

This document describes the work which was carried out for the Master Thesis Project EE4400, which is part of the master study Microelectronics. The project has been done in collaboration with Ford Motor Company and in context of the Ford Poling Challenge. The objective of this challenge is to stimulate research in a specific topic, in which multiple students are involved and work together. This work focuses on the different possibilities to implement a sensor system for the 'Flex-Fuel sensor', a sensor used in flex-fuel vehicles. This sensors should be able to solve a ternary mixture problem by determining the fraction of each component in mixtures consisting of gasoline, water and ethanol. This flex-fuel sensor is part of the fuel system in a car and monitoring is needed to provide important information about the fuel mixture to the engine control unit. The starting point of this work is based on the research and findings done by Giuseppe Lacerenza.

Two main domains have been investigated extensively within this work, the electrical domain and the optical domain. It was found that the imaginary part of the impedance up to 30MHz can provide valuable information of the composition. The real component of the impedance in this frequency range appeared not to be useful. Most important reasons are sample dependency, poor repeatability and a complex temperature dependency and mixing model. A coaxial impedance probe was designed and fabricated to enhance the impedance measurements. For the second independent selection parameter the optical domain was analyzed, where possibilities of absorption spectrometry were analyzed. It was found that gasoline specific absorption behavior is shown in the UV range between 220 nm and 300 nm. Two different implementation techniques are discussed. The work in the optical domain was published on the Eurosensors conference, which took place from 4 to 7 September 2016.

I would like to thank Ger de Graaf and Reinoud Wolffenbuttel for being a valuable source of advice on regular basis at the EI Department of TU Delft. Additionally I would like to thank Guido Sturm, from the Process & Energy Department, 3mE faculty for his time and availability at two important measurement series. Furthermore I would like to thank André Bossche for supervision and Jeroen Bastemeijer for technical help and advice, in addition to theoretical issues.

I acknowledge the contribution of Jaco Visser and Rick Soltis from the Research and Advanced Engineering department of Ford Motor Company, for the collaboration during the entire work. Also for their help and accompaniment during the Research Internship at their sensor research group in Dearborn. Furthermore, thanks are due to Ford Motor Company in general by facilitating the Ford Poling Challenge and let the author be a part of it.

Thanks are also due to Felix Wolffenbuttel for the collaboration on the design and production of the coaxial impedance probe. At last I would like to thank Amir Ghaderi for sharing his knowledge and view on a LVOF implementation and Johan Vogel for general tips and help with the impedance measurements.

L. M. Middelburg
Delft, September 2016

CONTENTS

List of Figures xi

1 Introduction 1
- 1.1 Context . . . 1
- 1.2 Social impact of the use and production of bio-fuel . . . 2
- 1.3 Bio-fuel . . . 2
  - 1.3.1 Static dissipators . . . 2
  - 1.3.2 Summer vs. winter grade fuels . . . 3
- 1.4 Methanol . . . 3
- 1.5 Selection methods . . . 3
- 1.6 State of the art . . . 4
- 1.7 Outline . . . 4

2 Feasibility study 7
- 2.1 Low-frequency impedance . . . 7
- 2.2 Dielectric relaxation in the GHz range . . . 8
  - 2.2.1 Debye Model . . . 8
  - 2.2.2 Measurements . . . 10
  - 2.2.3 Conclusion opportunities dielectric relaxation . . . 10
- 2.3 Calorimetry . . . 10
  - 2.3.1 Possible implementation technique - 3ω method . . . 10
  - 2.3.2 Conclusion thermal domain . . . 11
- 2.4 Optical domain . . . 11
- 2.5 Density measurement . . . 11
  - 2.5.1 Conclusion density measurement . . . 12
- 2.6 Surface Acoustic Waves . . . 12
  - 2.6.1 Conclusions measurements SAW Device . . . 15
- 2.7 Comparison and overall conclusions feasibility part . . . 16

3 LF impedance 17
- 3.1 LF impedance measurements . . . 17
  - 3.1.1 Measurement setup . . . 17
  - 3.1.2 Measurement I . . . 18
- 3.2 Double layer capacitance . . . 20
  - 3.2.1 Electrode Polarization . . . 20
  - 3.2.2 Measurements - II: Electrode polarization . . . 21
- 3.3 Series inductance . . . 22
- 3.4 Initial composition analyses . . . 23
  - 3.4.1 Possible strategy when only deionized water is assumed . . . 23
  - 3.4.2 Possible strategy when ion-rich water is assumed . . . 23
  - 3.4.3 Effective medium approximation: Maxwell-Garnett . . . 25
- 3.5 Measurements III - E85 . . . 25
  - 3.5.1 Empirical validity of linear mixing model . . . 26

3.6 Fouling detection E85 . . . 27
3.7 Total equivalent model and conclusions . . . 28

4 Probe Design **31**
4.1 Requirements . . . 31
4.2 Calibration . . . 32
4.3 Characteristic impedance and Comsol simulations . . . 33
4.3.1 Characteristic impedance . . . 33
4.3.2 Length of the coaxial probe . . . 33
4.3.3 Comsol simulations . . . 33
4.3.4 Relation between conductivity and parallel conductance . . . 34
4.3.5 Relation between relative permittivity and parallel capacitance . . . 36
4.4 Design and Realization . . . 37

5 Measurements Dedicated Probe **39**
5.1 Measurement setup . . . 39
5.2 Measurements . . . 39
5.3 Parallel conductance revisited . . . 42
5.3.1 Measurement Ethanol/Gasoline mixtures . . . 42
5.3.2 Reproducibility . . . 43
5.3.3 Literature . . . 44
5.4 Concluding remarks electrical domain . . . 46

6 Optical Absorption Spectroscopy **49**
6.1 Motivation optical domain . . . 49
6.2 Theory . . . 49
6.2.1 Absorption spectroscopy . . . 49
6.2.2 Beer-Lambert . . . 50
6.3 Measurement series I: Ocean Optics TUD . . . 50
6.3.1 Measurement Setup . . . 50
6.3.2 Measurements Ocean Optics Flame . . . 52
6.3.3 Measurements Ocean Optics Maya . . . 53
6.4 Measurement Series II: Varian Cary 500 FMC . . . 54
6.4.1 Different octane ratings . . . 54
6.4.2 Measurement Setup . . . 54
6.4.3 Single component Hydrocarbons . . . 55
6.4.4 Ethanol/Gasoline mixtures . . . 56
6.4.5 Octane content and Summer/Winter grade . . . 58
6.4.6 Near- & Mid-Infrared measurements . . . 58
6.5 Possible implementation techniques UV . . . 61
6.5.1 UV LEDs & UV enhanced photodiodes . . . 61
6.5.2 Linear Variable Optical Filters . . . 62
6.6 Conclusions Optical Absorption Spectroscopy . . . 62

7 Conclusion & Future Outlook **65**
7.1 Conclusions . . . 65
7.2 Proposed Measurement System . . . 67
7.3 Future outlook and Recommendations . . . 67
7.4 Publication Eurosensors XXX . . . 68

A Eurosensors Abstract Paper & Poster **69**

B Matlab code **75**
B.1 Medium approximation 75
B.1.1 The function Maxwell-Garnett 75
B.1.2 Code to generate comparison plots 75
B.2 Code to read out the Impedance Analyser 76

C S11 - Dielectric relaxtion **79**

D Accuracy in Cp - G calculation **81**

Bibliography **83**

List of Figures

1.1 The Continental Flex-Fuel sensor. Source: [1] . . . 4
1.2 Details of the measurement cell. Source: [2] . . . 4

2.1 The basic equivalent circuit model used for measuring the components. Source: [3] 7
2.2 Dielectric relaxation of water at 300K . . . 9
2.3 Dielectric loss of water as function of temperature . . . 9
2.4 Permittivity of ethanol at 320K against the frequency . . . 9
2.5 The different colors of American Regular Gas (left) and Dutch euro 95 (right) . . . 12
2.6 The density meter at the laboratory of Process & Energy department . . . 13
2.7 The used SAW device, bottom view . . . 14
2.8 The used SAW device, top view . . . 14
2.9 Results of the measurements with the SAW device . . . 14

3.1 The initial equivalent circuit model used for measuring the components. Source: [3] 17
3.2 The four different probes by number . . . 18
3.3 The measurement setup. Here the measurement of regular gasoline . . . 18
3.4 C_p of the three main components and tapwater . . . 19
3.5 G_p of the three main components and tapwater . . . 19
3.6 |Z| of the three main components and tapwater . . . 19
3.7 Φ of the three main components and tapwater . . . 19
3.8 An illustration about the charge buildup on both sides of the electrodes. Source [4] . 20
3.9 Equivalent model including the electrode polarization. Source [5] . . . 21
3.10 C_p including the 80%/20% ratio of D.I./tap water . . . 21
3.11 G_p including the 80%/20% ratio of D.I./tap water . . . 21
3.12 The equivalent circuit model including the parasitic inductance of the used probe . 22
3.13 The mean value of the dielectric constant according to the two different models . . . 25
3.14 The relative error of the linear model w.r.t. the Maxwell-Garnett model . . . 25
3.15 C_p including the methanol and the two versions of E85 . . . 26
3.16 C_p including the methanol and the two versions of E85 . . . 26
3.17 C_p for legitimate E85 mixtures with constant gasoline concentration . . . 27
3.18 G_p for legitimate E85 mixtures with constant gasoline concentration . . . 27
3.19 C_p for non-legitimate E85 mixtures, decreasing gasoline concentration when diluted 28
3.20 G_p for non-legitimate E85 mixtures, decreasing gasoline concentration when diluted 28
3.21 The total equivalent circuit model of the electrode/liquid under test system, using a coaxial impedance probe . . . 29

4.1 Both integrals in the coaxial structure, source [6] . . . 34
4.2 The obtained simulation result for the designed probe. . . . 35
4.3 The obtained simulation result for the designed probe. . . . 35
4.4 The cross section of the coaxial impedance probe. Source: [7] . . . 37
4.5 Cross section from the front. Source: [7] . . . 37
4.6 The realized coaxial impedance probe . . . 37
4.7 The realized coaxial impedance probe . . . 38

5.1 C_p measured with the dedicated coaxial impedance probe . . . 41
5.2 G_p measured with the dedicated coaxial impedance probe . . . 41
5.3 G_p for increasing ethanol concentration . . . 42
5.4 The used mixtures for the conductance measurements . . . 43
5.5 The measured parallel conductance at 9.98kHz . . . 43
5.6 The percent deviation of the parallel capacitance . . . 44
5.7 The percent deviation of the parallel conductance . . . 44
5.8 The conductivity of ethanol/gasoline mixture at 3 different temperatures . . . 45
5.9 Water, ethanol and gasoline interactions . . . 45
5.10 Temperature influence on ethanol-gasoline mixture conductivity. Source: [8] . . . 45

6.1 The spectrum of benzene among others. Source: [9] . . . 50
6.2 The used reflectance probe probe . . . 51
6.3 Fluorescence in the Dutch gasoline . . . 51
6.4 The measurement results of the flame Ocean Optics spectrometer. . . . 52
6.5 The measurement results of the Maya Ocean Optics spectrometer. . . . 53
6.6 Comparison of three different optical path lengths. . . . 55
6.7 The measured single component hydrocarbons and indolene with an optical path length of 1 mm. . . . 56
6.8 The measured single component hydrocarbons and indolene with dilution. . . . 56
6.9 The measured absorbance of different ethanol/indolene ratio's. The dilution ratio is included in the legend. . . . 57
6.10 The measured absorbance of different ethanol/gasoline ratio's. The dilution ratio is included in the legend. . . . 57
6.11 The absorbance as function of the gasoline fraction. Compared are the 87RON and indolene mixtures at two different wavelengths. . . . 57
6.12 Two representative American gasoline's, low and mid grade octane rating compared. Note the higher dilution ratio. . . . 58
6.13 The summer and winter grade E85 compared. The same dilution as previous gasoline/ethanol mixtures is used. . . . 58
6.14 The measured absorbance of different ethanol/indolene ratio's in the IR . . . 59
6.15 The measured absorbance of different ethanol/indolene ratio's in IR . . . 60
6.16 The measured absorbance of different ethanol/indolene ratio's in IR . . . 60
6.17 The measured absorbance of different ethanol/indolene ratio's in IR . . . 61
6.18 A schematic overview of the measurement system based on a LVOF. . . . 62
6.19 The LVOF on top of a detector array. . . . 62

C.1 The measurement results of the measurements with the impedance analyzer at Process and Energy Department . . . 79

D.1 Accuracy in measured G, source: Data sheet Agilent 4294A . . . 81
D.2 source: Data sheet Agilent 4294A . . . 82
D.3 source: Data sheet Agilent 4294A . . . 82

1

INTRODUCTION

1.1. CONTEXT

In the current context of ever increasing energy consumption and carbon emissions, an urgent claim for the usage of more sustainable energy sources is present. The exhaust emissions of cars and trucks play a big role in discussions about the environment and energy consumption. These emissions are in most countries strongly regulated by governmental rules. A health concern is also relevant, because of air pollution by cars, which can be very problematic in city areas where toxic exhaust gasses are a danger for the human health.

One possibility to form a more sustainable and clean solution, is the usage of bio-fuels, fuels that are produced from bio mass, such as sugar cane or corn. The carbon emissions caused by combustion of these fuels, have already been taken out of the air by the crops of which this fuel is made. Bio-fuel is represented in ethanol-gasoline mixtures which are globally used in all kinds of different ratio's. In some countries even 100% ethanol bio-fuel is available at gas stations. Cars which are able to run on these fuels are called flex-fuel vehicles, and should be able to run on mixtures of gasoline and ethanol in any ratio.

The stoichiometric air-fuel ratio, energy density, charge cooling due to vaporization, octane number and fuel volatility of bio-fuel are determined by the ethanol content. Therefore, it is important for the motor management system of Flex Fuel Vehicles to know what the volume fractions are in the gasoline/ethanol mixture, in order not to cause damage to the engine ([10],[11],[12]). To determine this fraction, a 'Flex-Fuel Sensor' is used. Currently available sensors, for Example the Continental Flex-Fuel Sensor, are not accurate when water is present in the bio-fuel. Water can be introduced to bio-fuel or to a bio-fuel/gasoline mixture by different reasons. Firstly, ethanol is hygroscopic and therefore attracts water vapor from the air. Secondly, water can be introduced by the production process of the ethanol, depending on the used origin, as will be described in section 1.3. Thirdly, water can be added by the vendors of car fuels, to increase profit. The fuel is adulterated with a few percent of water also called fouling.

This thesis work will proceed with the challenges when designing a sensor system that is capable of determining the volume fractions of a ternary mixture consisting of gasoline, water and ethanol. The starting point of this work is based on the research and findings done by G. Lacerenza [13].

1.2. SOCIAL IMPACT OF THE USE AND PRODUCTION OF BIO-FUEL

In the context of the Ford Poling Challenge, a multidisciplinary cooperation was set up with two graduates from Leiden University. Their work was focused on the social, environmental and political aspects of the use of bio-fuels in the European Union. During this cooperation several meetings have been arranged to discuss technical and non-technical issues. The advantage of the multi-disciplinary aspect is the exchange of valuable information about technical and non-technical impacts. This widening in context and view improves understanding of the 'big-picture' of mass scale integration of bio-ethanol as a fuel. Despite the advantages of bio-fuel such as energy security and reduced environmental impact, it is obvious that mass scale use of bio-ethanol will have a large impact in agricultural topics, land use, food security and also reduced fuel economy.

1.3. BIO-FUEL

Bio-fuel, or ethanol from sustainable sources, is produced from bio-mass (organic matter). The two main types of crop used for this bio-mass are sugar cane and corn [14]. Via fermentation of this bio-mass in distillation plants ethanol is formed. Ethanol production from sugar cane results in hydrous ethanol, also called wet-alcohol or AEHC. The wet-ethanol is only used in Brazil, mainly because of their enormous amount of sugar cane production. According to the ANP (National Agency of Petroleum, Natural Gas and Bio-fuels, Brazil) AEHC must have an ethanol content between 92.6 and 93.8 INMP (mass content, National Institute of Weights and Measures). When we translate these value to volume fractions, AEHC must contain between 94.1 and 95 GL (Degree Gay-Lussac), which means that the maximum water fraction is equal to 5.9%. Apart from this wet-alcohol, also dry alcohol or EACA is used, which is dehydrated and contains maximally 0.7 ° INMP of water, which corresponds with a volume fraction of 99.7 ° GL. [15] This dry-ethanol is usually mixed in different ratio's with regular gasoline and the ethanol fraction is denoted with an E. Some common ratio's are for example E10, E22 and E85. E100 or pure (hydrous) ethanol is mainly used in Brazil, whereas E22 and E85 are more available in the US. The flex fuel cars need to be able to run on as well hydrous ethanol (Brazilian E100) as gasoline-ethanol mixtures where dry-ethanol is applied. [16]

The added ethanol results in a cleaner combustion for multiple reasons. Since the energy resulting from the combustion of fuel is delivered by breaking down the C-H bonds, the ratio between C atoms and C-H bonds is relevant, because the C atoms result in CO_2 and/or CO. Because the ethanol molecule C_3H_5OH contains relatively few C atoms per C-H bond, compared to the components in gasoline (benzene rings and long carbon chains), less CO_2 is emitted for the same amount of energy when using ethanol as combustible.

Secondly, ethanol increases the octane rating of the fuel because of the presence of the oxygen molecule. A higher octane rating of the fuel results in a better anti-knocking ability. Therefore the combustion circumstances can be adapted such that a higher efficiency is reached. Knocking means the unwanted self-combustion of fuel under high temperature. Additional reasons for more efficient combustion circumstances are the broader flammability limits, higher flame speeds and higher heats of vaporization. [17]

1.3.1. STATIC DISSIPATORS

For safety reasons, anti-static additives are present in practical car fuels. When handling gasoline, it is possible that charge can accumulate and that static electricity will manifest itself, for example caused by flow or filtering. Because this static electricity can result in a spark in case of a sudden breakdown of the isolation between two potentials in the fuel/tank system, this causes a safety hazard. A spark causes a local place of high temperature which can ignite fuel-vapors. To prevent this from happening, so called static dissipators are present in the fuel, these are anti-static

additives added to the fuel. These additives increase the conductivity of the fuel, any static electricity will discharge trough this increased conductivity. The total conductivity of gasoline fuel is typically increased up to a value of 0.1 pS m^{-1} up to 1.0 pS m^{-1}. [18]

1.3.2. SUMMER VS. WINTER GRADE FUELS

Gasoline does contain a certain amount of volatile organic compounds (VOCs). When these compounds evaporate, they contribute to air pollution/smog. Because evaporation is increased when the environment temperature increases during summer, summer gasoline contains less VOCs and is therefore (marginally) better for the environment [19]. The volatility of gasoline is partially determined by the length of carbon chains of the hydrocarbons of which the gasoline exists. Roughly can be said that winter gasoline contains more volatile hydrocarbons, whereas summer gasoline contains less volatile hydrocarbons. When either summer or winter gasoline is used in a specific measurement, the grade will be denoted in the name between brackets.

1.4. METHANOL

Not only the alcohol ethanol is mixed with gasoline. In Asia, mainly in China, the alcohol methanol is mixed with gasoline. This methanol originates from coal gasification, a technique where thermal energy, steam and oxygen are used to form syngas out of coal. This syngas can be converted into methanol. Because the energy in this methanol still originates from a fossil source, namely coal, this can not be considered as sustainable energy or bio-fuel. However, because methanol-gasoline mixtures are used as car fuel, and because the methanol fraction is needed to be known for the same reasons as for ethanol, methanol is also considered in this work. The primary focus however is on ethanol-gasoline mixtures. [20]

1.5. SELECTION METHODS

To solve the ternary mixture problem, two measurement parameters are in search which are reliably measured, have a good reproducibility and repeatability. The two parameters should be selective to one or more of the components. An important aspect is the independency of the two parameters, with other words orthogonality should be introduced which result in a unique solution of the problem. There may be no dependency between the two measurement parameters. Furthermore introduced uncertainties, for example temperature effects, should be deterministic making correction possible.

The work of Lacerenca [13] concluded that promising possibilities would exist when using impedance spectroscopy as a detection method for the ternary mixture problem. Impedance spectroscopy, and more specific dielectric spectroscopy was investigated extensively within his work. This measurement technique is based on impedance of the liquid, which functions as a dielectric in an electrode/fuel interaction. The advantages are that this technique is non-destructive and robust. This thesis work will re-investigate the possibilities in the electrical domain by looking into the impedance behavior of the separate components and the ternary mixture. As well the low frequency range, so up to a frequency of 30MHz as high frequency range up to 15GHz will be covered. At the lower frequencies the considered possible selection parameters are the real and imaginary parts of the impedance, whereas in the GHz-range the mechanism of dielectric relaxation is considered.

Apart from the impedance spectroscopy, a significant part of this work was dedicated to optical spectroscopy. The mechanism of optical absorption spectroscopy was used. The UV range of $\lambda = 200$ nm up to $\lambda = 400$ nm will be treated, as well as the visible range and the infra-red range up to $\lambda = 3.3\mu m$. Also here, as well the separate components as ternary mixtures were considered. These measurements were carried out partly at TU Delft and partly at the Ford Motor Company, Dearborn.

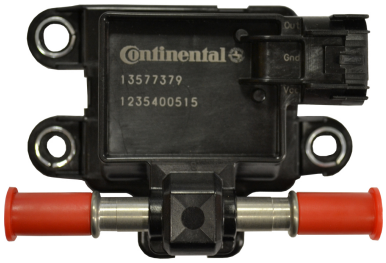

Figure 1.1: The Continental Flex-Fuel sensor. Source: [1]

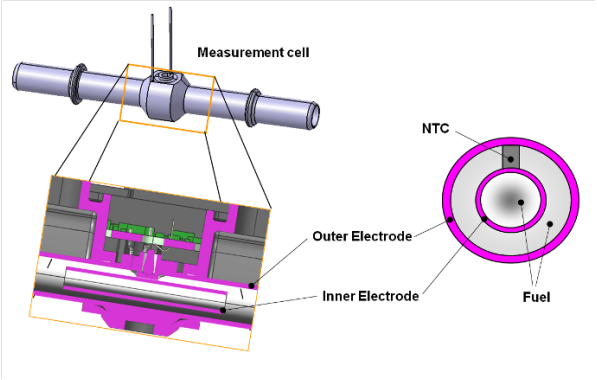

Figure 1.2: Details of the measurement cell. Source: [2]

1.6. STATE OF THE ART

The flex fuel sensor which is currently used by Ford is the Continental Flex Fuel sensor and is based on low frequency impedance measurement. The state of the art is now a measurement system which is capable of determining the ethanol/gasoline fractions in a *binary* mixture. To compensate for water content, a fixed water concentration is assumed and corrected for. Additionally a temperature sensor is embedded in electrode structure, in order to compensate for temperature effects. The determination of the gasoline vs. ethanol content is based on the dielectric constant of the fuel mixture present in the measurement cell. Since the dielectric constant of water ($\epsilon_r = 80$) is much higher than ethanol ($\epsilon_r = 25$) and gasoline ($\epsilon_r = 2$), a variable water content in the fuel strongly affects the measurement.

The sensor has an accuracy of $\pm$ 5% and a resolution of 0.1%, assuming no variable water concentration. Some practical measurements have been carried out using this sensor in an experimental setup. As expected, the error in the measured ethanol fraction increased dramatically if only 5% volume percent of water was present. Because a variable water concentration is introduced by the use of different kinds of ethanol (hydrous and anhydrous), fouling and the hygroscopic nature of ethanol, no commercially available flex-fuel sensor is present yet which is capable of measuring the three components.

1.7. OUTLINE

This thesis presents the research done in solving the ternary mixture problem when bio-ethanol is mixed with gasoline. This thesis is divided in 7 chapters and its outline is as follows:

This introduction chapter explains the context of the project, the practical and relevant information on bio-fuel and some important aspects of car fuel which are relevant to the measurement carried out in this work. It also describes the working principle of the state of the art.

Chapter 2 is meant to give an overview of the different possible domains, where selection parameters for the ternary mixture problem could be found. The small feasibility study is supported with measurements and examples. Furthermore, ideas about implementation techniques are given. At last an overview of all the domains is given.

Chapter 3 treats the first main domain which was extensively investigated. The goal of this chapter is to define the equivalent circuit model of the liquid-electrode system using a coaxial impedance probe structure. The derivation of this equivalent circuit model was done by finding explanations for effects which were observed during preliminary measurements.

Chapter 4 covers the design considerations of the dedicated coaxial impedance probe. Additionally, COMSOL simulations are included to support the calculations on the characteristic impedance. At last the realization of this probe is described.

Chapter 5 finalizes the low-frequency impedance part by describing the measurements carried out with the dedicated impedance probe. Important theoretical conclusions about the possibilities in this domain are drawn.

Chapter 6 introduces the second main domain, the optical domain, where absorption spectroscopy is investigated. This research is supported with two sets of measurements, partly carried out at Ford Motor Company, US.

Chapter 7 gives the conclusions which can be drawn. Secondly, the most promising combination of measurement techniques according to the author is described. At last, recommendations and future work is treated.

2

FEASIBILITY STUDY

In this chapter a brief overview of the possibilities in the different domains will be given. This short feasibility study was carried out in order to make a well argumented choice which domain would be worked out further, additionally to the electrical domain where the impedance was worked out. In an early stage it became clear that the electrical impedance in the low-frequency range would not give sufficient information to determine the composition of the ternary mixture. Details about the LF-impedance technique will be treated more extensively in chapters 3, 4 and 5.

2.1. LOW-FREQUENCY IMPEDANCE

The first possibility in the electrical domain is looking at the impedance behavior of the separate components of the bio-fuel mixture, water, ethanol and gasoline and mixtures of the three. This is typically done by using a certain electrode structure which interacts with the liquid under test. The frequencies where the impedance is determined ranges from approximately 10 Hz up to the MHz range. The lower limit is determined by the occurrence of electrolysis effects. The upper limit is determined by the RF-design and the occurrence of parasitic and resonance effects. Physical effects like the transport and polarizations of ions and dipole molecules present in the liquid can strongly affect the measured impedance. The typical *basic* equivalent circuit model of the electrode-liquid interaction is in this case a parallel circuit consisting of a resistance and a capacitance, see also figure 2.1. The topic of LF impedance measurements will be extensively treated in chapter 3, where the claims made in this section 2.1 will be supported with more theory and measurements.

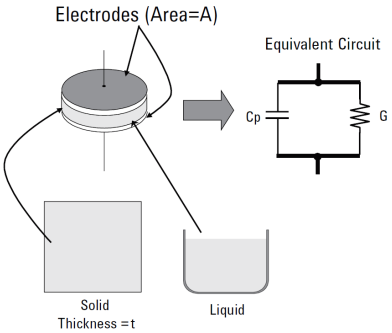

Figure 2.1: The basic equivalent circuit model used for measuring the components. Source: [3]

2.2. DIELECTRIC RELAXATION IN THE GHZ RANGE

The parallel capacitance of the equivalent circuit model of the low-frequency impedance behavior is determined by the dielectric constant ϵ and the cell constant of the used measurement cell. This dielectric constant originates from the different physical phenomena:

- Electronic polarization: Neutral atoms where the electric field displaces the nucleus with respect to the electrons
- Atomic polarization: Adjacent positive and negative ions stretch under an applied E-field
- Di-polar polarization: An electrical field exhibits torque on a dipole molecule

In dipolar liquids like water and ethanol, this dipolar polarization effect is dominating the total polarization, and therefore contributing most significantly to the total dielectric constant ϵ. When the E-field changes, the torque changes and the dipolar molecules need to turn according to the new orientation of the E-field. This turning does not happen frictionless. This friction is called 'loss', introducing ohmic losses ϵ''. This turning also costs time, the dipolar molecules can not follow the orientation of the E-field infinitely quick. A measure for the time it costs to follow the field is called relaxation time τ, this is the time it takes for a displaced system to return to 1/e of its random equilibrium value. At low frequencies, there is no phase difference between the polarization and the electric field, and the resulting dielectric constant is constant over frequency. At a certain frequency, the period of the alternating E-field is comparably smaller than the relaxation time, and the dipolar molecules can not follow the E-field anymore. Here the dielectric constant starts to roll off. At this point the loss peaks, because it increases proportional with frequency, up to where the dipolar polarization starts to disappear. The dielectric constant ϵ_∞ is mainly determined by atomic and electronic polarization.

2.2.1. DEBYE MODEL

The frequency where the permittivity starts to roll off is determined by the relaxation time τ. The Debye equation gives the relation between the total permittivity $\epsilon(\omega)$, the relaxation time τ and the real and imaginary parts of the permittivity. The model describes a first order roll off, and the position where the loss peaks is always at the same location of the 'transition band'. As a selection parameter to distinguish between the three components, the frequency where the permittivity starts to roll off and the amount in which the permittivity rolls off (the difference between $\epsilon_\infty - \epsilon_S$) can both be used. In figure 2.2 the dielectric relaxation of water is included, where the dashed trace represents the loss. In figure 2.3 the dielectric relaxation is of water is included as function of temperature. In figure 2.4 the relaxation of ethanol is included, as can be seen the relaxation frequency is approximately 2 GHz.

$$\epsilon(\omega) = \epsilon_\infty + \frac{\epsilon_S - \epsilon_\infty}{1 + j\omega\tau} \tag{2.1}$$

Table 2.1: Overview of different relaxation frequencies at 300K. Source: [21], [22]

Component	Relaxation frequency[GHz]
Water	20
Ethanol	2
Gasoline	no dipole

Debye equation: $\varepsilon(\omega) = \varepsilon_\infty + \frac{\varepsilon_s - \varepsilon_\infty}{1 + j\omega\tau}$

For $\omega = 0$, $\varepsilon(0) = \varepsilon_s$

For $\omega = \infty$, $\varepsilon(\infty) = \varepsilon_\infty$

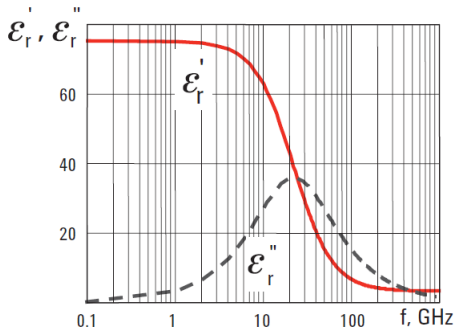

Figure 2.2: Dielectric relaxation of water at 300K. Source: [3] The total permittivity is divided in the real and imaginary part, where the real part ϵ_r' represents the polarization, whereas the imaginary part ϵ_r'' represents the ohmic losses.

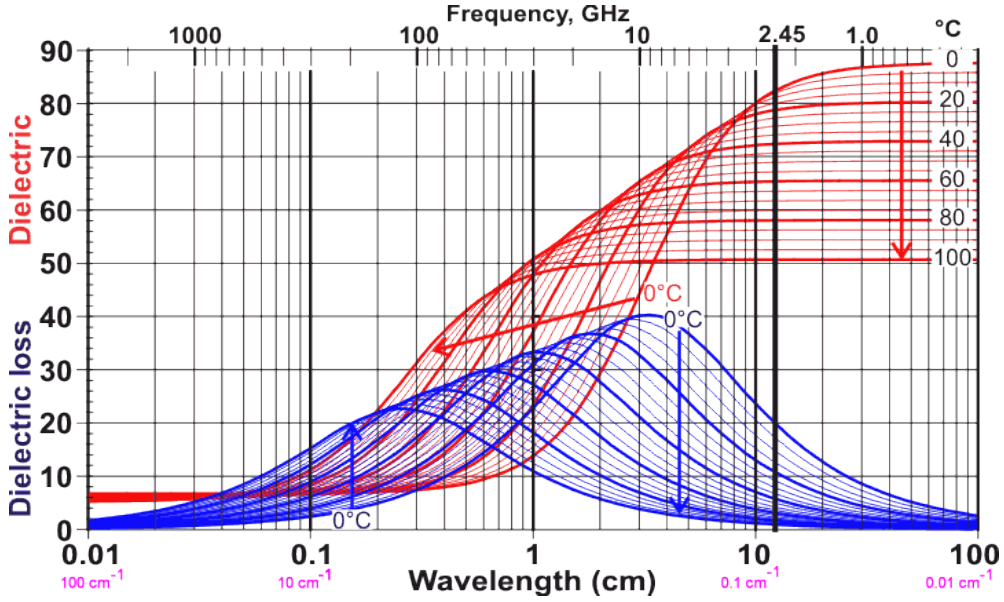

Figure 2.3: Dielectric loss of water as function of temperature in blue, dielectric constant of water in red. Source: [21]

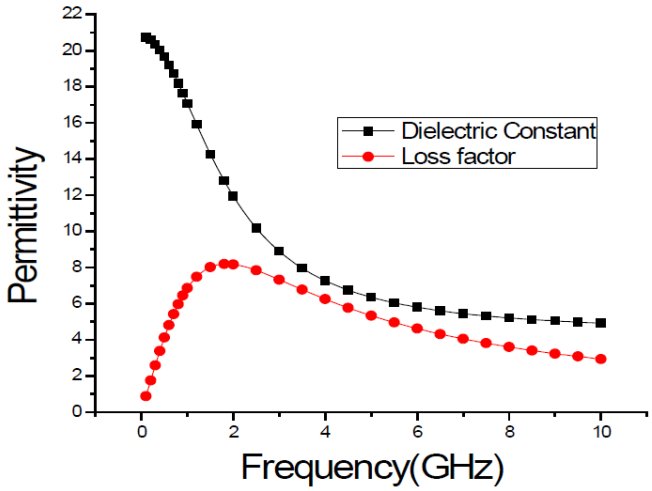

Figure 2.4: The graph of permittivity of ethanol at 320K against the frequency. Source: [22]

2.2.2. MEASUREMENTS

In the context of this feasibility part, some measurements were carried out at the department of Process and Energy at the 3ME faculty of the Delft University. The method used, was an open ended coaxial probe, the 85070E Dielectric Probe from Agilent in combination with an Agilent E5071C ENA Network Analyzer, which ranges from 300kHz up to 14GHz. With this combination, the magnitude of the scattering parameter S11 was measured. From this parameter, the permittivity ϵ can be determined. However, the measurement setup was not capable of delivering a reliable phase measurement. Therefore, the S11 measurements can not yet be used to fully extract the real and imaginary part of the complex permittivity. An algorithm like the SCL algorithm or the NRW method could be used for this purpose. For completeness this measurement plot is included in appendix C.

2.2.3. CONCLUSION OPPORTUNITIES DIELECTRIC RELAXATION

The frequency at which dielectric relaxation takes place differs significantly for ethanol and water. Theoretically, this would offer an ability to distinguish between these two components very well. Because gasoline does not contain dipole molecules, the effect of dipolar relaxation can not be utilized to say something about the gasoline content. The effect of dielectric relaxation is therefore only selective between ethanol and water.

During the RF measurements up to 14GHz it was experienced that the measurement of the phase of the S_{11} parameter is challenging with the setup which was available in the P&E department. When the mechanical properties of the setup were changed, a significant step in the phase response was read. Therefore, the obtained data did not yet give sufficient information to determine all the relevant details about the relaxation time and the real- and imaginary parts of the complex permittivity.

2.3. CALORIMETRY

In the thermal domain the thermal capacitance and thermal conductance can be considered as selection parameters. When comparing the thermal domain with the electrical domain, the electrical capacitor is analogous to the thermal capacitor and the electrical conductance to the thermal conductor. The voltage is analog to temperature now, and the heat source is the power source in the system. The combination of a parallel conductance and capacitance in the thermal domain also contains a corner frequency and thus a spectrum, however with frequencies within another order of magnitude.

2.3.1. POSSIBLE IMPLEMENTATION TECHNIQUE - 3ω METHOD

One example for the implementation of a measurement system which is capable of measuring as well the thermal capacitance as the thermal conductance, is the 3ω method. This method is a transient method, and has the advantage of a short response time and the minimization of radiation effects [23]. The 3ω method can be implemented by a so called hot wire, which functions as a heat source and temperature sensor simultaneously. Since the heat capacitance of the wire is relatively small, it results in a small error in the measurement. By injecting a current with frequency Ω through the wire, the power (which causes the wire to heat up) is proportional with 2ω, see also equations 2.2 and 2.3. This heating causes a temperature increase in the medium of the wire and the wire itself. The temperature of the wire is mainly determined by the temperature of the medium and influences the resistance of the wire. The influence of the temperature of the wire on its resistance is described by equation 2.4. Because the current through the wire is determined by the current source, and since the voltage over the hot wire is equal to the multiplication of current and resistance, a voltage proportional to 3ω arises. In an experimental setup, this voltage could be read out with the aid of a lock-in amplifier.

$$I = I_0 cos(\omega t) \tag{2.2}$$

$$P = I^2 R = \frac{1}{2} I_0 R_0 (1 + cos(2\omega t)) \tag{2.3}$$

$$R = \frac{dR}{dT} T_{2\omega} cos(2\omega t) \tag{2.4}$$

Table 2.2: Overview of the thermal conductivity and thermal capacity at 298K

Component	Thermal conductivity [$W\,m^{-1}\,K^{-1}$]	Thermal capacity [$J\,cm^{-3}\,K^{-1}$]
Ethanol	0.179	1.925
Gasoline (Octane)	0.15	1.64
Water	0.58	4.1796

2.3.2. CONCLUSION THERMAL DOMAIN

Based on the values presented in table 2.2 the largest difference between the thermal conductivity and capacity of the three components is between water versus ethanol and gasoline. Water has a significantly higher value for the thermal conductivity and thermal capacity. This domain could thus be exploited to be a good estimator for the water content. This measurement principle could be suitable in combination with the already designed probe, since this thermal system can be miniaturized which improves integration possibilities.

2.4. OPTICAL DOMAIN

In this section, the optical domain will shortly be addressed, because it will be treated more extensively in chapter 6. The technique which is treated here is absorption spectroscopy, the absorption of electromagnetic waves by (mainly) organic molecules. The full optical range from 200 nm up to 3300 nm will be treated in this work and two different measurement setups are used. Based on measurements which were carried out it could be concluded that the absorption behavior in the UV range is dominated by gasoline content and that deionized (D.I.) water has a flat spectrum in the UV range. Ethanol does contain spectral information, but its magnitude of absorbance is orders of magnitude lower than for gasoline. Concluding one could say that the absorption behavior in the UV range can be utilized as an estimator for gasoline content. Additionally, the absorption behavior in the IR range can be utilized to say something about the ethanol content. Because of the coloring which is added to gasoline, the visible range will not be usable. When the American Regular gasoline is compared to the euro 95 Dutch gasoline, an obvious difference in color can be observed. See also figure 2.5.

2.5. DENSITY MEASUREMENT

To investigate if the density would be a good parameter to distinguish between the three components, some density measurements were carried out at the department of Process & Energy, faculty of 3mE at TU Delft. These density measurements were carried out with an Anton-Paar DMA-5000 density meter. This meter uses the principle of an oscillating U-tube. When the material inside the tube changes, the frequency on which the tube is resonating, changes. By measuring this frequency, assuming the tube is completely filled (constant volume), the density of the liquid can be determined. The measurement results are included in table 2.3.

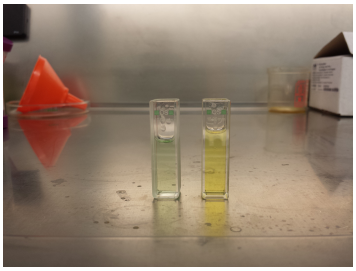

Figure 2.5: The different colors of American Regular Gas (left) and Dutch euro 95 (right)

Table 2.3: Overview of different measured density's. T=293K

Component	Density [g cm^{-3}]
Air	0.005056
D.I. Water	1.00025
Ethanol	0.789507
Gasoline	0.749365
50% D.I./50% ethanol	0.927996
50% gas/50% ethanol	0.769591
85% ethanol/15%gas	0.783379
80% ethanol/15% gas/5% D.I.	0.800523
75% ethanol/15% gas/10% D.I.	0.816620

2.5.1. CONCLUSION DENSITY MEASUREMENT

The density of air and water are conform expectations. The difference in density between ethanol and gasoline is only 6% w.r.t. the density of ethanol. Additionally none of the three components is showing a value which is far from the other two in magnitude, and therefore no orthogonality is present. This makes this domain in terms of selectivity less interesting. Factors which do advocate for this domain may be robustness and insensitivity for contamination.

2.6. SURFACE ACOUSTIC WAVES

To support the feasibility discussion of this chapter, it was decided to carry out some measurements with an SAW device. The Surface Acoustic Wave technique works with a surface effect. It is based on the piëzo electric effect, which is an interaction between the electrical en mechanical domain. More specifically the propagation of the wave on the boundary between the deposited liquid on the device and the solid state material of the device itself. The sensitivity of this type of devices (in contrary to Bulk Acoustic Wave devices) can be maximized by using wave types which show a high concentration of acoustic energy at the surface.

The SAW device which was used, was the sensor described by the thesis 'A smart lamb-wave sensor system for the determination of fluid properties' [24]. Lamb waves are related to Rayleigh waves and contain both shear and normal displacement components. The a lamb wave sensor considered here is consisting of two sets of two interdigital transducers (IDTs) of aluminum on a zinc oxide layer. This zinc oxide layer is deposited on aluminum, silicon oxide, a Si-epi layer and at last the silicon bulk. This device is fabricated in the DIMES laboratory. For all the details about this sensor, see also the Ph.D. work of M.J. Vellekoop [24]. Two pictures of both sides of the sensor package have been made, see therefore figures 2.7 and 2.8.

The measurement principle is as follows: Both IDTs are connected to the Vector Network An-

Figure 2.6: The density meter at the laboratory of Process & Energy department

alyzer, which is determining the transfer between both two-ports, whereas at the same time a droplet of the liquid under test is put on the device. The relevant parameter is then the scattering parameter S_{21} (the forward voltage gain). At a certain frequency the transfer between in- and output of the device is maximum. The velocity of propagation of the acoustic waves is dependent on multiple mechanical parameters, namely the mass adsorption, the viscosity, the density and the sound speed through the liquid. The sensitivity to either of these parameters is dependent on the liquid which is measured. For example, viscosity sensitivity is very low for low-viscous liquids. Since we are dealing with low viscous liquids, this effect is negligible compared to the other mechanical parameters. The two major parameters are therefore sound speed and density. This speed is generally highest in the solid state, followed by the liquid state and the gas state. When a liquid with certain properties is deposited on the back of the SAW device, the total speed will be an average of the velocity of the waves trough the device itself and through the liquid. A lower velocity of propagation will result in a lower frequency where the transfer peaks.

The results of the measurements can be seen in figure 2.9. The frequencies where the voltage transfer is maximum is clearly a function of the medium, as significant difference in peak frequency is present between ethanol, water and gasoline. The traces of the mixtures between both three are located on places which seem logical considering the peaks of the pure components. The 50% ethanol/50% D.I. mixture however peaks above the value of water, which seem not logical. An explanation might be that the viscosity still plays a significant role, despite the application on low-viscous liquids. This could be explained by the sensitivity function of this SAW device, which is included in equation 2.5. The sensitivity of the resonance frequency ω to the speed of sound c_f is a function of multiple parameters: ρ_f is the density of the fluid, c the in plane wave velocity, δ_f the fluid layer thickness, k the propagation constant, m the mass adsorption and η the viscosity. The sensitivity of the resonance frequency to the speed of sound is therefore also a function of the the fluid layer thickness δ_f. Since in this small experiment droplets were used, and because the surface tension of gasoline and ethanol is much smaller than that of water, the layer thickness is introduced as a disturbing uncertainty. A recommendation for this experiment is to control the layer thickness, for example by putting the surface of the device on or inside the liquid under test.

$$S_\omega^{c_f} \approx \frac{\rho_f c^2 c_f^{-3} \delta_f^3 k^2}{2(m + \rho_f \delta_f + \sqrt{\frac{\rho_f \eta}{2\omega}})} \tag{2.5}$$

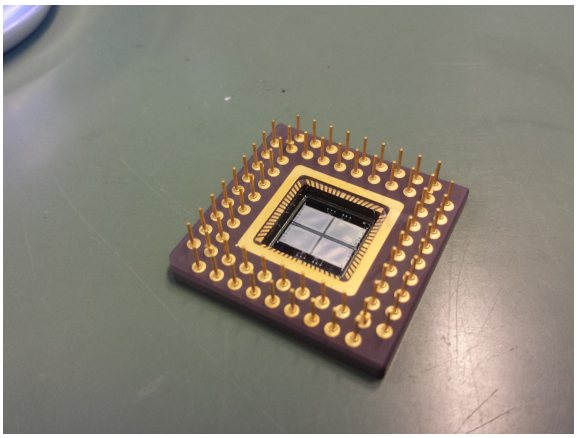

Figure 2.7: The used SAW device, bottom view of the package. The 2 times two IDTs are located on this side

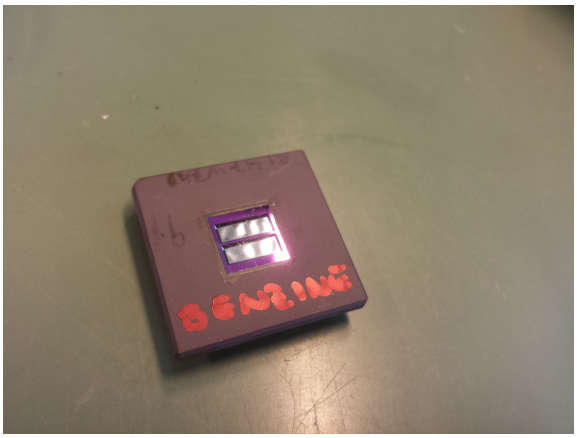

Figure 2.8: The used SAW device, top view of the package. The two separate devices can clearly be distinguished

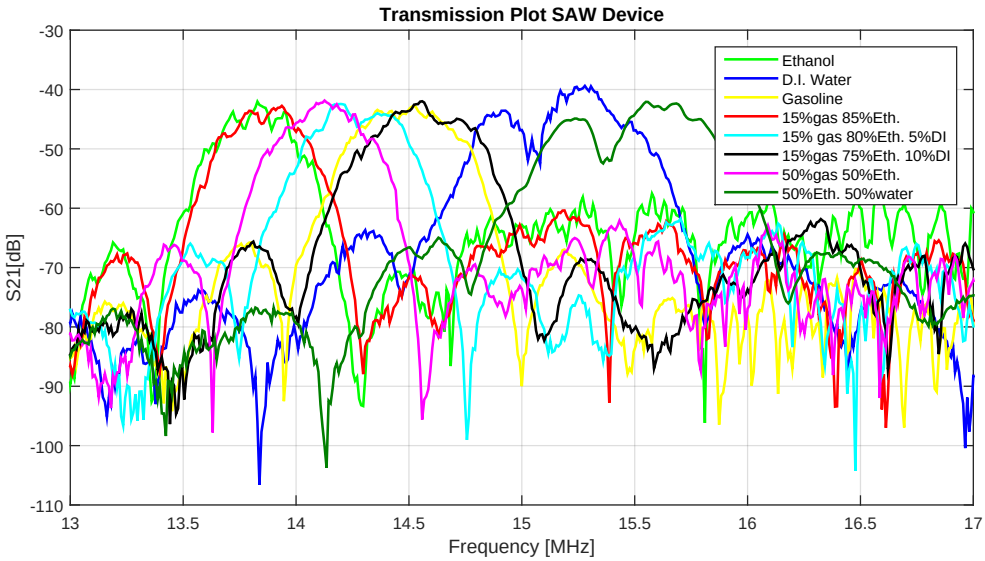

Figure 2.9: Results of the measurements with the SAW device

Table 2.4: Overview of different speeds of sound, T=298.15K. And of different viscosity's, T=293K. Source: [25]

Component	Speed of sound [m/s]	Viscosity [mPa s]
Water	1250	0.894
Ethanol	1480	1.074
Gasoline	1144	0.6

2.6.1. CONCLUSIONS MEASUREMENTS SAW DEVICE

Since the field of Acoustic Wave devices is very broad, this set of measurements was only intended to give a glance about the existence and possibilities of this technique. In terms of selectivity, none of the three components is dominating the response, so no large orthogonality is supplied when using this technique. However, it might very well be used to supply additional information in combination with a measurement technique of a different domain, for example LF impedance in the electrical domain. It is expected based on literature that when the uncertainties of the viscosity and liquid layer thickness are taken away, this technique is robust in terms of repeatability and relatively insensitive to contamination.

2.7. COMPARISON AND OVERALL CONCLUSIONS FEASIBILITY PART

In the comparison between different possible quantities and domains, the aspect which will impose the limiting specifications on a measurement system, will be the selectivity of a certain domain to either of the three combinations. Therefore a ranking of the selectivity between each of the three components has been made. Since the selectivity is expressed differently in either of the domains (differences in equivalent medium approximations and orthogonality of the separate components), this ranking has not been done with numbers, but with a plus/minus scale. See also table 2.5. The behavior which would be ideal, talking about selectivity, is a measurement result where there exist a certain (frequency/wavelength) range where one of the three components is 100% dominating the parameter, or dominating it within acceptable ranges, taking into account the final inaccuracy of the fuel composition ratios. This seems to be happening with the optical absorbance in the range from 280nm up to 315nm, here the absorbance is practically dominated by gasoline, as will be treated extensively in chapter 6. The thermal domain in addition, shows a large difference between water content and the other two components. It could be concluded, based on this introduction to the different domains, that the optical measurement methods in the UV range delivers information about the gasoline content, whereas the thermal domain gives information about the water content. For completeness, also some measurement in the mechanical domain have been carried out. The SAW implementation by Vellekoop has been picked as a starting point. Many more implementations could be possible, for example oscillating U-tubes or the usage of bulk acoustic waves instead of surface acoustic waves.

Table 2.5: Selectivity comparison for gasoline (**G**), ethanol (**E**) and water (**W**). Range: - -, -, 0, +, ++

Domain	Selectivity W w.r.t. G	Selectivity W w.r.t. E	Selectivity E w.r.t. G
LF permittivity	++	+	++
Thermal	++	++	0
Optical visible	0	- -	0
Optical IR	++	- -	++
Optical UV	++	0	++
Density	+	0	- -
Viscosity	0	0	+
Speed of sound	0	0	0

3

LF IMPEDANCE

In this section the equivalent circuit model will be derived of a electrode/liquid under test system. For this analysis some experimental probes were used, because a dedicated impedance probe was not yet available. In chapter 4 the design considerations of the coaxial impedance probe will be treated. In chapter 5 the measurements with this dedicated probe will be treated.

3.1. LF IMPEDANCE MEASUREMENTS

Because the initial technique to be investigated, taking into consideration the work of Lacerenza [13], is impedance spectroscopy, it was decided to re-investigate the possibilities in the range up to 100 MHz first. To get an idea about how the impedance of the liquid/electrode combination will behave and to which extent we can gather information in the 'low-frequency' (LF) range, impedance measurements are done on the different components of the ternary mixture. One of the key goals for this measurements is to derive an equivalent circuit model for the fuel mixture/electrode system. This model is needed to be able to interpret the measurement results correctly by mapping the raw impedance (|Z| and θ) data on this model. The changes in the liquid under test will manifest themselves as variations of the components of the equivalent circuit model. The 'standard' equivalent circuit model to start with, is the parallel capacitance/conductance. This model will be the starting point of this analysis.

3.1.1. MEASUREMENT SETUP

The impedance analyzer used is the Agilent 4294A in combination with an extension probe 42941A. This extension probe is calibrated with respectively a short, a 50Ω and an open termination. Parasitic effects of the extension probe are calibrated out, possible effects originating from the exper-

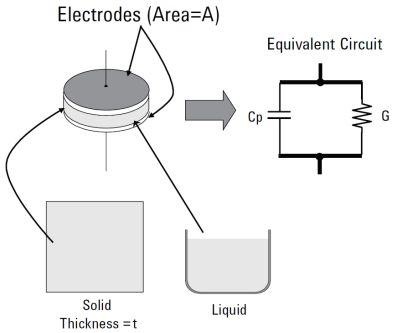

Figure 3.1: The initial equivalent circuit model used for measuring the components. Source: [3]

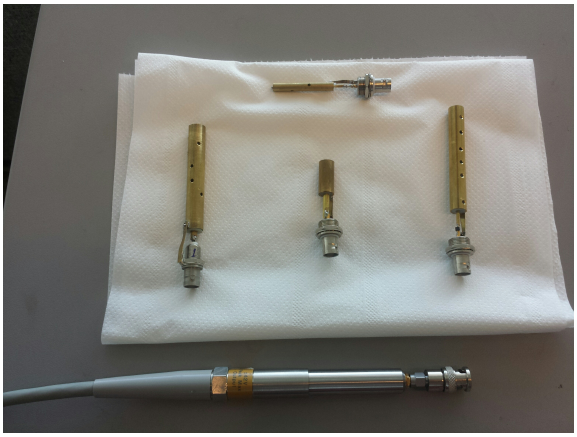

Figure 3.2: The four different probes by number. Only the bottom three are used, from right to left nr. 1-3. Bottom: the extension probe 42941A

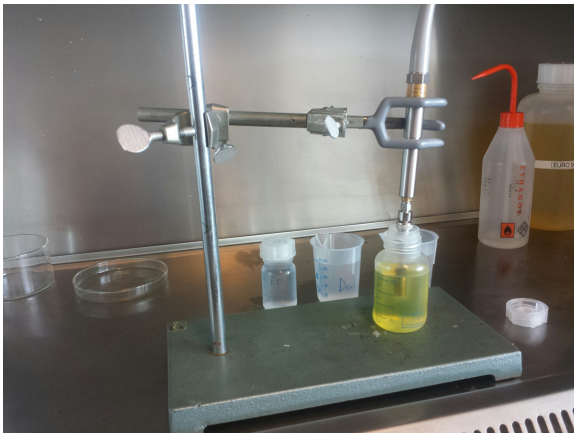

Figure 3.3: The measurement setup. Here the measurement of regular gasoline

imental probe can still manifest themselves. A practical advantage is that by using the extension probe, no 4 cable connection is needed. A 4 cable configuration is typically used to correct for capacitive and inductive effect by the leads (Van der Pauw Method), because of an independent voltage sensing path and and independent signal current path. The data is read out via a LAN connection and is sent to an Excel file delivered by Keysight. This raw data is imported in Matlab.

The measurements that were carried out are the following:

- $|Z| - \theta$ for the following liquids over the frequency range 100Hz up to 110MHz
  - Air, empty measurement
  - Deionized water
  - Tap water
  - Regular 'Dutch' gasoline 95RON
  - 100% ethanol

3.1.2. MEASUREMENT I

For this series of measurements probe number one was used, because of its best performance in preliminary measurements. In figure 3.4 the comparison of the parallel capacitance among the different dielectrics is plotted. As written above the frequency range is from 100Hz up to 100MHz. The empty and the gasoline measurement confirm that the medium behaves purely capacitive. Further deionized water and ethanol have the same behavior, but tap-water shows a particular behavior from 100kHz and below. As can be observed, this capacitance increases up to the μF range. It can therefore be questioned if the model of a capacitor in series with a resistor (figure 2.1) is correct for measuring the medium in the case of tap-water. This model seems to be correct for ethanol and deionized water, also when one looks to the impedance plot, figure 3.6. However if we consider the phase plot for tap-water, figure 3.7, it seems that there is a *zero* in the origin, and there are two *poles*, one at approximately 10kHz and one at approximately 1MHz. Another effect which is evident when looking at the parallel conductance 3.5 is the resonance peak around 50MHz. This can be explained by the existence of parasitic effects of the experimental measurement probe. This issue will be solved, when an dedicated impedance probe is designed later on in this work.

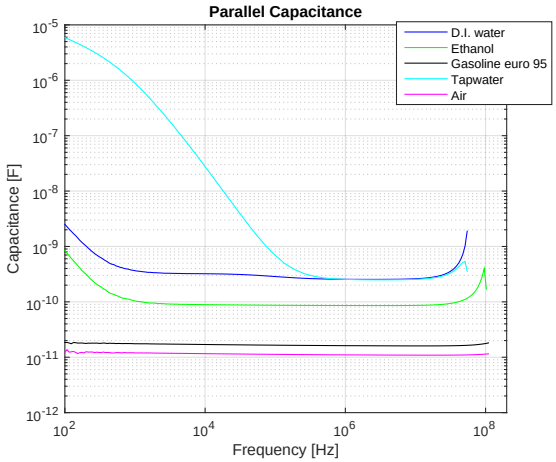

Figure 3.4: C_p of the three main components and tapwater

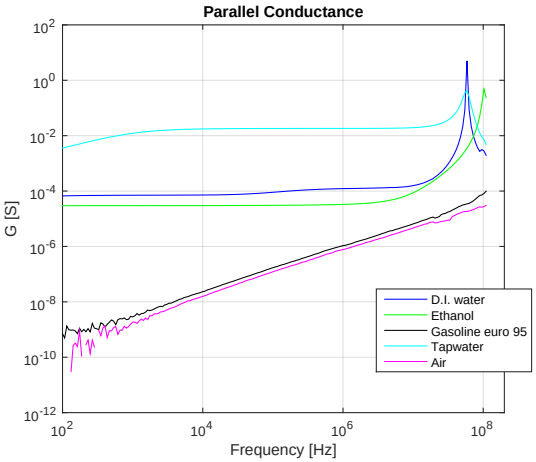

Figure 3.5: G_p of the three main components and tapwater

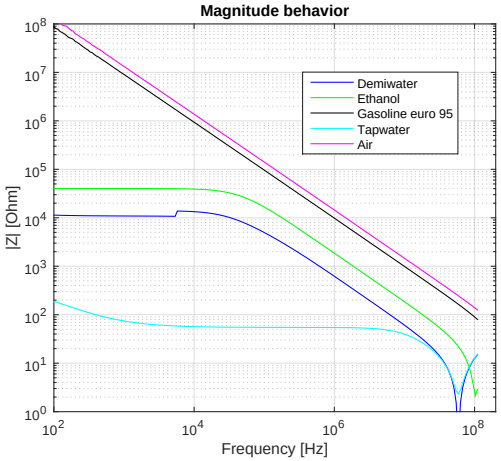

Figure 3.6: |Z| of the three main components and tapwater

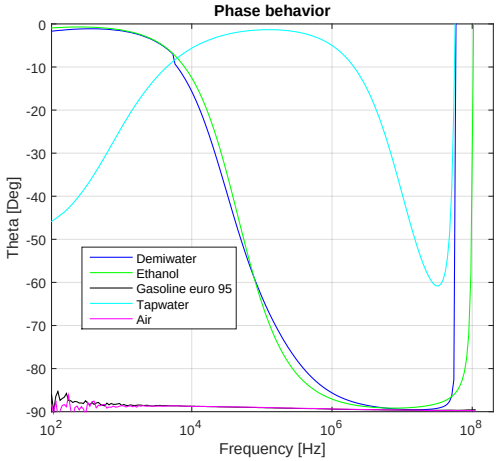

Figure 3.7: Φ of the three main components and tapwater

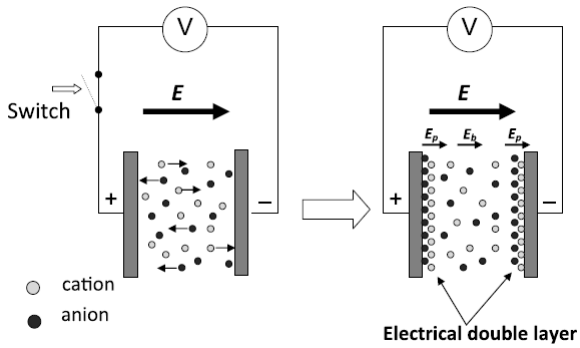

Figure 3.8: An illustration about the charge buildup on both sides of the electrodes. Source [4]

3.2. DOUBLE LAYER CAPACITANCE

An issues to investigate is that the capacitance is increasing up to the μF range in the case of tap-water. This effect was noticed during the impedance measurements described in section 3.1. In the case of ethanol and deionized water, the parallel capacitance also increases, but in a much smaller amount. If the model of the parallel capacitance with conductance would be correct, the projected values of C_p and G_p would be constant. This is not the case here.

3.2.1. ELECTRODE POLARIZATION

The increase in measured parallel capacitance from approximately 1MHz and below for tap-water and in smaller amount, for ethanol and deionized water, is the result of the so called 'double' layer capacitance. When a liquid contains many free ions, these ions will diffuse through the liquid as a result of the electric field. At the boundaries, c.q. the electrodes, this diffusion causes a charge build up. When the field is opposite (AC excitation), this process is reversed and the charge will be build up on the opposite side. This effect is called electrode polarization and the resulting impedance is the polarization impedance.

The equivalent model resulting from this effect to describe the probe/liquid interaction is depicted in figure 3.9. The polarization capacitors and resistors are placed in series with the sample R-C parallel network. The two values of Cp/2 and Rp/2 can be taken together since they are equal. When this model is 'mapped' onto the simpler R-C model, the equivalent parallel capacitance is equal to.

$$C = C_s + \frac{1}{\omega^2 R^2 C_p} \tag{3.1}$$

Now the increase in parallel capacitance at frequencies below approximately 1 kHz can be explained. Tap water used in this measurements contains a high concentration of free ions. These ions will contribute largely to the polarization capacitance. Since tap-water is a good conductor too, R_p and R_s will be low, yielding a high capacitance at lower frequencies, as can be seen in figure 3.4. Both resistors need to be small, to let the two capacitors be in parallel. Only in this configuration the double layer capacitance can add to the total measured parallel capacitance. This is the case with good conducting liquids like tap water, where R_s is relatively small. When frequency increases, the period of the signal decreases, as a result less charge is build up at the boundaries (since the drift velocity of the free ions can be considered constant for the same E-field), resulting in a lower polarization, and thereby lower overall capacitance. This explains the second order roll-off of the added capacitance by the electrode polarization effect. The equivalent circuit model of the liquid/electrode system is as in figure 3.9. A parallel capacitance/conductance in series with the double layer capacitance. The value of the series resistance is in most literature neglected.

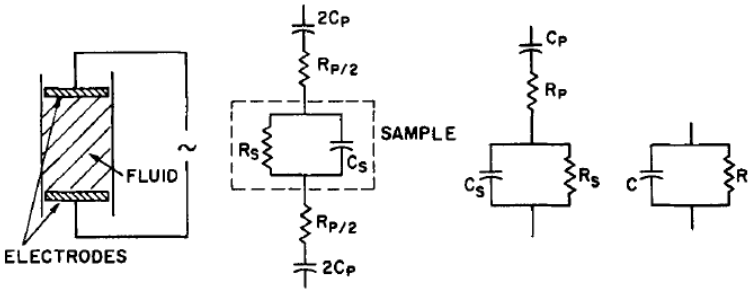

Figure 3.9: Equivalent model including the electrode polarization. Source [5]

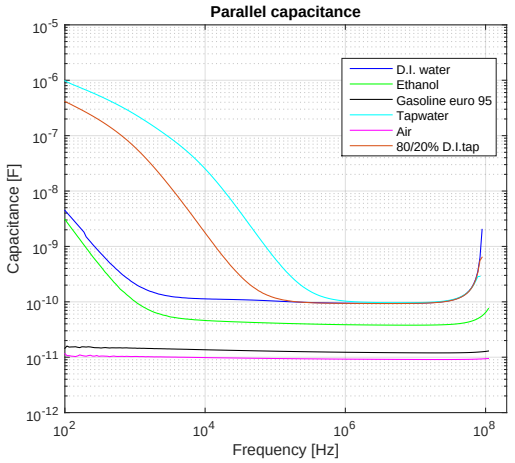

Figure 3.10: C_p including the 80%/20% ratio of D.I./tap water

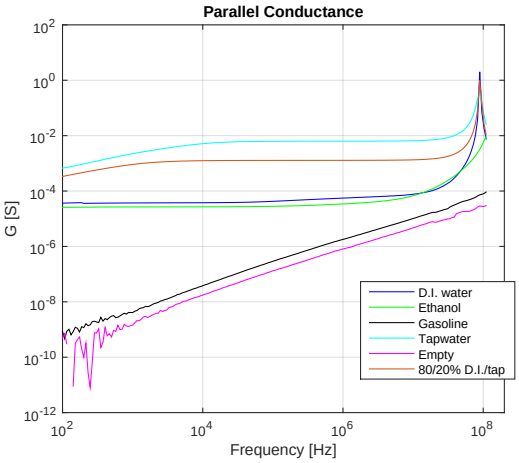

Figure 3.11: G_p including the 80%/20% ratio of D.I./tap water

3.2.2. MEASUREMENTS - II: ELECTRODE POLARIZATION

To verify if the increasing capacitance is indeed the effect of the electrode polarization/the presence of the double layer capacitance, a mixture with 80 volume percent deionized water with 20 volume percent tap-water was measured. It is expected that the measured values for capacitance and conductance are in between the values for deionized water and tap water. Because there were some mechanical issues with probe number 1, the probe which is most similar to probe 1 was chosen, namely probe number 3. The cleaning and drying in between the different measured components is extra important in this series, since a small residue of tap water contains a lot of free ions. The change in probes is influencing the response in terms of absolute value to a small extent, but is not problematic for verifying the influence of ions and the concepts op double layer capacitance. For a complete overview, and to verify the first measurement series with probe 1, additionally to the 80/20 measurement, the gasoline, ethanol, DI-water, air and tap-water measurements are redone. The results are included in figures 3.10 and 3.11. It can be concluded that the capacitance and conductance behavior resembles the results obtained with probe 1 during the first measurement series. The graph of the capacitance and conductance of the 80/20 mixture lays in between the graphs of 100% deionized and 100% tap water. This result is according to prior expectations based on the theory about ion transportation and double layer capacitance. The free ion concentration is a measure for the amount in which the double layer capacitance adds to the total measured parallel capacitance. Additionally, the parallel conductance is strongly affected by the free ion concentration.

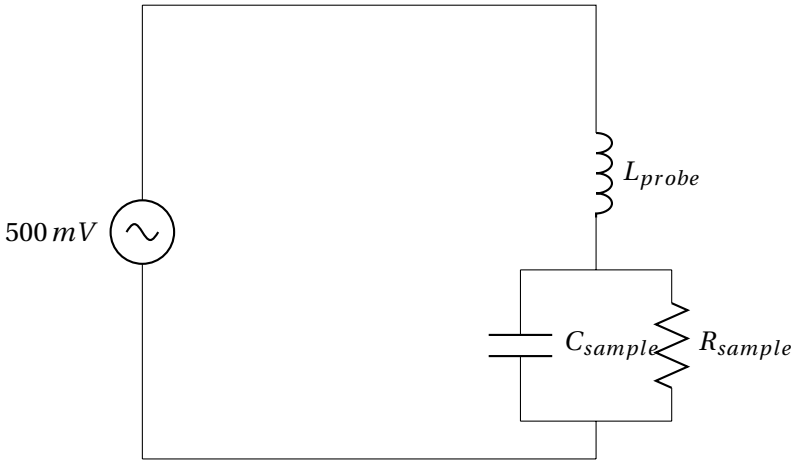

Figure 3.12: The equivalent circuit model including the parasitic inductance of the used probe

3.3. SERIES INDUCTANCE

A second effect which can be noticed from the measurements (section 3.1) is that the measured conductance is increasing with increasing frequency. This frequency dependency is approximately first order behavior and is most strongly present in the measurements where the medium is formed by air and by gasoline, both have relatively low ϵ media compared to water and ethanol. The increase of the measured parallel conductance can be explained by the presence of a series inductance. To get an idea about the size of this inductance, the inductance along the coaxial probe of probe 1 was measured and found to be 49 nH. As a result, the parallel resistor/capacitor model is not covering all effects for low ϵ materials. When the impedance of the model with included series inductance is calculated and used as 'data' to the simpler model (without series inductance) we see the following expression for R.

$$R_{RC}^2 = \frac{-L - \omega^2 R^2 L C^2 + R^2 C}{\omega^2 L C^2 + \omega^4 R^2 L C^2 + C} \tag{3.2}$$

When no inductor would be present this model is correct(L=0):

$$R_{RC}^2 = \frac{R^2 C}{C} = R^2 \tag{3.3}$$

Now, if there *is* a parasitic inductor L present, but not taken into account in the used equivalent circuit model, then the L terms do not fall out of equation 3.2. By leaving out the constant terms and looking to the terms which are frequency dependent in this fraction, the effect of the inductor on the calculated resistance can be found.

$$R_{RC}^2 \propto \frac{-\omega^2}{\omega^2 + \omega^4} \propto \frac{-1}{\omega^2 + 1} \propto \frac{1}{\omega^2} \tag{3.4}$$

Taking the square root:

$$R_{RC} \propto \frac{1}{\omega} \tag{3.5}$$

This effect will only be visible when the inductance and capacitance are in the same order of magnitude. So when a dielectric with low ϵ is inside the probe, just as was the case with gasoline and air. When a liquid with a large permittivity is measured, C is big compared to L, and the parasitic effect has a negligible effect on the determined parallel resistance. The equivalent circuit model including the series inductance is included in figure 3.12.

3.4. INITIAL COMPOSITION ANALYSES

Knowing that the ion concentration influences the parallel capacitance and conductance significantly, initially one would think that the low frequency domain is not giving opportunity to fulfill the requirement of this sensor system. However, as described in section 3.2, these ions cause the double layer which only manifest itself up to a certain frequency. From measurements described in section 3.1 it can be noticed that this polarization effect vanishes from a certain frequency, depending on the ion concentration in the measured liquid and the dimensions and characteristics of the probe. A safe worst case estimation from where the electrode polarization will be vanished is approximately 1 MHz. The fact that the double layer capacitance is present up to a certain frequency, and is not present at a higher frequencies, means theoretically that this effect can actually be *used* to determine the ion concentration and to deal with a fourth unknown in the ternary mixture problem.

3.4.1. POSSIBLE STRATEGY WHEN ONLY DEIONIZED WATER IS ASSUMED

If only the water is taken into account which results from the production of bio-ethanol, the problem can quite easily be solved using the conductance and capacitance. This procedure is also described in the paper [26]. Capacitance is completely flat for all types of water from approximately 1 MHz, so the first independent equation can be determined from this frequency and beyond. The second equation can be taken using the parallel conductance. The used frequency should be high enough that no 'DC-effects' are present and low enough that no resonance effects take place. Ideally the parallel capacitance and conductance is determined at the same frequency, which simplify the sensor implementation in later design stages. The three equations will be the following, where the α represent the volume fraction of each of the components and C represent the measured parallel capacitance.

$$C_{mix} = \alpha_w C_w + \alpha_g C_g + \alpha_e C_e \tag{3.6}$$

$$G_{mix} = \alpha_w G_w + \alpha_e G_e + \alpha_g G_g \tag{3.7}$$

$$\alpha_w + \alpha_e + \alpha_g = 1 \tag{3.8}$$

Subscript	Meaning
mix	mixture
d	deionized water
t	tap-water
w	water (general)
g	gasoline (general)
e	ethanol

3.4.2. POSSIBLE STRATEGY WHEN ION-RICH WATER IS ASSUMED

For the case of the impedance domain we actually do have four components now instead of three, namely deionized water (originated from condensation and the production process of bio-ethanol), gasoline, ion-rich water(i.e. tap-water), ethanol. In the context of the final application, it is needed to determine the amount of *water* in general. At the low frequencies it is clear that the capacitance is for a large amount determined by the free ions originating from the ion-rich water. At higher frequencies, above 1MHz, tap-water and deionized water behave exactly the same

speaking about the parallel capacitance. A possibility to deal with unknown free ion concentrations is to measure the capacitance at reasonably low frequencies, say 1kHz-100kHz, and subtracting the 'HF' (around 1MHz) capacitance which is independent of the free ions. The resulting capacitance is a result of the electrode polarization effect caused by free ions, and can be used as an estimator for the free ion concentration. The measured parallel conductance G_{mix} can now be corrected for the influence of free ions by this estimator of the free ion concentration, whereafter the problem can be considered again as ternary. When using the polarization capacitance effect to correct the measured conductivity, it is important that a change in viscosity of the medium has the same influence on as well the conductivity as on the capacitance, to maintain the relating function between measured capacitance increase by free ions and conductance correction of the mixture to be valid. The problem contains now four different components: ion-rich water, deionized water, ethanol and gasoline and can be considered as quaternary. Overall, the measurement strategy to determine the volume fractions of the separate components is as follows.

- Measure the increase in capacitance caused by electrode polarization, by first measuring at the lower frequencies (1-100kHz), then measuring the capacitance above 1 MHz and subtracting both values. Let this ΔC_{mix} be an estimator for the free ion concentration.
- Use this value to correct the measured conductivity of the mixture later on.
- Measure the parallel capacitance in the regime above 1 MHz, where C_p of deionized water and tap water are the same, and let this deliver the first independent equation.
- Measure the conductivity and let this deliver the second independent equation. The ambiguity in the conductivity is now removed by subtracting an correction value as function of the ΔC_{mix} (the double layer capacitance effect).
- The third independent equation is delivered by knowing that the sum of all three fractions is equal to 1.

At lower frequencies (1kHz) ΔC_{mix} can be determined. $C_{mix,1MHz}$ is measured at higher frequencies, i.e. above 1MHz, here the parallel capacitance of tap-water is equal to the capacitance of deionized water. At higher frequencies, approximately above 1MHz, the equation 3.10 can be obtained. Now the other parameter that is taken into account is the conductivity, where the conductivity of the water can be considered as the conductivity of deionized water (ion free) because G_{mix} is corrected for the influence of free ions by a function of $(C_{mix} - C_{mix,1MHz})$, see also equation 3.11.

$$\Delta C_{mix} = (C_{mix} - C_{mix,1MHz}) \tag{3.9}$$

$$C_{mix,1MHz} = \alpha_w C_w + \alpha_g C_g + \alpha_e C_e \tag{3.10}$$

$$(G_{mix} - f(C_{mix} - C_{mix,1MHz})) = \alpha_w G_w + \alpha_e G_e + \alpha_g G_g \tag{3.11}$$

$$\alpha_w + \alpha_e + \alpha_g = 1 \tag{3.12}$$

Now we have a set of 3 unknowns and 3 independent equations, so this is mathematically solvable.

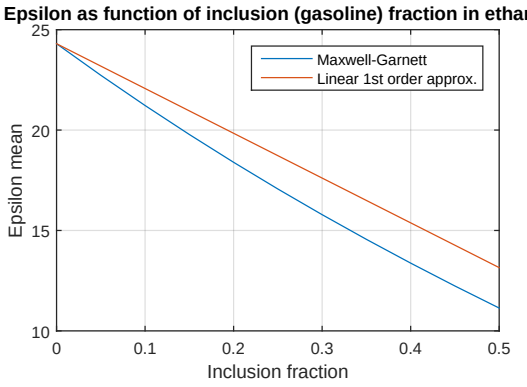

Figure 3.13: The mean value of the dielectric constant according to the two different models

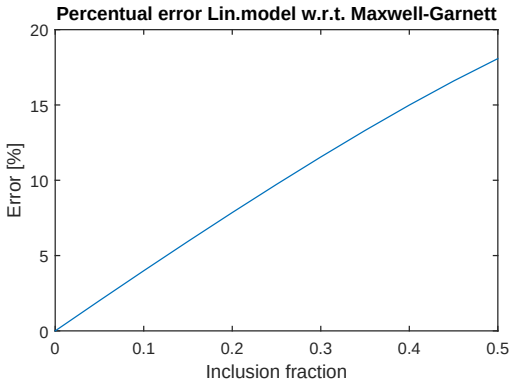

Figure 3.14: The relative error of the linear model w.r.t. the Maxwell-Garnett model

3.4.3. EFFECTIVE MEDIUM APPROXIMATION: MAXWELL-GARNETT

In this section a medium approximation will be worked out and will be compared with the linear mixing model used up to this point. The motivation for this, is to get an idea about the error which will be introduced when the linear mixing model is used. One approximation to determine the resulting dielectric constant of a mixture is the effective medium approximation by the Maxwell-Garnett model. This model assumes a base medium in which an inclusion medium is included with a certain volume fraction. The Maxwell-Garnett approximation assumes that the domain of the base material and the inclusions are spatially separated, and therefore only valid at low inclusion fractions. For that reason, only inclusion fractions up to 0.5 are taken into consideration, but validity may be restricted to even much smaller inclusion fractions. [27], [28] The Maxwell-Garnett equation is solved by equation 3.13, where δ_i represents the inclusion medium fraction. To compare the linear mixing model (as proposed in this project up to this moment) with the Maxwell-Garnett approximation, the effective dielectric constant was calculated with both models using an inclusion fraction ranging from 0 up to 0.5. The base is considered ethanol with a gasoline inclusion. The results are presented by figures 3.13 and 3.14. When the Maxwell-Garnett approximation is assumed as correct, the error made by a linear approximation already exceeds the 5% when a gasoline inclusion of 10% is present.

$$\epsilon_{eff} = \epsilon_m \frac{2\delta_i(\epsilon_i - \epsilon_m) + \epsilon_i + 2\epsilon_m}{2\epsilon_m + \epsilon_i + \delta_i(\epsilon_m - \epsilon_i)} \tag{3.13}$$

3.5. MEASUREMENTS III - E85

An additional measurement series is treated in this section, to investigate the mixing behavior in practice. To see if the E85 delivered by the Ford Motor Company will behave the same as an 'self-made' mixture E85, these two mixtures have been measured. Also for future project possibilities, methanol is measured. Because it was experienced from earlier measurement series that no additional information is provided at frequencies above 30 MHz, this is used as upper limit of the frequency range for this series. For comparison and completeness the impedance measurements on pure ethanol and gasoline euro 95 are redone. From figure 3.15 it can be observed that the traces of the self-mixed E85 and the E85 FMC fit between the measured capacitance of pure ethanol and gasoline. In the lower frequency range, from 2 kHz and below, the increase in parallel capacitance caused by the double layer capacitance is present again. The extent to which this effect is occurring is significantly higher for the E85 fuel mixture originating from FMC. This implies that the free ion concentration is significantly higher for the FMC fuel than in the self-mixed case. Looking at the conductance, see figure 3.16, this expectation is confirmed. The conductivity

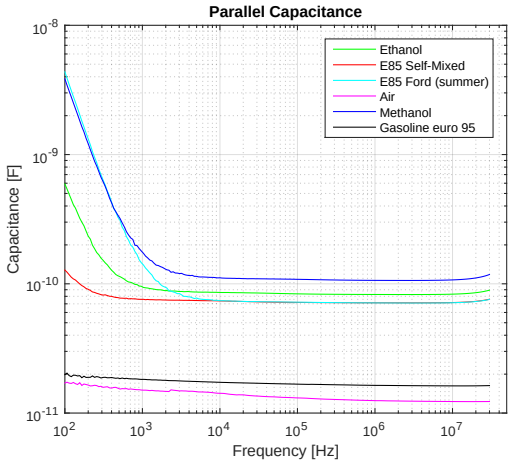

Figure 3.15: C_p including the methanol and the two versions of E85

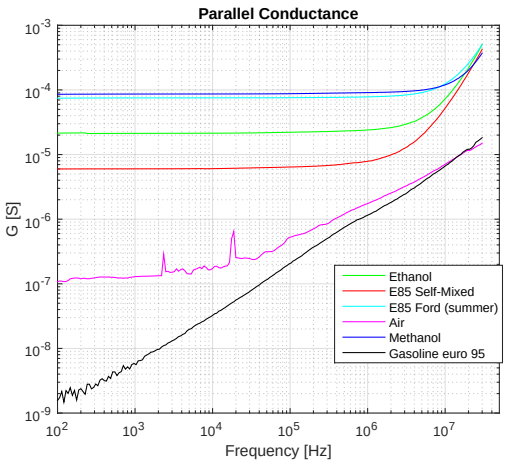

Figure 3.16: C_p including the methanol and the two versions of E85

of the E85 FMC fuel mix is with 75.4 µS more than one order of magnitude larger than the 6.05 µS measured for the conductivity of the self-mixed E85. This observation confirms again the theory about the double layer effect caused by free ions in the liquid. A resonance effect is visible from the MHz range and beyond.

3.5.1. EMPIRICAL VALIDITY OF LINEAR MIXING MODEL

After some theoretical analysis done in section 3.4.3, the additional measurements done in this section give a good opportunity to verify. Because E85 was measured, an binary mixture is considered. The values are considered at a frequency of 100 kHz. This frequency provides stable values for as well the capacitance as the conductance values. More specifically, at and around this chosen frequency, the spectral behavior does not show variations over frequency in both domains.

$$\begin{aligned} C_{p,e} &\quad 83.60\,\text{pF} \\ C_{p,g} &\quad 16.73\,\text{pF} \\ C_{p,E85} &\quad 71{,}77\,\text{pF} \end{aligned}$$

According to the linear mixing model:

$$C_{p,E85} = 0.15 \cdot 16.73\,\text{pF} + 0.85 \cdot 83.60\,\text{pF} = 73.57\,\text{pF} \tag{3.14}$$

The resulting difference between the measured self-mixed E85 mixture and the calculated capacitance value for this binary mixture:

$$\Delta_{C_p} = \frac{73.57 - 71.77}{71.77} \cdot 100\% = 2.51\% \tag{3.15}$$

- The impedance measurement accuracy is within 1% in this measurement range according to the data sheet of the device.
- The E85 sample was made by manually mixing the two components using an medical syringe. An accuracy of some tenth of a percent can be assumed this way.

Considering these uncertainties, the determined error is within acceptable boundaries, Ford Motor Company would agree with an total system error of approximately 3-5%. In agreement with

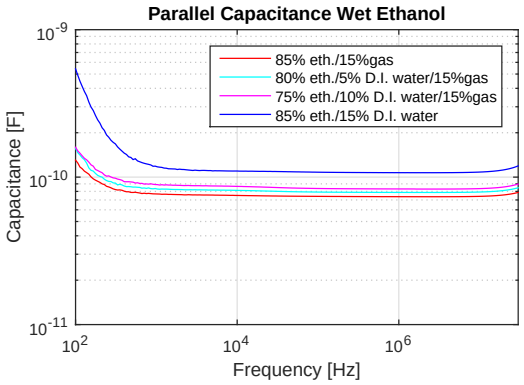

Figure 3.17: C_p for legitimate E85 mixtures with constant gasoline concentration

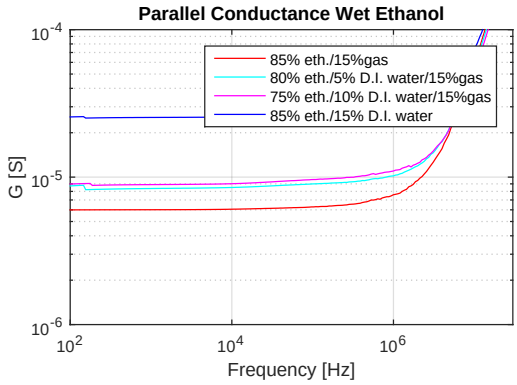

Figure 3.18: G_p for legitimate E85 mixtures with constant gasoline concentration

the theory of effective medium approximations the linear mixing model estimates the equivalent ϵ higher than the true value. Contrary, the predicted error by the Maxwell-Garnett model is much higher than the error determined here. It can be concluded that the linear mixing model is a better approximation than the Maxwell-Garnett effective medium approximation.

3.6. FOULING DETECTION E85

A very common mixture is E85. Assuming that this mixture contains water, there are two scenario's possible. Either the water can be part of the ethanol part in the E85 mixture, when so called wet ethanol is used. When this is not the case, the water can be added after the mixture was made, for example by the trader of the mixture. Then this can be considered as adulteration of the bio-fuel, and thus fouling. In the latter case, the percentage gasoline, which should be 15%, is affected. In the first case, this percentage will not be affected by the presence of water. Practically, this implies that without looking to the double layer effect or the influence of free ions/tap-water, even adulteration with deionized water is detectable as long as it is known that the mixture should be E85. In this section, a strategy to check for this form of fouling is worked out.

As an example for this statement, some measurements were carried out. In the first series of measurements, the non-fouling set, the water content was at the cost of the ethanol content, thereby keeping a constant 15% gasoline. The capacitance and conductance plots can be seen in figures 3.17 and 3.18. In the second set, a pure E85 mixture was taken and water was added to it, resulting in adulteration of this fuel. The capacitance and conductance plots can be seen in figures 3.19 and 3.20. If one would like to say something about fouling, without working out the linear mixing models, one can start by looking at the measured capacitance of an adulterated mixture. Suppose an adulterated E85 mixture is measured with 5% water. The parallel capacitance of this mixture is 82 pF (at 100kHz) and this value corresponds with a legitimate mixture with water content between 5% and10%. To check whether this mixture could be legitimate, we now look at the conductivity of this legitimate mixtures (figure 3.18), the corresponding values for this range (water between 5 and 10%) are between $9\mu S$ and $9.6\mu S$. When we look at the measured (adulterated) conductance, this value is equal to $6.6\mu S$, so these measured values don't 'pass' this test, and it can be concluded that the measured mixture is adulterated → fouling. With other words, there is no linear combination possible of both the capacitance and conductance of an legitimate mixture which satisfy both the measured conductance and capacitance values of the adulterated E85 mixture.

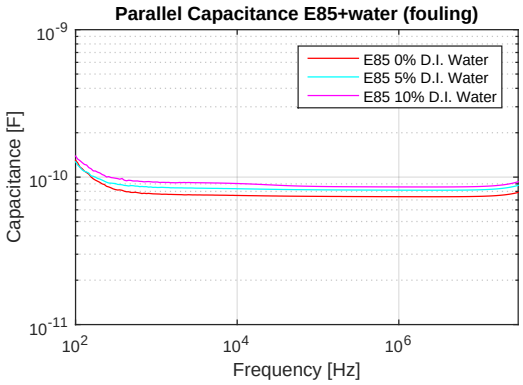

Figure 3.19: C_p for non-legitimate E85 mixtures, decreasing gasoline concentration when diluted

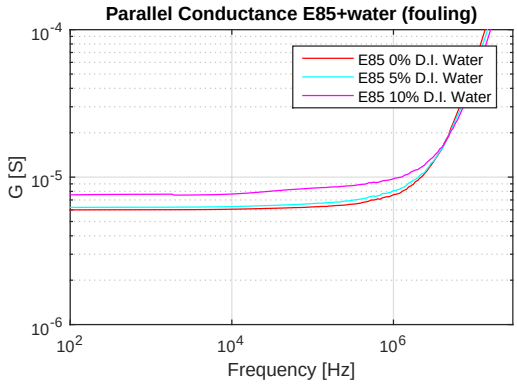

Figure 3.20: G_p for non-legitimate E85 mixtures, decreasing gasoline concentration when diluted

3.7. TOTAL EQUIVALENT MODEL AND CONCLUSIONS

After the analysis done in sections 3.2 and 3.3, the total equivalent circuit model consists of the sample parallel capacitance and conductance. Additionally a series capacitor originating from the double layer capacitance (in the case of ion rich water) is present and a series inductance originating from the distributed inductance in the probe. The total equivalent circuit model is included in figure 3.21. As proposed earlier, the double layer capacitance might theoretically be eligible to correct for the influence of free ions on the measured parallel conductance. This will only be relevant if ion rich water is considered, for example in fouling scenario's. Exploiting the double layer effect by correcting the conductance will in practice be challenging for multiple reasons. For example the 'mapping' function from a increased capacitance to a correction in the measured conductance has to be derived and be deterministic in different measurement conditions (varying temperature for example). Another issue is that the conductance increases dramatically as function of the ion concentration. Because of this high sensitivity, with only a small error in capacitance measurement, a large error in conductance correction will be made. Because of these reasons, this measurement strategy to deal with the fourth unknown, the ion concentration, will be worked out further in this work. The series inductance is due to the fact that the coaxial probes themselves are not calibrated. There are multiple options to remove the influence of this inductance. Firstly, calibration can be done before measurements are taken out. However a change in (measured) impedance will cause a deviation from the calibration point, and therefore introduce again an influence by the parasitic series inductance. This topic will be further explained in chapter 4.

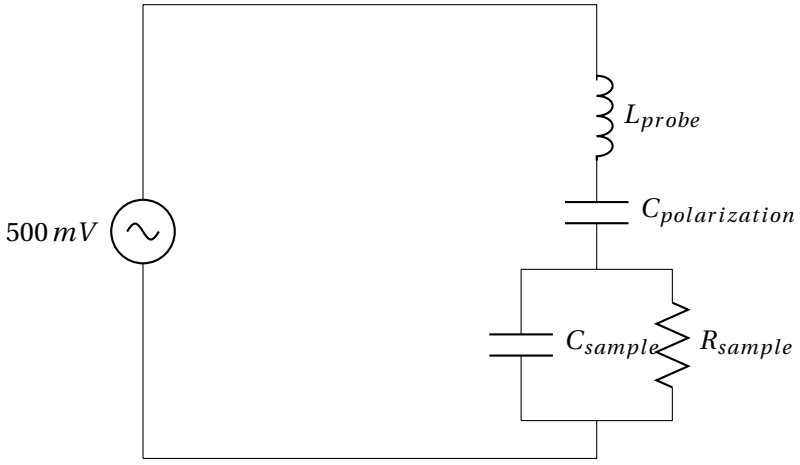

Figure 3.21: The total equivalent circuit model of the electrode/liquid under test system, using a coaxial impedance probe

4

PROBE DESIGN

In cooperation with a mechanical engineering internship student, Felix Wolffenbuttel, it was decided to design a probe for lab applications. Because the measurements described in chapter 3 were carried out with probes which experienced some unwanted parasitic effects, for accuracy reasons it would be better to work with an probe dedicated to measure the impedance of these liquids and is able to be calibrated.

4.1. REQUIREMENTS

The probe that is concerned here, is a lab-purpose probe. The probe will be used to characterize the components in the test phase. The design flow and experience of this probe may help to design the possible industrial probe later on in the project. The motivation for the probe to be coaxial is that the probe needs to be calibrated, in order to correct for the parasitics of the probe itself, here mainly the series inductance. Calibration requires a characteristic system, the probe can be terminated with an impedance with the same value as the characteristic impedance of the probe itself. 50Ω is a standard value for the characteristic impedance, because it is a compromise between the best peak power handling and lowest cable loss. For standardization reasons, this value is also used here for the design of the characteristic system. Further reasons for a coaxial geometry are that the probe is easy to clean and that the liquid under test will flow in and out of the structure reliably.

Requirements

- Probe has to be coaxial
- The characteristic impedance of this coaxial probe has to be 50Ω
- It must be possible to reliably terminate the probe with a short and a load with a 50Ω impedance in order to proper calibrate the measurement system
- The materials of which the probe is fabricated should be resistant to the components which are measured: ethanol, gasoline and water
- The inner conductor has to be robust, such that no deformation/movement of the electrode is possible
- Aeration of the probe is an important aspect, the liquids must be able to enter and leave the probe easily
- Multiple signs on the outside of the probe must be present to mark the level of the mixture

4.2. CALIBRATION

To improve sensitivity and to minimize the effect of parasitics when performing LF impedance measurements, it is advantageous to calibrate as close as possible to the dielectric constant of the mixture to be measured. This can also be viewed as a 'common-mode' problem, calibrating in air with an ϵ_r of one, and measuring a liquid with an ϵ_r of 25 (ethanol) may induce more errors than calibrating at an ϵ_r of 24. To investigate if the measurements are getting more accurate if the calibration takes place in a liquid with an ϵ_r closer to the to be measured MUT, a probe with interchangeable inner conductor was designed. By using different inner electrodes, the characteristic impedance is held on 50 Ω, with the ability to calibrate at higher values of ϵ_r. An overview of the different possible calibration ϵ_r in combination with the coaxial probe dimensions, is included in table 4.1. These dimensions are based on commercially available brass cylinders of with the probe will be designed. The range of ϵ_r goes up to 17, because above this value the inner conductor is getting to small to be mechanically feasible in combination with an outer diameter of 16 mm.

Table 4.1: An overview of different $\epsilon_r's$ in combination with the inner conductor diameter

D/d [mm]	designed for ϵ_r
16/0.5	17
16/1	11
16/2.5	5
16/5	2
16/7	1

For completeness, an overview of ϵ_r for different components is given in table 4.2. Further, in this context it might be relevant to consider some possible practical mixtures, these are included in table 4.3. For the water containing ethanol, the worst case water concentration of 'wet-ethanol' AEHC is considered. According to ANP AEHC must have an ethanol content between 92.6 and 93.8 INPM (mass content). When we translate these value to volume fractions, AEHC must contain between 94.1 ° GL and 95 ° GL, which means that the maximum water volume fraction is equal to 5.9% [15].

Table 4.2: An overview of different ϵ_r of the relevant components at 293,15 K

Component	ϵ_r
Deionized water	80.4
Gasoline	2.0
Ethanol	24.3

Table 4.3: An overview of different ϵ_r of the relevant mixtures at 293,15 K according to the linear mixing model

Mixture	ϵ_r
E22 (pure components)	6.9
E85 (pure components)	21.0
E85 (ethanol containing 5.9% water)	23.8
E100 (containing 5.9% water)	27.6

4.3. CHARACTERISTIC IMPEDANCE AND COMSOL SIMULATIONS

4.3.1. CHARACTERISTIC IMPEDANCE

As was discussed in section 4.1, the characteristic impedance is a key aspect in designing a coaxial impedance probe. A coaxial probe can be viewed as a piece of an infinitely long transmission line. The characteristic impedance can be viewed as the ratio between voltage and current when an pulse is traveling along an infinitely long line at t=0. When the inner and outer conductors are from a well conductive material, the two most important parameters are the series inductance and the parallel capacitance. (Where the latter is employed in our measurement system) The two formulas describing them are included in equations 4.1 and 4.2, where D is the inner diameter of the outer conductor, and d is the outer diameter of the inner conductor. The characteristic impedance is then obtained by 4.3, assuming that the resistance per unit length is zero.

$$(\frac{C}{l}) = \frac{2\pi\epsilon_0\epsilon_r}{ln(D/d)} \tag{4.1}$$

$$(\frac{L}{l}) = \frac{2\pi\mu_0\mu_r}{2\pi} ln(D/d) \tag{4.2}$$

$$Z_0 = \sqrt{\frac{L}{C}} \tag{4.3}$$

4.3.2. LENGTH OF THE COAXIAL PROBE

Since the characteristic impedance is in principle only determined by the ratio of the conductor diameters, varying the length does not affect this value. The length of the probe however, has significant implications on various parameters. When increasing the length of the probe:

- The value of C_p will increase
- The value of L_s will increase
- As a result of the increase of both values, the resonance frequency will decrease
- ΔC_p will increase, the increase in the parallel capacitance of the coaxial probe will increase when the probe is longer. The insertion of a MUT with a higher ϵ_r will cause a larger increase of the absolute value of the parallel capacitance. This effect is not yet advantageous or disadvantageous, but can be taken in mind when an analog back and/read-out is designed.
- To prevent the case of having standing waves on the probe, the length of the probe may not exceed approximately a tenth of λ
- As a compromise between ΔC_p and a lowering of the resonance frequency, an effective probe length of 50 mm has been chosen

4.3.3. COMSOL SIMULATIONS

To verify if the calculations on the characteristic impedance were done correctly, and to gain some extra insight in the Electro-Magnetic field distribution inside a coaxial structure, some 2-dimensional RF simulations were done on a coaxial cable. For these simulations the RF module in Comsol was used. This simulation uses the dimensions of the coaxial structure, the dielectric constant of the medium and calculates at first the analytic value of the characteristic impedance.

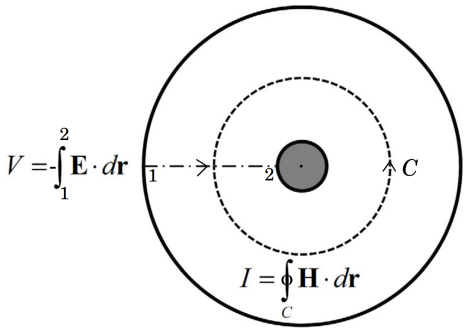

Figure 4.1: Both integrals in the coaxial structure, source [6]

Then the electric and magnetic fields are calculated and graphically plotted. Now the voltage between the inner and outer conductor is determined by integrating the electric field over a boundary which can manually be allocated. Secondly the current is determined by evaluating a contour integral, where the closed contour is the circle along the outer conductor. Finally the characteristic impedance is determined by dividing voltage and current. This value can now be compared to the analytic value. Both integrals are depicted in figure 4.1. Further, the setup settings of the simulation are included in table 4.4.

Table 4.4: Comsol 2-dimensional RF coaxial cable simulation setup for the $\epsilon_r = 17$ case

Figure	Value
outer conductor	16 mm
inner electrode	0.5 mm
ϵ_r medium	17
μ_r medium	1
σ medium	0
frequency	1 GHz

Table 4.5: Comparison of the characteristic impedance's

D/d [mm]	designed for ϵ_r	$Z_{0,analytic}$	$Z_{0,simulated}$	error [%]
16/0.5	17	50.399 Ω	50.484 Ω	0.168
16/7	1	49.566 Ω	49.653 Ω	0.175

In table 4.5 as well the analytic values of the characteristic impedance as the simulated values are included. It was chosen to simulate both 'extremes', so for an ϵ_r of 1 and 17. The error is only around 0.2% when the analytic approach is used, so with this simulation the calculation of the characteristic impedance has been validated.

4.3.4. RELATION BETWEEN CONDUCTIVITY AND PARALLEL CONDUCTANCE

When doing the impedance measurements, the measured values will be mapped on the most appropriate model, the parallel capacitance and conductance. Now, when one would like to compare the measured value for the parallel conductance with the bulk parameter 'conductivity' $[S \cdot m^{-1}]$ or 'resistivity' $[\Omega \cdot m]$, there is a cell constant between both of them. The relation between resistance and resistivity ρ is described by Pouillet's law.

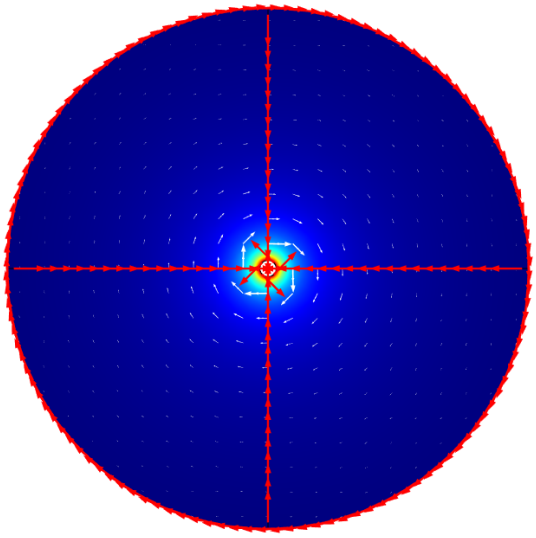

Figure 4.2: The obtained simulation result for the $\epsilon_r = 17$ designed probe. The electric field is depicted in colors, whereas the magnetic field is marked by the arrow vector field. The red vectors are the tangential components of the magnetic field used for integration.

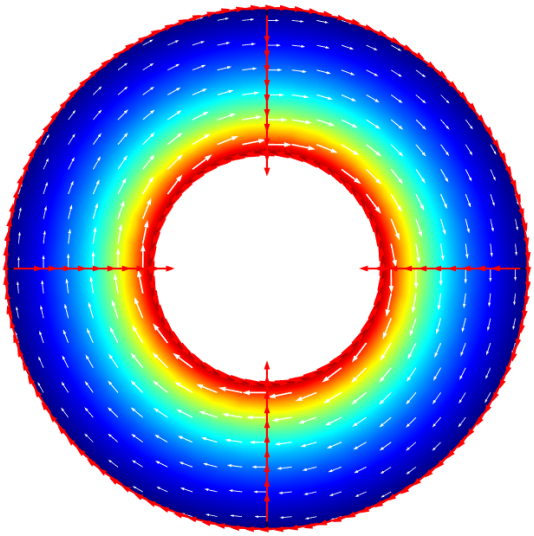

Figure 4.3: The obtained simulation result for the $\epsilon_r = 1$ designed probe. Clear is that the ratio of conductor diameter is different from the previous simulation. The electric field is depicted in colors, whereas the magnetic field is marked by the arrow vector field. The red vectors are the tangential components of the magnetic field used for integration.

$$R = \rho \cdot \frac{l_d}{A} \tag{4.4}$$

In the case of a coaxial impedance probe, the length l_d is equal to the distance between the inner and outer electrode. The calculation will be done, assuming the probe for $\epsilon = 1$.

$$l_d = \frac{D-d}{2} = \frac{16-7mm}{2} = 4.5\,\text{mm} \tag{4.5}$$

The area A is not a constant in the case of a coaxial structure, since the area of medium between the two electrodes is increasing when going from the inner to the outer conductor. The area of a cylinder is now considered and filled in, in Pouillet's law. Neglecting the parasitic effects on the end of the coaxial structure, the inner electrode can be seen as a cylinder.

$$R = \rho \cdot \frac{l_d}{2\pi r l} \tag{4.6}$$

Now integrating this formula for the radius r.

$$R = \int_{r=R_i}^{r=R_o} \rho \frac{l_d}{2\pi r l} dr = \frac{\rho l_d}{2\pi l} \ln \frac{R_o}{R_i} \tag{4.7}$$

Filling in the constants for the distance between the electrodes, the length of the coaxial probe and the outer- and inner radius, yielding:

$$R = \rho \cdot 1.18 \times 10^{-2}\,\Omega \tag{4.8}$$

After measuring R_p, the resistivity is thus.

$$\rho = R_p \cdot 84.5\,\Omega\,\text{m} \tag{4.9}$$

4.3.5. RELATION BETWEEN RELATIVE PERMITTIVITY AND PARALLEL CAPACITANCE

Analog to the calculation of the resistivity from the parallel conductance, the relative permittivity is also directly linked to the parallel conductance via a cell constant. The (parallel) capacitance for a coaxial structure is described by the following equation:

$$C_p = \frac{2\pi\epsilon_0\epsilon_r l}{ln(D/d)} \tag{4.10}$$

Solving this equation for ϵ_r yields:

$$\epsilon_r = \frac{C_p ln(D/d)}{2\pi l \epsilon_0} \tag{4.11}$$

Filling in the values for a D/d ratio for an ϵ_r of 1 gives:

$$\epsilon_r = C_p \frac{ln(16/7)}{0.05 \cdot 2\pi\epsilon_0} = C_p \cdot 2.97 \times 10^{11}\,\text{F}\,\text{m}^{-1} \tag{4.12}$$

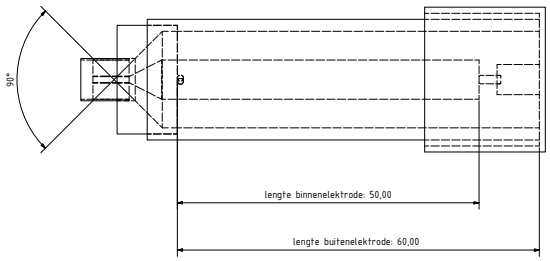

Figure 4.4: The cross section of the coaxial impedance probe. Source: [7]

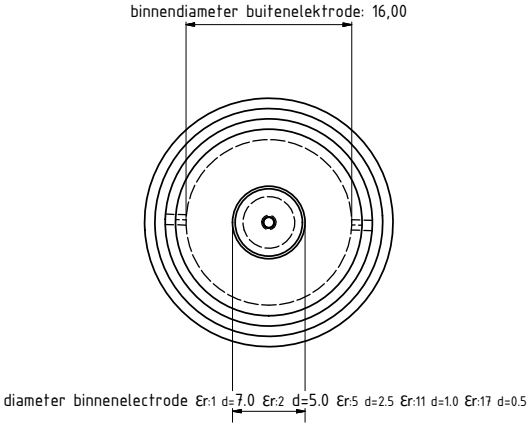

Figure 4.5: Cross section from the front. Source: [7]

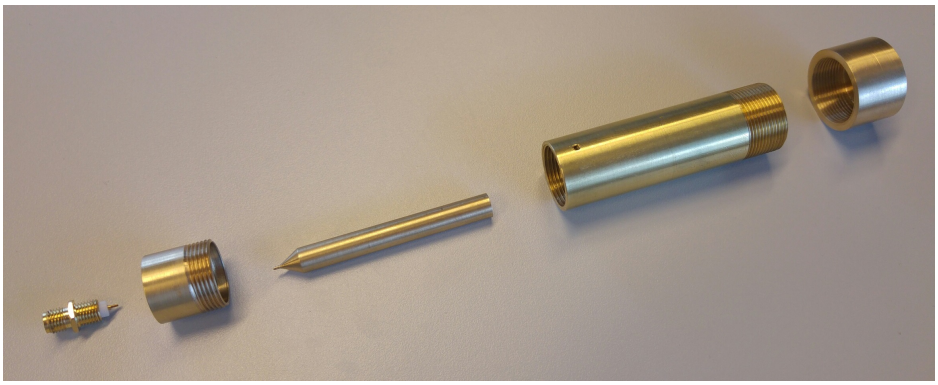

Figure 4.6: The realized coaxial impedance probe

4.4. DESIGN AND REALIZATION

In figures 4.4 and 4.5 the design of the coaxial impedance probe is included. The design process is carried out in communication with the author and with the advices and consultation of J. Bastemeijer. The interchangeable inner electrodes can be used for higher ϵ calibration as explained earlier, the parts of the probe are cashed (chemically silver plated) to improve series conductivity and to prevent contamination and oxidation of the brass material. The design has been carried out with the help of autoCAD design software. In the final assembly of the probe, some epoxy material has been used. For all technical details, the report of F. Wolffenbuttel can be adressed. [7]

Figure 4.7: The realized coaxial impedance probe, note the different inner conductor diameters, as well as the different calibration terminations

5

MEASUREMENTS DEDICATED PROBE

5.1. MEASUREMENT SETUP

All included measurements in this section were carried out on the same afternoon, to prevent possible errors due to fluctuations in temperature. Secondly, the characteristic system was calibrated with the available load and short extensions of the dedicated probe, after the impedance analyzer was warmed up (30 min.). At last, after every measurement with possible high ion concentration or other contamination sources, the probe was cleaned by putting it into a sample with 'cleaning' ethanol, where after the probe was partly disassembled and dried with compressed air. Then the measurements with resulting samples were continued. For the measurements, a Matlab script was used, which triggers the analyzer, such that no possible drift effects are visible. The used Matlab code is included in section B.2. A complete overview of the measurement setup is included in table 5.1.

Table 5.1: Measurement Conditions

Impedance Analyzer	Agilent 4294A
Extension Probe	Agilent 42941A
Meas. Probe	Dedicated, coaxial
Measurement Range	100 Hz - 30 MHz
Calibration Medium	air
Number of points	201
Sweep	frequency, logarithmic
Excitation	Sinusoidal
Exc. amplitude	500 mV
Raw data	|Z|, θ

5.2. MEASUREMENTS

For this series it was decided to redo the measurements on all liquids done earlier using the experimental probes, to get a complete overview of the results with one probe and setup. As described above, measures have been taken to remove uncertainties. Apart from the three components (ethanol, regular gasoline euro 95 and D.I. water) also Methanol and some E85 mixtures were measured. Additionally two 'E85' mixtures contain respectively 5% and 10% D.I. water. This water content is of cost of the pure ethanol content to mimic a practical situation where hydrous

ethanol is used. The results for the parallel capacitance of the liquid are included in figure 5.1. These results resemble the measurements done with the experimental probes, they are however more stable over frequency. Again the double layer effect is present, however in a much smaller extent than with tap water. The different liquids differ from eachother only in magnitude, and the spectrum is flat over the whole frequency range. If no double layer effect is taken into account, impedance measurements in the MHz range do not provide additional information compared to measurement above the frequency where no double layer effect takes place, say 10 kHz. To investigate if the capacitance meets the linear mixture model also in the case of a ternary mixture, and to validate the measurements carried out with the designed dedicated probe, a comparison between the calculated value according to the linear mixing model using the measured values for the pure components and the measured values of the mixtures has been made. The data points at the frequency 102.9 kHz have been chosen, because at this frequency the possible influence of the double layer effect is absent. For the case of self mixed E85 at 102.9 kHz for example, the calculated value from the mixing model of 71.21 pF is close to the measured value of 69.36 pF. A difference of 2.68% w.r.t. the measured value. For the two ternary E85 mixtures, see table 5.2 below .The influence of the inaccuracy introduced by the impedance analyzer was calculated and found to be 0.894% for the parallel capacitance at this specific frequency and for these specific impedances. The full calculation is included in the appendix D.

$$0.85 \cdot C_{ethanol} + 0.15 \cdot C_{gasoline} = 0.85 \cdot 82.8p + 0.15 \cdot 5.54p = 71.21\,\text{pF} \tag{5.1}$$

Table 5.2: The calculated capacitance according to the linear mixing model and based on the capacitance measurements of the pure components at 102.9 kHz.

Mixture	C_p linear mixing model [pF]	C_p measurement Mixture [pF]
85%Eth. 15%Gas	71.21	69.36
80%Eth. 15%Gas 5%D.I.	81.92	82.77
75%Eth. 15%Gas 10% D.I.	92.63	91.00

In figure 5.2 the measured parallel conductance is shown. Also this parameter resembles the results from earlier measurements using the experimental probes. Interesting is that the conductance of methanol is close to D.I. water instead of ethanol, because larger similarity between the two alcohols would be expected when their molecule structure in taken into consideration. To say more about the results of the conductance measurements, again the results of the mixture are compared with the linear mixture approximation using the measured values of the pure components. Doing so it was found that the conductance values do not meet this linear mixing model at all. Looking at the binary E85 mixture, again at 102.9 kHz, and taking zero conductance for gasoline (conductance of gasoline is so small that it is with this setup barely measurable and approximately 5 order of magnitudes smaller w.r.t. the conductance of D.I. water), the total conductance of the self mixed E85 will be determined by the ethanol part. When we compare the calculated value below with the measured value of $6.51\mu S$, we see a discrepancy of a factor of 3. The inaccuracy in the measured conductance originating from the impedance analyzer is found to be 6.16%, see also appendix D.

$$0.85 \cdot 24,0\mu S = 20.4\mu S \tag{5.2}$$

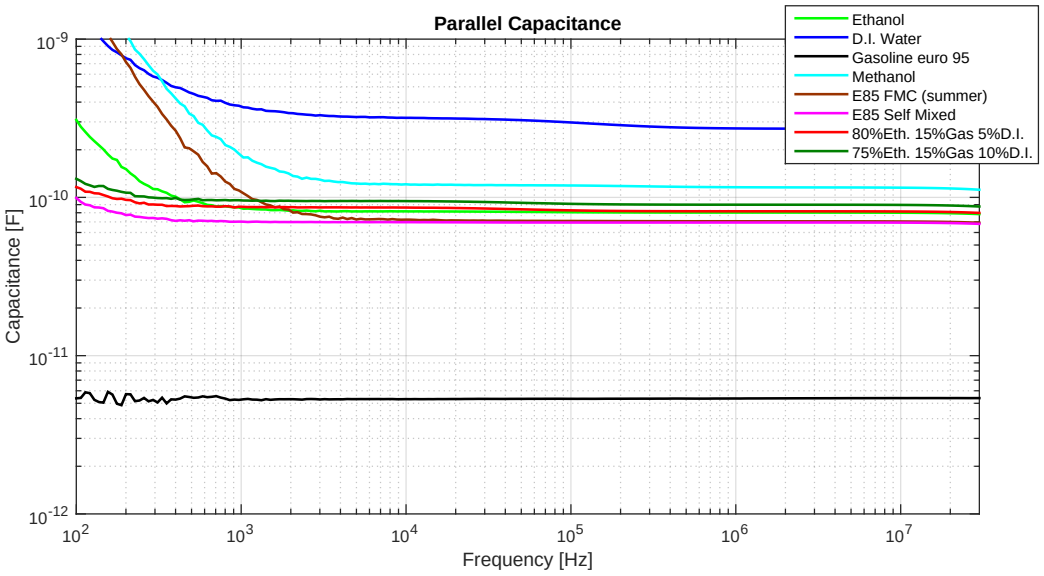

Figure 5.1: C_p measured with the dedicated coaxial impedance probe

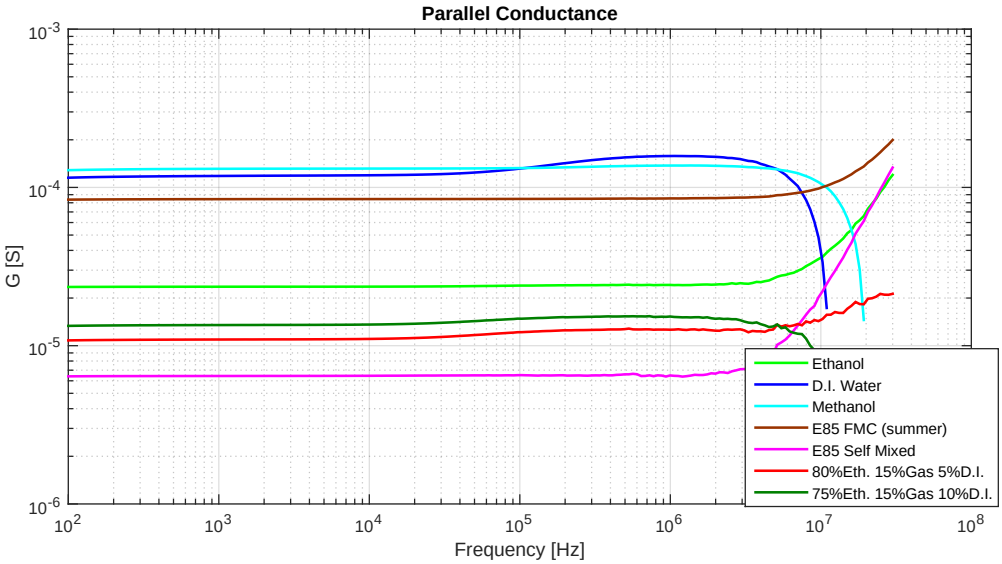

Figure 5.2: G_p measured with the dedicated coaxial impedance probe

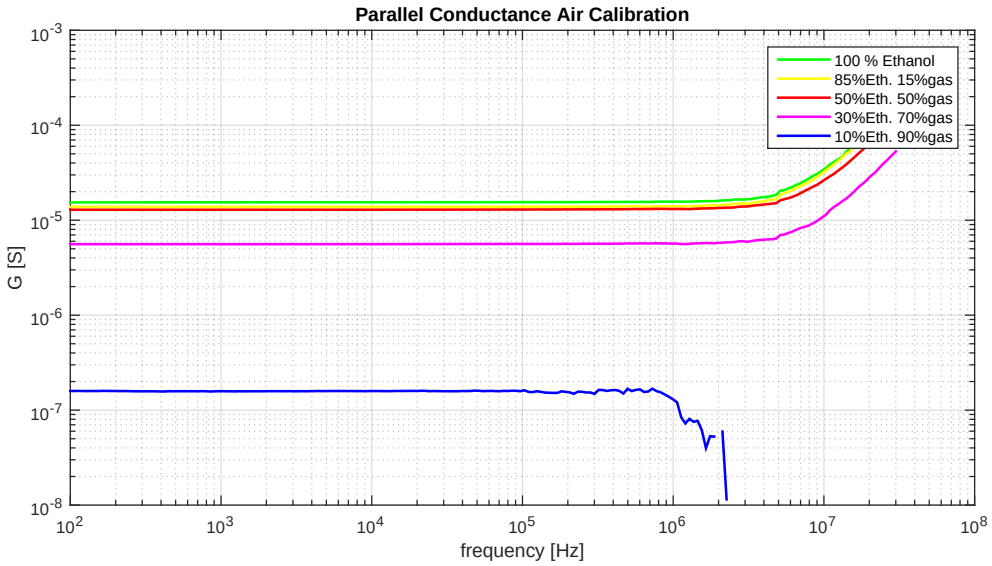

Figure 5.3: G_p for increasing ethanol concentration to investigate the parallel conductance further as possible selection parameter

5.3. PARALLEL CONDUCTANCE REVISITED

Since, as described in section 5.2, the measured parallel conductance did not meet the expectation at all, this issue was revisited. Some more gasoline/ethanol ratios were measured using the same principle as the method used earlier in this chapter. The purpose of this measurements was to investigate any possible interaction between both components.

5.3.1. MEASUREMENT ETHANOL/GASOLINE MIXTURES

In figure 5.3 the conductivity of different gasoline/ethanol mixtures is measured. The ethanol fraction is increasing from 10% up to 100% to see the effect on the conductivity. As can be noticed on the conductivity level of the different traces, the equivalent medium approximation is not behaving linearly. The conductance difference between an ethanol concentration of 10% and 30% is significant, whereas from 50% and beyond, the steps in conductance as function of the increasing ethanol concentration are really small. To have a good overview of this trend, the conductance values are put in table 5.3, using the datapoints at a frequency of 9.98 kHz. There seems to be a 'saturation' effect at approximately 1.4×10^{-5} S. Another point of concern is the *reproducibility* of the conductivity measurements. It was experienced that the conductivity measurements in particular varied over different days and that the measurements were strongly sample dependent. Therefore, the repeatability will be treated in the next subsection 5.3.2.

Table 5.3: The measured parallel conductance as function of ethanol concentration at f=9.98kHz

Ethanol concentration	Parallel conductance
10%	1.52×10^{-7} S
30%	5.41×10^{-6} S
50%	1.08×10^{-5} S
85%	1.21×10^{-5} S
100%	1.36×10^{-5} S

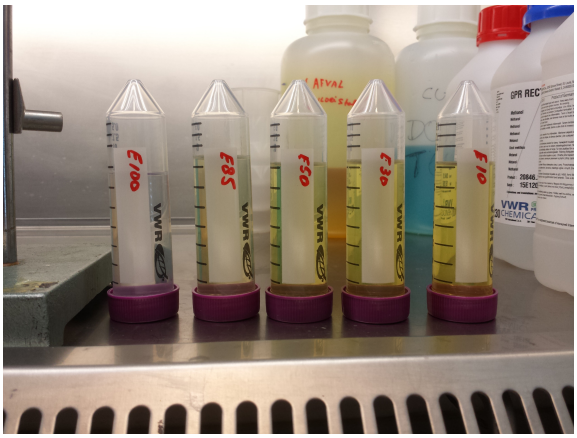

Figure 5.4: The used mixtures for the conductance measurements

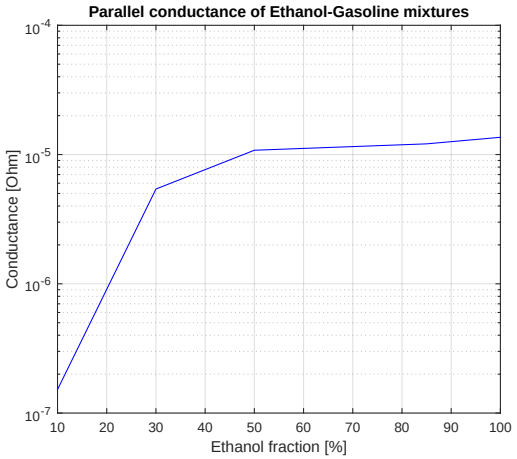

Figure 5.5: The measured parallel conductance at 9.98kHz

5.3.2. REPRODUCIBILITY

In order to obtain measurements as precise as possible, some actions were taken. The mixtures under test were all made new at the same day, using new disposable containers. Three different conductivity and capacitive measurements were carried out on the same afternoon, using the same calibration. The mixtures were measured from 100 down to 10% ethanol, to start with the 'cleanest' mixture. The coaxial impedance probe was soaked completely, to prevent any possible differences caused by a different degree of filling. And at last, after each series of measurements, the probe was cleaned using pure ethanol. Time between each set was approximately 1 hour. These circumstances could be considered as a test for *repeatability*. The result is plotted as percent deviation of the second and third series with respect to the first series. For readability reasons only the graphs of the 10%, 50% and 90% ethanol have been plotted. In figure 5.6 the percent deviation of the different capacitance measurements is included. It can be seen that the repeatability error is largest in the lower frequency ranges. This can be explained by a higher inaccuracy of the impedance analyzer at the lower frequency, because here the magnitude of the impedance of the electrode/liquid interaction is much higher (capacitive). The repeatability error is between 0 and 5% for the capacitance measurement. What also can be noticed, is that the deviation of the third measurement is just a scaled version of the deviation of the second. In figure 5.7 the percent deviation of different conductance measurements is included. First thing noticeable, is that the deviation is much higher, especially the mixtures containing a higher ethanol content are showing significantly higher deviation. It can be concluded after this experiment in lab circumstances that the capacitance measurement is much more stable and reliable in terms of reproducibility while the conductance measurement shows deviations up to 35%. Obvious from both figures is that the capacitance measurement obtains a better repeatability.

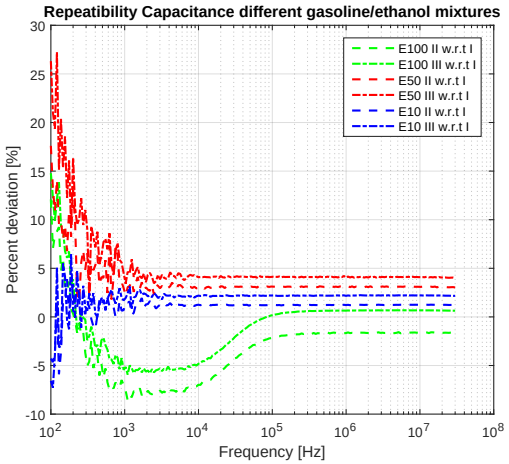

Figure 5.6: The percent deviation of the parallel capacitance of resp. the second and third measurement w.r.t. the first measurement

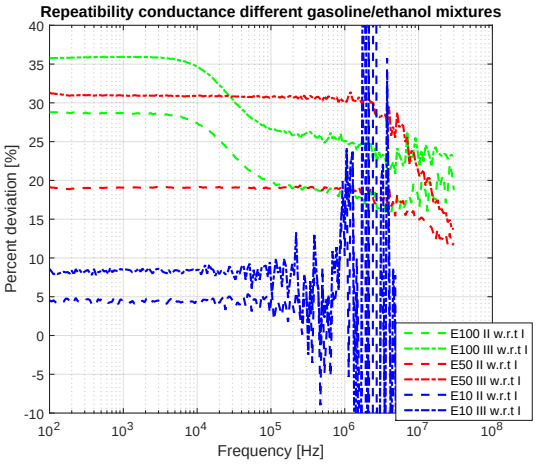

Figure 5.7: The percent deviation of the parallel conductance of resp. the second and third measurement w.r.t. the first measurement

5.3.3. LITERATURE

Because the conductance measurements still show poor repeatability and strong non-linear mixing behavior, more research was done in literature about this topic. Literature about gasoline/ethanol conductivity can be found [[8],[29]]. D.W. Kirk did measurements specifically on the parallel conductivity of gasoline, ethanol, water mixtures. Some important theoretical conclusions can be drawn from his data of ethanol-gasoline mixtures.

- For low ethanol concentrations, up to 30%, the conductivity increase can be considered logarithmic. See also figure 5.8 where the measured values by [29] have been plotted on a logarithmic y-axis.
- For an ethanol concentration between 5% and 40% an increase in temperature decreases conductivity, whereas for ethanol concentration outside this interval an temperature increase increases the conductivity. [29]. No explanation for this phenomenon was found yet.
- The influence of water on the conductivity is dependent on the ethanol, gasoline ratio. See also figure 5.9.

From the prototype and measurements done by Moreira et al.[8], important conclusions can be drawn about the ethanol/gasoline conductivity.

- The conductivity measurements are general strongly sample dependent.
- The temperature dependency is dependent on the ethanol concentration. Ethanol conductivity drops quicker than gasoline's when temperature drops. See also figure 5.10
- Temperature effects will be more drastic when static dissipators are added. This claim is made in literature, but is within this work not verified.

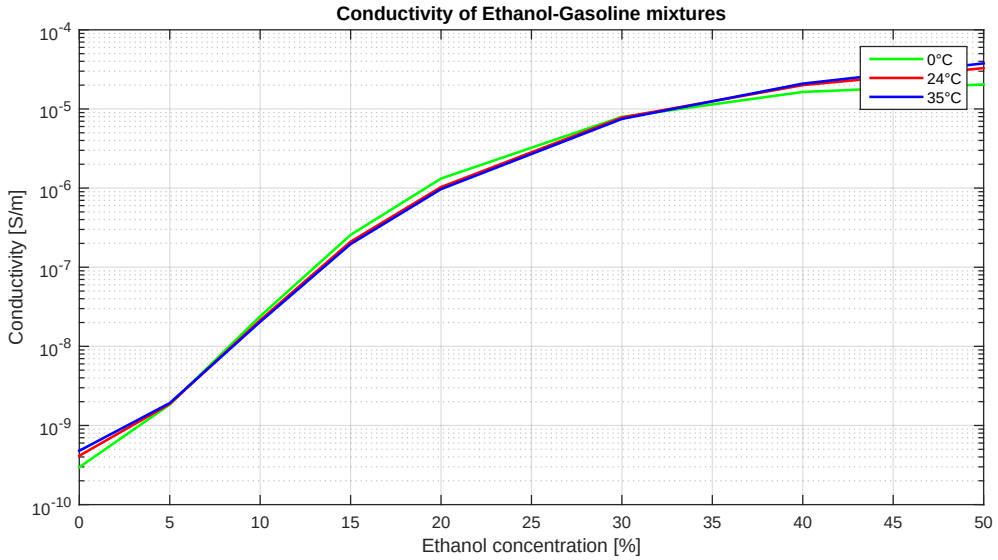

Figure 5.8: The conductivity of ethanol/gasoline mixture at 3 different temperatures as function of ethanol content. This plot has been reproduced with data originating from [29].

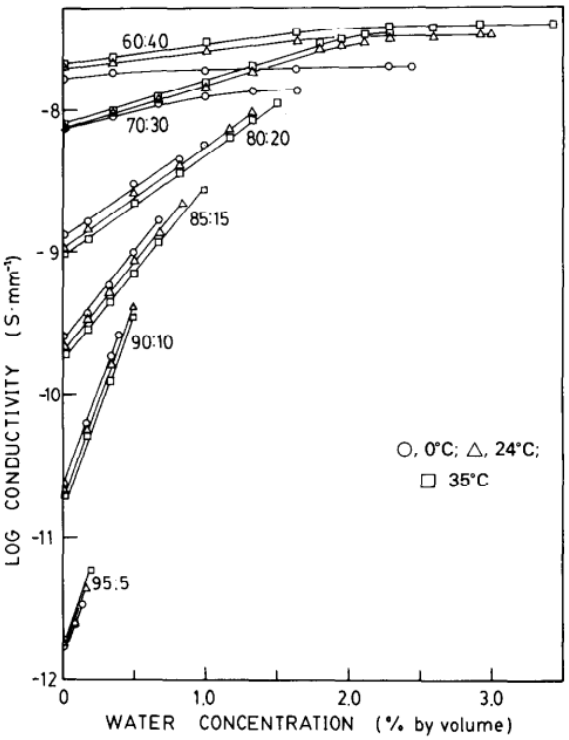

Figure 5.9: The added water was double distilled. The amount of water that can be added to the gasoline/ethanol mixture increases with the ethanol concentration, Source:[29]

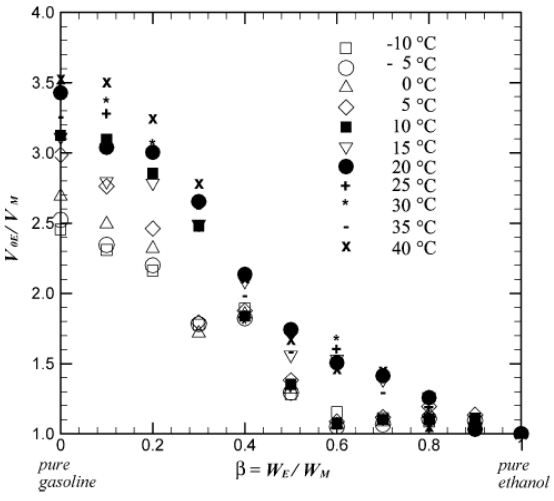

Figure 5.10: Temperature influence on ethanol-gasoline mixture conductivity. Source: [8]

5.4. CONCLUDING REMARKS ELECTRICAL DOMAIN

As was already stressed in the introduction of this thesis, to solve the ternary mixture problem two measurement parameters are in search which are reliably measurable, have a good reproducibility and repeatability. The two parameters should be selective to one or more of the components. An important aspect is the independency of the two parameters, with other words orthogonality should be introduced which result in a unique solution of the problem. There may be no dependency between the two measurement parameters. Furthermore introduced uncertainties, for example temperature effects, should be deterministic making correction possible.

In this thesis work, the primary domain of interest was the electrical domain, independent of the frequency used. The question if impedance behavior could be exploited as a selection parameter to fully solve the ternary mixture problem was kept in mind up to this point in the thesis work. During the explorative feasibility study, it soon became clear the the dielectric relaxation effect is certainly measurable. However, the high relaxation frequency of water (20GHz) requires dedicated RF design and forms a challenge with was not intended to address within this work. The low frequency impedance domain was investigated. By measuring the impedance, two possible selection parameters can be thought of, namely the magnitude and phase behavior, or equivalently the real and imaginary part. It was found that the real part is directly linked to the parallel conductance, whereas the imaginary part is directly linked to the capacitance.

After the measurements with the dedicated impedance probe were carried out, it can be concluded that the capacitance part of the equivalent circuit model meets the linear model as was expected and seems promising to function as a selection parameter. The conductance however doesn't follow this line. As supported by the described measurements and the discussed literature some major disadvantages became clear. The most important ones are the complex mixing model, the composition dependent temperature dependency, the sensitivity to the ion concentration, contamination and static dissipators and the ethanol sample dependency. In addition, the difficulties in obtaining proper repeatability and the temperature dependency which reverses direction in certain ranges for the ethanol fraction. Due to all these reasons, it was decided to abandon the parallel conductance as a selection parameter for the ternary mixture problem.

To summarize all the findings on the electrical domain up to this point:

- The dielectric relaxation of water happens around 20GHz
- Reliable magnitude/phase measurements in this frequency range appeared to be challenging 2.2. A prototype will most likely need to be an integrated chip, requiring a RF design procedure.
- Imaginary part of LF impedance, c.q. parallel capacitance, provide a robust and stable first parameter. Repeatability was measured as good. Effective medium approximation is best described using a linear mixing model.
- Real part of LF impedance, c.q. parallel conductance, is not useful for multiple reasons:
  - Complex mixing algorithm
  - Composition dependent temperature dependency, sign of coefficient reverses
  - Sensitive to free ion concentration
  - Dependency on static dissipators
  - Conductivity strongly sample dependent
  - Poor repeatability

With these remarks the research in to the electrical domain is concluded. The second domain which will be worked out further is the optical domain, exploiting absorption spectroscopy. The motivation for this domain is mainly based on selectivity. More about the motivation will be explained in chapter 6.

6

Optical Absorption Spectroscopy

6.1. Motivation optical domain

From the final conclusion of the electrical domain it became clear that only one useful independent measurement parameter is delivered by this domain. At this point a second independent measurement parameter is required. From the feasibility study (see also chapter 2) two domains offer both good selectivity to one of the three components and interesting possibilities for implementation and integration in the final application. When looking at the selectivity aspect, water is dominating the permittivity in the electrical impedance behavior whereas gasoline is comparatively weak. In the thermal domain, water again has the largest values for thermal capacitance and conductance. Simultaneously, gasoline is dominating the absorption behavior in the UV range whereas water does not contribute to the optical absorption in this range. So in the LF impedance domain water is the strongest component, but in the optical domain, gasoline seems to be the dominating one. Combining both techniques, so LF impedance spectroscopy and UV absorption spectrometry, would introduce a large orthogonality between gasoline and water in solving the ternary mixture problem.

6.2. Theory

6.2.1. Absorption spectroscopy

Spectroscopy focuses on the interaction between light and matter as function of wavelength λ. This interaction can change the state of electrons and molecules. As a result different effects can occur, namely scatting, emission or absorption of light. The measurement technique which is considered here is absorption spectroscopy applied to organic compounds. When light is absorbed by matter, electrons of molecules are excited to a higher quantized energy level in the atomic structure. Absorption at certain wavelengths happens if the energy difference of the electron transition between the two atomic states matches the energy level of the incident photons. By analyzing the light before and after the interaction with the matter under test, the absorption behavior can be determined. This data can give valuable information in characterization of materials. [30]

In this study where the considered matter consists of organic compounds and water, the effect which is studied is mainly the interaction between the incident photons and the electrons in the organic compounds. Gasoline contains a lot of components containing aromatic bonds [31], for example benzene and toluene (methyl-benzene), which strongly contribute to the electronic interaction. According to literature [32], benzene for example shows strong light absorption near 180 nm (which is in practice not very useful because air starts to absorb too). It has further absorption bands at 200 nm and 254 nm, see also figure 6.1 for the spectrum of benzene, which was

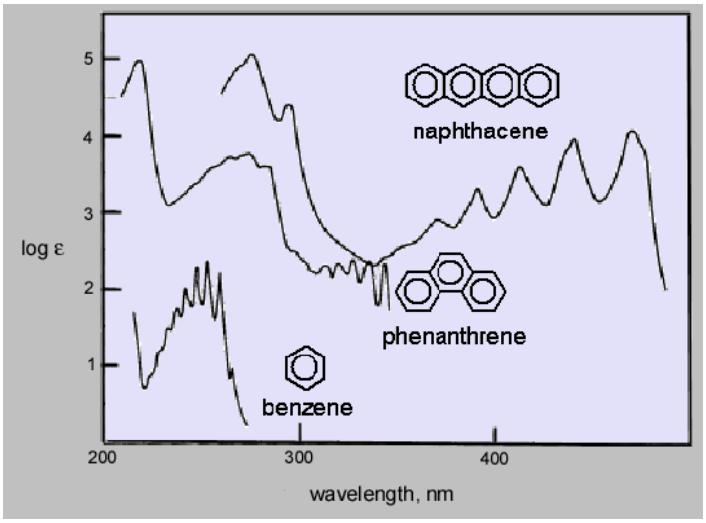

Figure 6.1: The spectrum of benzene among others. Source: [9]

found in literature [9]. Further it can be noticed that when these topics are discussed, a small exploration in the field of chemistry is made, and that the absorption spectroscopy measurements are not solely limited to the field of electronic instrumentation.

6.2.2. BEER-LAMBERT

The absorbance of a liquid can be described by the law of Beer-Lambert. It states that the total resulting absorbance is determined by the extinction coefficient ϵ_i, the molar concentration of the absorbing component c_i and the optical path length l. Theoretically it can be thought of as the number of absorbing molecules which are present in the optical path. It also states that, when considering a mixture, the total resulting absorbance A is a summation of the separate absorbances, assuming that no interaction takes place between the molecules of the components of which the mixture consists. In the situation of gasoline, water and ethanol mixtures, this would mean that the absorbances of the separate components will add up. Preliminary measurements showed that the absorbance of water is negligible and that the absorbance of gasoline is orders of magnitudes larger than the spectrum of pure ethanol.

$$A = \sum_{i=1}^{N} \epsilon_i c_i l \tag{6.1}$$

6.3. MEASUREMENT SERIES I: OCEAN OPTICS TUD

6.3.1. MEASUREMENT SETUP

To correctly measure the absorption spectrum, the right measurement setup is key. The first set of measurements is carried out using spectrometers from Ocean Optics in combination with a reflectance probe, which is put into the liquid under test, see also figure 6.2. The first spectrometer is the Ocean Optics Flame and is capable of determining the absorption behavior from 337 - 1023 nm, so the visible range as well as part of the Near-Infrared (750-1400 [nm]) and a small fraction of the UV spectrum (10-400 nm) is covered. The second available spectrometer is the Ocean Optics Maya, which is a dedicated UV spectrometer, and is capable of measuring the absorption behavior from 200 up to 400 nm. In the used setup however, the results got unreliable from 250 nm and below, because of the absorption of the used fibers. Both Ocean Optics devices use dark and full-exposure calibration, to correct for back-ground light and for the spectrum of the light source itself. The medium for calibration is air. Because the transmission through the boundary between

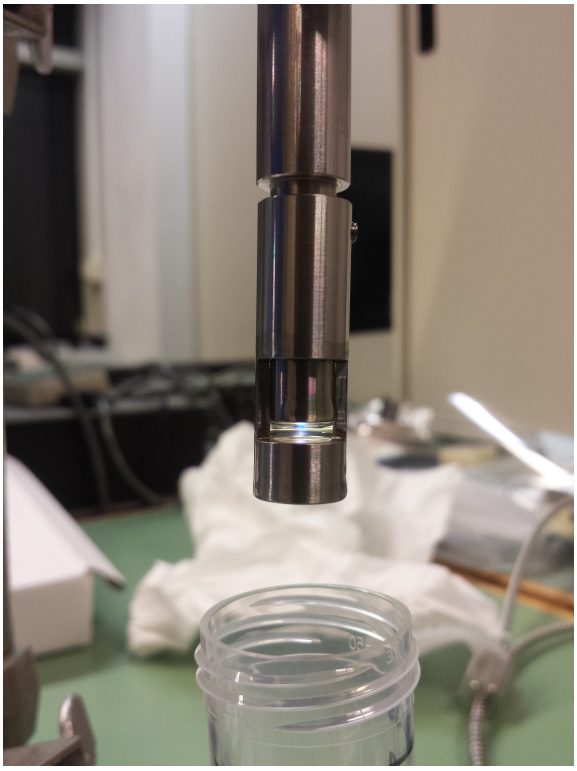

Figure 6.2: The used reflectance probe probe

Figure 6.3: Fluorescence in the Dutch gasoline

the coupling fiber and the medium is higher when a liquid is used instead of air, some absorption result will give negative values. This 'offset' will not affect the spectral behavior. The light source used in this set up is a halogen-deuterium source, to cover the full spectrum. The calibration is done before the measurement and during measurement the signal from the detector is corrected with the calibration values. See also table 6.1 where a summary of the measurement parameters is included. The used absorption quantity is the absorbance, because its scale is logarithmic and therefore suitable to cover the range of absorption for the measured liquids. Secondly because of the linear addition when a mixture is considered, as already described above. The absorbance A_λ for a certain wavelength λ is defined as follows, where S is the sample intensity, R the reference or calibration intensity and D the background of dark intensity.

$$A_\lambda = -log_{10}(\frac{S_\lambda - D_\lambda}{R_\lambda - D_\lambda}) \tag{6.2}$$

Table 6.1: An overview of the different measurement parameters

Parameter	Value
Optical pathlength	20 mm
Lightsource	Halogen/Deuterium
Measurement range Flame	337-1023
Measurement range Maya	171-389 nm
Calibration medium	air

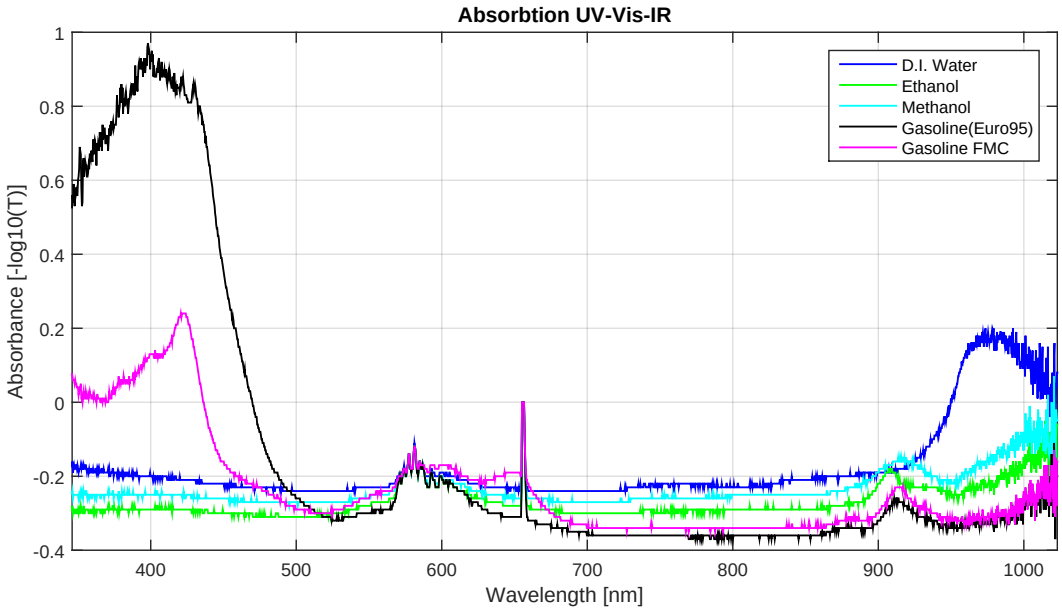

Figure 6.4: The measurement results of the flame Ocean Optics spectrometer.

6.3.2. MEASUREMENTS OCEAN OPTICS FLAME

The measured components are D.I. water, pure ethanol, pure methanol, regular dutch gasoline Euro 95 and Regular American gasoline supplied by Ford Motor Company and therefore denoted as FMC here. Visually, this FMC gasoline differs from the regular gasoline, because the FMC fuel is green and more transparent w.r.t. the Dutch fuel, which is dark yellow. This already implies that the visible range of the spectrum will not be suitable to distinguish between different kinds of gasoline. The measurement result using the Flame spectrometer is included in figure 6.4. It can be seen from these results that in the IR range, water starts to absorb significantly and that in most of the visible range no component is showing a specific spectral behavior. From 500 nm and below, the two different gasolines start to absorb dramatically, but a large difference between both is present. More detailed measurements on these two gasolines from 400 nm and below will be treated in the next section 6.3.3.

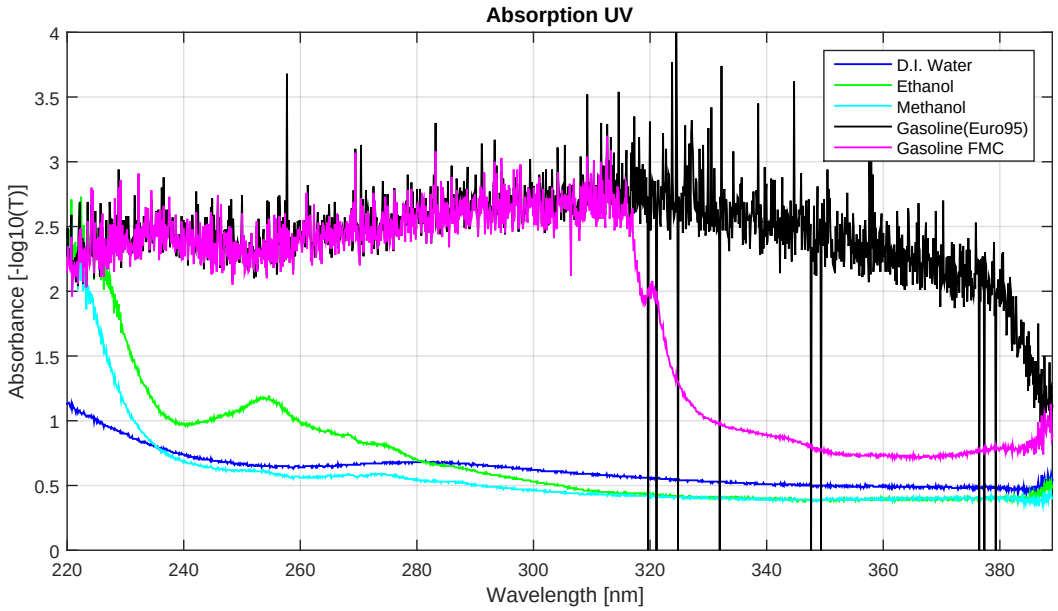

Figure 6.5: The measurement results of the Maya Ocean Optics spectrometer.

6.3.3. MEASUREMENTS OCEAN OPTICS MAYA

In this section, the measurements in the UV range are treated. The same components as in the visible measurements are measured. The result is included in figure 6.5.The range goes down to 171 nm, but since the results get unreliable from 220 nm and below, only these are included. As was expected from the measurements with the Ocean Optics flame spectrometer, around 400 nm a domination of the absorption by gasoline is present. This time however, the gasolines dominate also the rest of the UV range and even behave equal from approximately 315 nm and below. This result is actually promising, because a measurement parameter is desired which is independent of the type of gasoline. It is further the case that the absorption is that high, that the obtained values are close to the noise floor and are not ideally located within the dynamic range of the measurement setup. This is the case because in this first measurement series, an overview of the absorbance spectra of multiple components was meant to be given. Now it became clear that for more spectral information, the gasoline mixtures need to be either diluted or a smaller optical path length should be used. More about the UV measurements on gasoline mixtures will be treated in section 6.4. Looking at the other components of the measurement result included in figure 6.5, it can noticed that the absorption of D.I. water is very small and ethanol shows a specific peak around 250 nm. Methanol does not show this peak but follows the trend of ethanol to a smaller extent. An important conclusion up to this point is that both gasolines absorb orders of magnitude more than the other two components of the ternary mixture.

6.4. MEASUREMENT SERIES II: VARIAN CARY 500 FMC

In this section the measurements carried out at the Research and Advanced Engineering Department of Ford Motor Company in Dearborn are described. During the internship project 'Particulate Matter Measurement by Impedance Spectroscopy'.

6.4.1. DIFFERENT OCTANE RATINGS

In this section, more test fuels and off the shelf fuel originating from the fuel house at Ford, Dearborn, are measured. Since an important parameter of gasolines is the octane rating, some comments about parameter will be made. The octane rating is a very important parameter in relation to uncontrolled combustion of the air/fuel mixture in combustion engines. When the combustible gas is compressed in the engine, it is important that combustion takes place only when the mixture is ignited by the spark plug. When, due to high pressure and thus resulting temperature increase, the gasoline/air will spontaneously ignite itself, serious engine damage can be the result. This effect is also called knocking.

Three different indexes are used world wide to denote the octane rating, namely RON, MON and AKI. RON stands for research octane number is obtained under laboratory conditions, using different compression ratios. MON stands for motor octane number and is obtained using a motor running on 900 rpm and variable ignition timing. AKI stands for anti-knock index and is obtained by the following formula: $AKI = \frac{RON+MON}{2}$. [33]

6.4.2. MEASUREMENT SETUP

For this set of measurements, a Varian Cary 500 Spectrophotometer was used in combination with quartz cuvettes. This device uses a double beam, one for a reference sample and one for the actual measurement. So apart from the initial dark- and full-exposure calibration, the device is correcting real time for possible variations of the spectrum of the light source over time. Since the output power of the light source and the integration time of the detector were not adjustable, the optical path length is critical.

To determine which optical path length would be best suitable in this setup, three different values for the optical path length were used, namely 10 mm, 5 mm and 1 mm. Some preliminary measurements were carried out using the three main components of our ternary mixture, as well as 1 type of 'off the shelf' fuel, summer E85. The gasoline used is indolene 50E clear gasoline, which is a standardized test gasoline free of additives and coloring. The used version here has a premium octane rating, which corresponds to an AKI index of 93. This is equivalent with the RON98 index used in Europe.

The result is included in figure 6.6. From these results it is obvious that the indolene gasoline and the E85 saturate strongly against the detection limit of the spectrometer in the case of optical path lengths of 10 mm and 5 mm. Because of this 'clipping' a horizontal shift in the transition from the transmission to the absorption region is shown. This effect can be explained by the law of Beer-Lambert. When the extinction coefficient is multiplied by a large number for the optical path length, the extinction coefficient graph will be 'blown up' and this horizontal shift will occur. When the optical path length is decreased to 1 mm, spectral information below 280 nm is visible again for the gasoline containing E85, see also the local minimum peak in absorbance in figure 6.6 in the red dash-dotted trace.

The comparison measurements could be summarized by concluding that the 1 mm path length is the most suitable to obtain best spectral information. Since saturation still exists with the 1 mm cuvettes, it was decided to dilute the gasoline (mixtures) with a suitable solvent. In this way the absorption behavior of the gasoline (mixtures) would fall into the lower absorption ranges and the measurements would give the best spectral information. Cyclo-hexane was chosen as the solvent, because of the low absorption over the entire UV spectrum and the fact that it dissolves

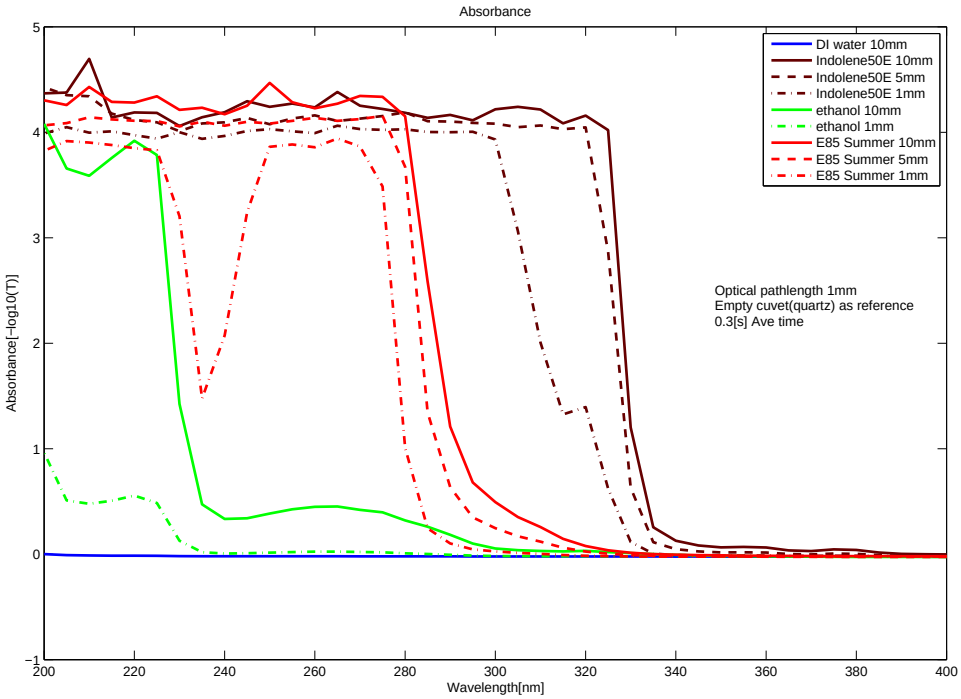

Figure 6.6: Comparison of three different optical path lengths.

the relevant components well. According to literature [34] the cut-off wavelength in the UV range of cyclo-hexane is 195 nm. In table 6.2 a summary of the measurement parameters is included. During initial measurements it was already found that D.I. water does not absorb significant light in the UV range, hence does not interfere using this measurement technique.

Table 6.2: An overview of the different measurement parameters.

Parameter	Value
Average time	0.3 s
Spectral BW	2.000 nm
Measurement range	200-400 nm
Optical Pathlength	1 mm
Cuvettes	Quartz
Solvent	Cyclo-hexane

6.4.3. SINGLE COMPONENT HYDROCARBONS

Since gasoline is a mixture of tenths of different hydrocarbons, it was thought that it would be good to investigate some single component hydrocarbons. Then the measured liquid is exactly defined, and can therefore also be used to check for the setup and the way the measurements are carried out. Available were cyclo-hexane, hexane and toluene. Toluene is a compound of gasoline, and typical gasoline compound analysis yields values ranging from 3.5 up to 22 mass percent [31]. The result is included in figure 6.7. It is clear that hexane and cyclo-hexane do not show absorption in the UV range, which corresponds with literature [34]. It is obvious that the

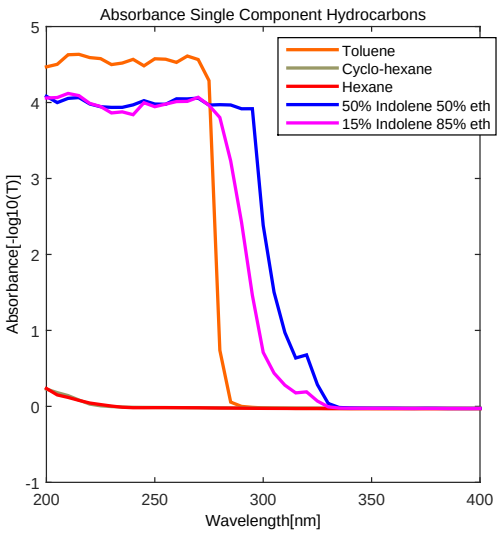

Figure 6.7: The measured single component hydrocarbons and indolene with an optical path length of 1 mm.

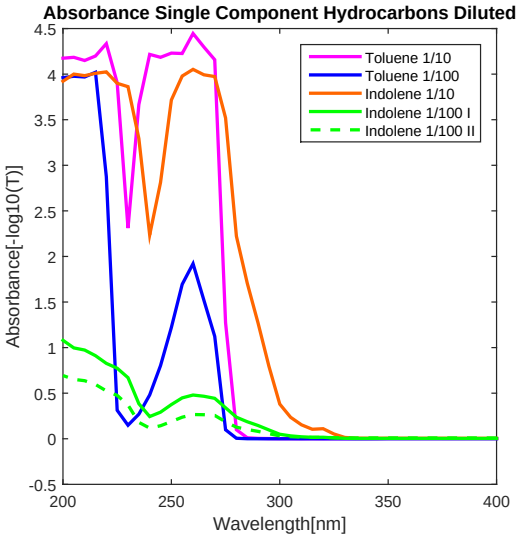

Figure 6.8: The measured single component hydrocarbons and indolene with dilution.

absorbance values of toluene and indolene gasoline strongly saturate against the detection limit of the device, as also described above 6.4.2.

Therefore measurements where toluene and indolene are diluted have been carried out and two different dilution ratios have been used, 1/10 and 1/100. Because the influence of the diluted liquids, here indolene and toluene, is investigated, now a cuvette with the solvent is used as a reference (instead of air, an empty cuvette). The result of this measurement including dilution, is included in figure 6.8. Obvious is now that there is much more spectral information, than in the earlier measurements. Especially the 1/10 and the 1/100 dilution of the toluene show clearly some peaks.

It can be concluded that the 1 mm measurements without any dilution just absorbs too much light to show the specific absorbance peaks. For toluene specifically it can be concluded that the 1/10 dilution is still absorbing too much light, because the 1/100 dilution show a much sharper peak. Indolene (test gasoline without additives) behaves similar as the toluene with a small horizontal shift to larger wavelengths, also called red shift. This could be caused by the presence of different other components in the indolene fuel which decreases the energy needed to result in an energy transition which causes the absorption behavior. Since the longer wavelength light carries less energy, this might explain this red shift [34].

6.4.4. ETHANOL/GASOLINE MIXTURES

Since the optimal path length and dilution ratio is investigated, now the absorption of gasoline/ethanol in different ratios was measured. Indolene 50E clear was used in combination with the so-called 200 proof ethanol (>99.98% pure). The dilution ratio of 1/10 is used to optimally use the dynamic range of the spectrophotometer. No dilution is applied when measuring pure ethanol to prevent further loss of spectral information. As can be seen in figure 6.9 two absorption features are present. One local minimum in the absorption at 240 nm and a peak around 265 nm. Despite the dilution ratio of 1/10 and the path length of only 1 mm, saturation at minimum sensitivity occurs at 70% indolene concentration and beyond. On the other hand, no saturation is present and the absorption is dominated by gasoline content at 240 nm.

To investigate if this gasoline-dependent absorption behavior could be utilized in determining the composition of the initial ternary mixture problem, indolene 50E was replaced with a differ-

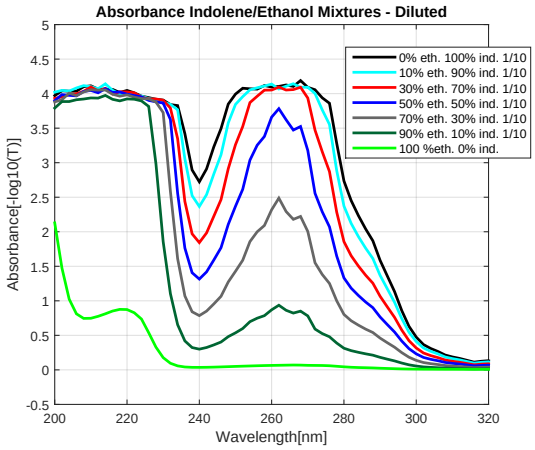

Figure 6.9: The measured absorbance of different ethanol/indolene ratio's. The dilution ratio is included in the legend.

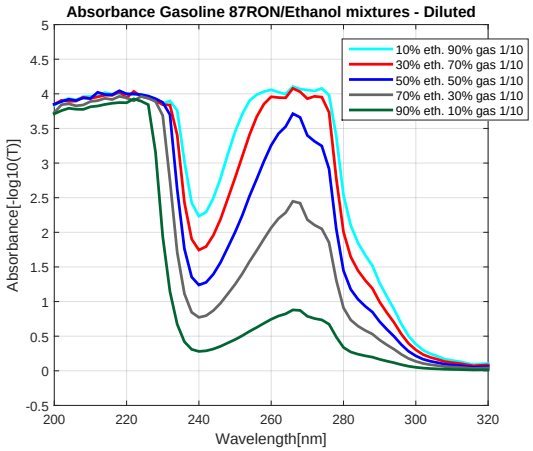

Figure 6.10: The measured absorbance of different ethanol/gasoline ratio's. The dilution ratio is included in the legend.

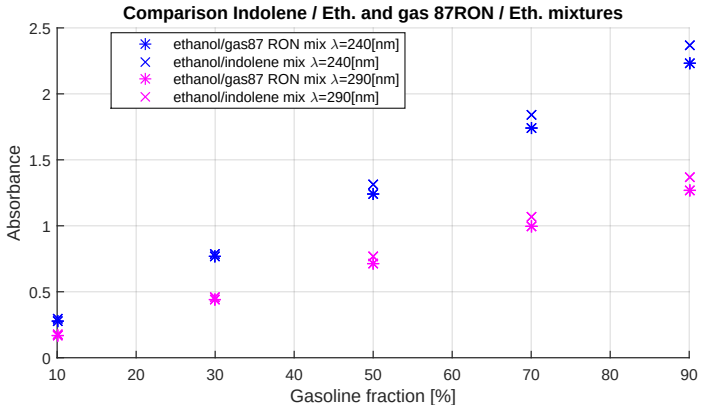

Figure 6.11: The absorbance as function of the gasoline fraction. Compared are the 87RON and indolene mixtures at two different wavelengths.

ent kind of an 'off the shelf' test fuel, namely Unleaded Low Octane gasoline 87RON (Research Octane Number) in a new series of identical measurements. The results are shown in figure 6.10. The absorption behavior seems to resemble the measurements of indolene gasoline, the spectral behavior is very similar. This result can be considered as promising in the final application of a future optical extension of the fuel composition sensor system in flex fuel vehicles.

To look if the relation between absorbance and gasoline content is linear, as predicted by the theory described in section 6.2, two different points in the UV spectrum have been taken for both the indolene as the 87RON mixtures. At these points the total absorbance was plotted against gasoline content. The 240 nm wavelength was chosen, because of the local minimum, which has turned out to be typical for different gasolines. Because of the saturation effect at 265 nm, a higher dilution ratio or smaller optical path-length should be used at and around this wavelength. Instead of this peak, the wavelength 290 nm was chosen instead, to still supply a second wavelength where the absorption behavior can be analyzed. The result of this plot is included in figure 6.11. It can be concluded from this plot that the relationship between gasoline content and optical absorbance is linear, and the slope between both is dependent on the used wavelength. Since both gasolines have different compositions, this explains the discrepancy at higher gasoline content.

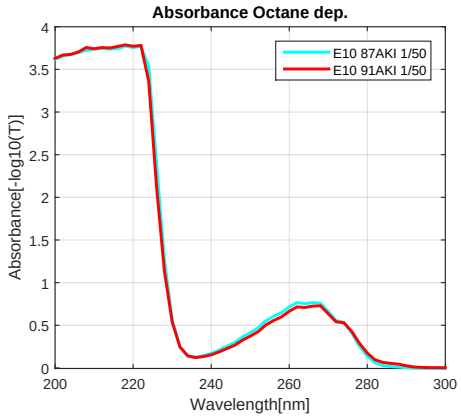

Figure 6.12: Two representative American gasoline's, low and mid grade octane rating compared. Note the higher dilution ratio.

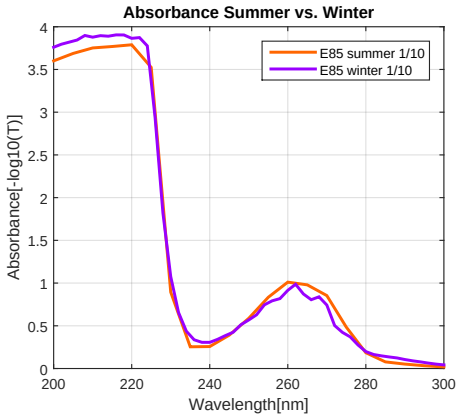

Figure 6.13: The summer and winter grade E85 compared. The same dilution as previous gasoline/ethanol mixtures is used.

6.4.5. OCTANE CONTENT AND SUMMER/WINTER GRADE

During the research, some practical 'off the shelf' fuel blends were available. Again, absorption measurements were carried out to investigate the dependency on octane number and summer/winter blends. The results are included in figures 6.12 and 6.13. The effect of the octane content on the absorption behavior is very small, it can also be concluded that the higher volatility winter fuel behaves similarly to the E85 summer version. This result can be considered as promising, since insensitivity for this type of uncertainties is preferred. Note the different dilution ratios that were used to prevent loss of spectral information.

6.4.6. NEAR- & MID-INFRARED MEASUREMENTS

In this section the same ethanol/gasoline mixtures as in the previous section are treated, however this time the infra-red range is considered. The absorption behavior was measured up to 3300 nm. No interesting results were measured from 700 up to 2000 nm, for that reason these results are not included here. The range from 2000 up to 3300 nm is divided in two plots. The results for the 2000-2700 nm range for the mixing series with both gasolines are included in figures 6.14 and 6.15. In the first figure 6.14 both the diluted gasoline/ethanol mixtures and the absorbance behavior of pure ethanol are included. From this plot it is obvious that in this range ethanol is dominating the optical absorbance. Note further that from 90% ethanol content and below (and thus 10% gasoline content and beyond) a dilution with 1/10 ratio was used, since the IR measurements were carried out in the same series with the UV measurements. In the second figure 6.15 the absorption behavior of 87RON gasoline is included. Because no pure ethanol is included this time, the y-axis is much more zoomed in. At multiple wavelengths in the spectrum the linearity between ethanol concentration and optical absorbance is shown. For example at and around the peaks at 2084, 2270 and 2482 nm.

In figures 6.16 and 6.17 the second part of the IR range is included for the mixing series with both gasolines. In the first figure 6.16 it can be remarked that from an ethanol concentration of 30% and beyond the absorbance strongly saturates and that the measurement results get very noisy. The trend of increasing absorption with increasing ethanol concentration is still exhibited. A typical absorption peak for ethanol appears to be present around 3000 nm. In the second figure 6.17 the result of the 87RON gasoline is included, which resembles the result of the absorption measurements which were carried out using indolene measurement. This was expected, since in the IR range the absorbance is strongly determined by ethanol, instead of gasoline.

When comparing both sub-ranges within the UV, for example for 87RON gas (see also figures

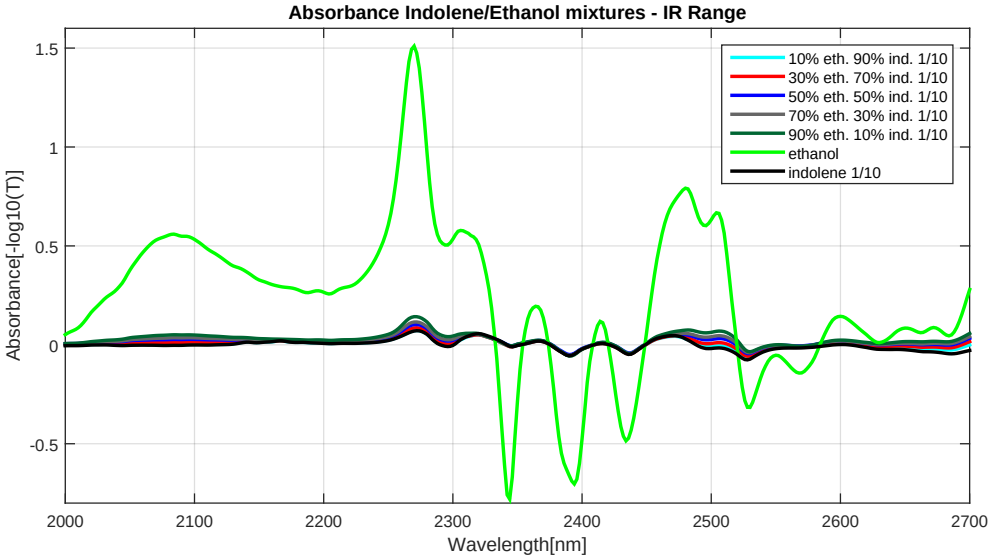

Figure 6.14: The measured absorbance of different ethanol/indolene ratio's in the IR range. The dilution ratio is included in the legend.

6.15 and 6.17 and taking into account the different scaling of the y-axis, it can be concluded that the extent to which ethanol absorbs varies strongly between the two ranges. In other words the sensitivity of the optical absorbance to ethanol concentration differs strongly between the two wavelength ranges. This effect could be exploited in a practical implementation for redundancy or multiple channel purposes.

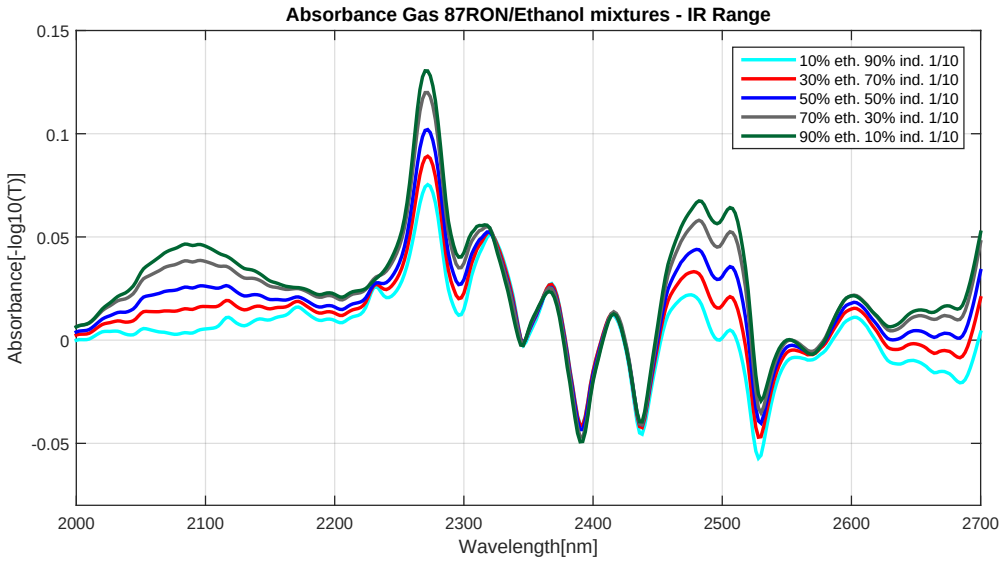

Figure 6.15: The measured absorbance of different ethanol/indolene ratio's in the IR range. The dilution ratio is included in the legend.

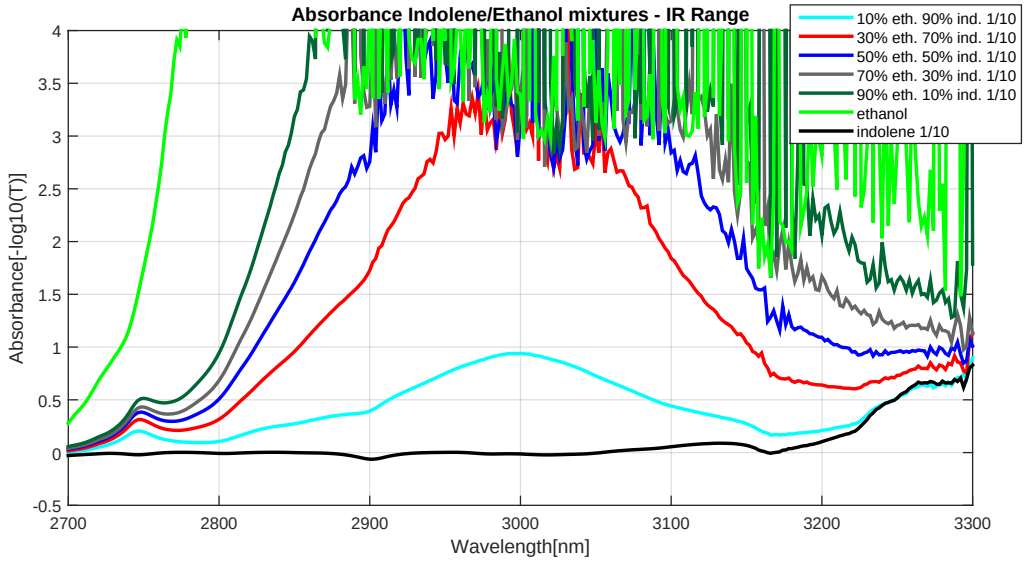

Figure 6.16: The measured absorbance of different ethanol/indolene ratio's in the IR range. The dilution ratio is included in the legend.

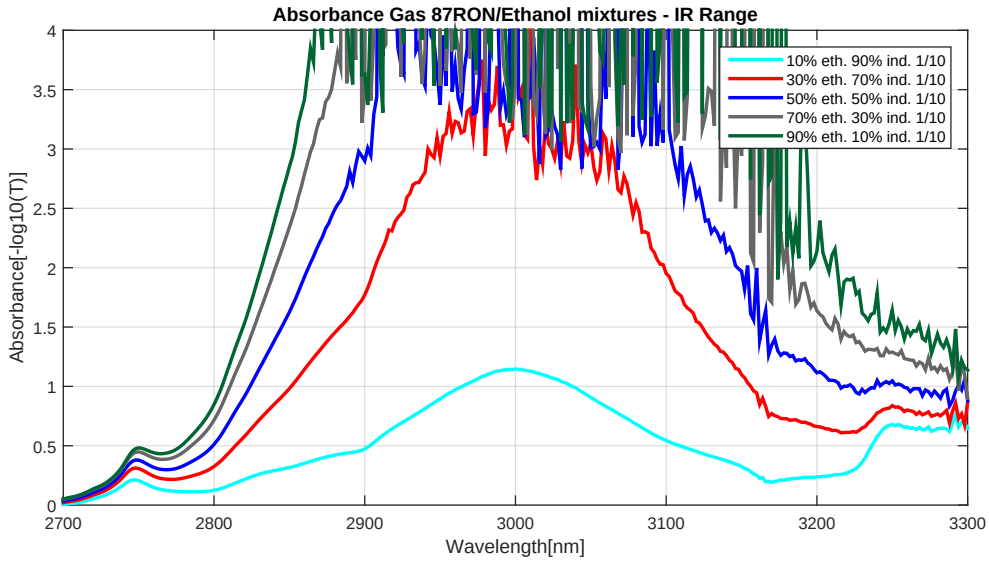

Figure 6.17: The measured absorbance of different ethanol/indolene ratio's in the IR range. The dilution ratio is included in the legend.

6.5. POSSIBLE IMPLEMENTATION TECHNIQUES UV

As can be concluded from the measurements in the UV range, described in section 6.4 is that gasoline shows useful features in the UV domain between 220 nm and 300 nm. In this section implementation techniques for a microspectrometer are proposed. With these propositions theoretical and chemical issues related to the measured spectral behavior are left open for later discussion in this thesis.

6.5.1. UV LEDS & UV ENHANCED PHOTODIODES

The advantage of the availability of a full spectrum in the measurement range of interest is that full information about the absorption features is present, more specifically the peaks and local minima in the absorption behavior. This information may be useful in the case of unexpected values in the measured spectrum, for example caused by so called blue or red shifts. The extent to which this possible uncertainty plays a role is not yet determined within the measurements carried out up to this point. When it is assumed that the spectrum is stable and reproducible and that unexpected changes to the spectrum of gasoline are within the error range, it might be possible that significant information is provided by determining the absorption only on specific wavelengths.

A simple implementation for the microspectrometer system which can be thought of is a multi channel combination of multiple LEDs and photodiodes. Within the wavelength of interest multiple UV LEDs are commercially available, for example at 265 nm and 280 nm. [35] The combination of LEDs and photodiodes could be implemented in a 3D prototype, most likely with the use of collimators. When designing a microscectrometer using LEDs and photo diodes also the different refractive indices of ethanol, gasoline and water have to be taken in to consideration. Different optical path lengths could be utilized according to absorbance sensitivity to gasoline content, since it was discovered that this sensitivity is dependent on the used wavelength, see also figure 6.11.

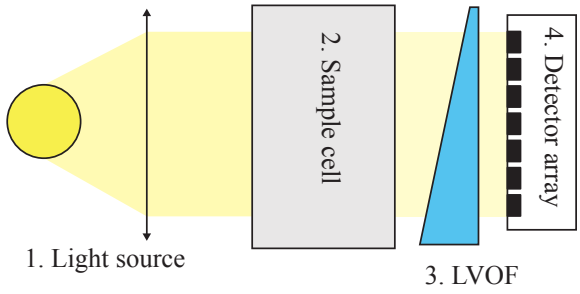

Figure 6.18: A schematic overview of the measurement system based on a LVOF.

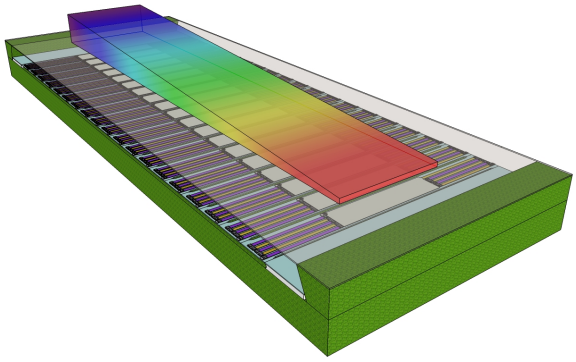

Figure 6.19: The LVOF on top of a detector array.

6.5.2. LINEAR VARIABLE OPTICAL FILTERS

The second proposal for a possible future implementation for the microspectrometer application describes a more advanced technique. A system based on a Linear Variable Optical Filter (LVOF) is proposed. The main advantage of this implementation compared to the LED implementation is that more spectral information is provided. In case of unexpected changes in the spectrum of gasoline (for example by a blue or red shift, or contamination other UV absorbing compounds) the location of the absorption features might still be determined and corrected for. The three main optical channels of interest (taking into account most interesting ranges of gasoline absorption) are therefore centered at 240 nm, 265 nm, and 290 nm. A value of about $\delta_\lambda = 1$ nm is required for a proper gasoline content estimation, considering measurement results of gasoline absorbance.

The LVOF is composed of two reflectors separated by a cavity. The depth of the cavity determines the transmission wavelength. The resolution is determined by both the reflectivity and the cavity depth. Figure 6.18 shows the schematics of the optical sensor design. The structure consists of four main components: 1) a light source, 2) a sample cell, 3) LVOF, and 4) the photo detectors. Further advantages of LVOF-microspectrometer designs are the CMOS compatibility and high spectral resolution when operated over a relatively narrow band. To conclude, a sensor system based on multiple-LVOFs centered around the intended spectral channels is promising for this application [36]. In figure 6.19 an illustration of the LVOF is included, on top of a detector array.

6.6. CONCLUSIONS OPTICAL ABSORPTION SPECTROSCOPY

In this section two different setups have been utilized to investigate the absorption behavior of the three main components of the ternary mixture problem. By combining the measurement results valuable information of the absorption behavior was obtained. As a result conclusions can be drawn on the application of absorption spectroscopy as measurement technique. As was already expected by the use of different colorings, the visible range does not provide sufficient component specific spectral information and is dependent on the type of gasoline measured. In the IR range, most interesting results were obtained in the range 2000 nm to 3300 nm. Ethanol is strongly dominating the absorption behavior. However, also water is a strong absorber in this range. Therefore it was decided to work out further the UV range of the spectrum. It was namely found that different kinds of gasolines showed similar absorbance spectra. Features such as different peaks resp. local minima were positioned on the same location. Variations originating from winter vs. summer grade gasolines or different octane ratings showed negligible discrepancies in absorption behavior. Since questions relating to these topics ask for a more chemical analysis,

more research in to this field might be needed to fully explain the effects which were measured up to this point. At last two proposals for a practical implementation of a microspectrometer are given. Concluding, it can be said that the optical domain, in particular the absorption behavior of gasoline in the UV range between 230 and 300 nm certainly provides promising possibilities in delivering the second measurement parameter for the ternary mixture problem.

7

CONCLUSION & FUTURE OUTLOOK

7.1. CONCLUSIONS

The research work was focused on a measurement system capable of determining the composition of a ternary bio-fuel mixture containing water, gasoline and ethanol. A starting point for the measurement uncertainty was based on the state of the art and maximally 3-5% of the final determined composition fractions. A number of different domains were studied, namely the electrical, optical, thermal and mechanical domain.

Low-frequency impedance The first domain which was treated was the impedance domain up to 30 MHz. Multiple measurement series on the LF impedance behavior, as well of the separate components of the ternary mixture, as of mixtures of them have been carried out. Additional measurements were carried out on methanol for possible future applications, mainly meant for the Chinese market.

For these impedance measurements a dedicated coaxial impedance probe was designed. With this probe, better calibration, higher accuracy and more stable results were obtained compared to the preliminary measurements using experimental probes. It was found that free ions in the liquid cause an electrode polarization effect, resulting in an increase of the measured parallel capacitance below a certain frequency. This effect results in an additional series capacitance, to the parallel capacitance/conductance equivalent circuit model.

Parallel capacitance It can be concluded that the parallel capacitance, or equivalently, the relative permittivity, can be exploited as a selection parameter. The permittivity for the three main components is significantly separated and constant throughout the whole frequency range up to 30 MHz. The effective medium approximation for the relative permittivity of a binary or ternary mixture is highly linear. Repeatability measurements yielded percent deviation values below 5%. Considering other uncertainties such as mixing errors and temperature effects, it is expected that repeatability is sufficient to comply with the desired final inaccuracy range. Additionally, when the electrode polarization effect is accounted for, this selection parameter is not sensitive to free ions.

Parallel conductance In contrary, the parallel conductance, or equivalently the conductivity, was found to be not a useful selection parameter for three of reasons. Firstly, the mixing model to determine the conductance of a mixture is found to be piecewise logarithmic as function of ethanol concentration, which makes the mixing model composition dependent. The temperature de-

pendency is composition dependent which makes it challenging to compensate for temperature effects, before the composition is known.

Secondly is the conductance dramatically influenced by free ion concentration as also supported by measurements. The static dissipators that are present in gasoline for safety reasons also have a non-negligible influence on the conductance.

Thirdly it was found from measurements that the conductance of ethanol is strongly sample dependent. This effect effect was supported by literature.

Fouling scenario When the application of the sensor system is limited to the use of a specific gasoline/ethanol ratio, for example E85 or E22, the LF impedance measurement technique can be used to detect fouling. Since in such a scenario additional information is supplied, namely that the gasoline content is fixed and known, it can easily be checked whether the parallel capacitance and conductance meet the subset of a legitimate mixture. Even if ion-free water is added, the mixture will not fit a legitimate combination of capacitance *and* conductance, and it is evident that fouling has occurred. Because the application of the parallel conductance as selection parameter is now restricted to a specific expected ethanol content, the uncertainties originating from sample temperature dependency and mixing model are not applicable here. The other uncertainties in measuring conductance, such as static dissipators and sample dependency, are still an issue if a practical implementation is considered.

Domain analysis Since the impedance measurements up to 30MHz deliver only one useful and valuable parameter, namely the parallel capacitance, a second selection parameter is required to solve the ternary mixture problem in all mixture scenario's. G. Lacerenza proposed the effect of dielectric relaxation as selection parameter. The relaxation frequency of ethanol is around 2 GHz, whereas the relative permittivity of water rolls off around 20 GHz. Since a prototype in this frequency range will most likely be an integrated chip and because this RF topic would fall out of the framework of this thesis, it was decided to consider more domains.

A feasibility study has been carried out, which resulted in two promising domains, the thermal domain, exploiting the thermal capacitance and conductance, and the optical domain, exploiting absorption spectroscopy.

In the thermal domain, water is by far the strongest parameter, its thermal capacitance and conductance are significantly higher than those of gasoline and ethanol. Water also has the largest relative permittivity ($\varepsilon_{r,water} = 80$ as compared to $\varepsilon_{r,gas} = 2$), and is thus dominating in this domain too.

Based on preliminary measurements, it was found that gasoline is dominating the absorption behavior in the UV. For selectivity reasons, the combination of LF impedance with optical absorption is preferred over the combination of LF impedance with thermal conductance/capacitance.

Optical absorption spectroscopy For the research in the optical domain, numerous measurements over the whole wavelength range have been carried out using the three components of the ternary mixture, but also practical car fuels and test gasolines originating from Ford Motor Company have been measured.

For the UV range 200-400 nm it was found that the optical absorbance is strongly dominated by gasoline. Ethanol does have a spectrum in the UV too, but its absorption is more than four orders of magnitude smaller in this range. D.I. water does not show any absorption in the UV range at all, which can be considered advantageous, since it improves orthogonality in distinguishing the three components.

The visible range can be considered as not useful, because of the application of colorants that are added to gasoline. For different regions of the world, different colorants were observed. In the

infra-red range from 2000-2700 nm, a useful ethanol-specific spectrum was found, but an even stronger ethanol absorption was measured in the range 2700-3300 nm.

Furthermore, it was found from measurements that the octane content of the measured gasolines and the summer or winter grade had a negligible influence on the spectral behavior. Gasoline consists of a large range of various hydrocarbons. To fully understand which hydrocarbons cause the gasoline specific absorption behavior, more research is, for example a chemical composition analysis of different gasolines.

7.2. PROPOSED MEASUREMENT SYSTEM

Based upon the in-dept analysis of the LF impedance and the optical domain, and after the feasibility study was performed, in this section a measurement system for the application of a Flex-Fuel sensor will be described. The best combination of domains to form a measurement system based on the findings of this work is given and motivated.

First, the relative permittivity should be used as selection parameter for reasons as described above: non-destructiveness, linear mixing behavior, non-sensitivity to free ions, high stability and good reproducibility. Another advantage is that a low frequency can be used. Depending on the free ion concentration in the liquid under test, a lower limit is approximately 10kHz, based on experiments with the gasoline from Ford Motor Company.

Because water is the dominating component in the relative permittivity, and because the highest orthogonality is obtained when different components dominate over different domains, the choice for the optical domain is the best option, compared to the thermal domain. The local minimum at 240 nm and the peak at 265 nm are very suitable spectral features where the optical absorbance can be exploited as gasoline estimator. But even more experiments in the frequency range 270 nm to 300 nm are expected to give useful results for the application of gasoline estimation based on the optical absorbance.

However, the important condition that has to hold for this reasoning: The absorption behavior of different gasolines should be constant or within acceptable error ranges (max. 5% system error in final measurement system) in the range of interest, 220-300 nm. This means that gasoline originating from different locations within a country or even continents must show the same spectral behavior in the UV range of interest.

Two different implementation techniques have been proposed. One proposal contains a combination of UV LEDs in combination with UV enhanced photo diodes. When it turns out that the variations introduced by shifts in the gasoline spectrum yields an unacceptable error, more spectral information is needed. In that case the implementation using a linear variable optical filter in combination with a broad band UV light source, and a detector array of photo diodes is an option. Two channels can be implemented for the two peaks 240 nm and 265 nm. For redundancy an additional channel can be used at a wavelength of 290 nm. Spectral resolution is in the order of $\delta_\lambda = 1$ nm.

7.3. FUTURE OUTLOOK AND RECOMMENDATIONS

To study whether the the absorption behavior is constant for different gasolines, more research on the chemical composition of gasoline is needed. Gasoline can be considered as a 'black-box' liquid, it consists of numerous hydrocarbons and its exact composition can vary from source to source. It is important to find out which of all these hydrocarbons is causing this domination in absorption behavior. Then it will be more clear to which extent the absorption spectroscopy in the UV can be applied, although promising results have been obtained up to this point.

Based upon the obtained optical data of this work, it is likely that the benzene and the benzene compounds, such as toluene, account for the measured UV absorption of the different gasolines. The aromatic structures are known to be a strong absorber in the range of interest. This assump-

tion is supported by the performed measurements on benzene and toluene.

When it is clear which components of the gasoline are responsible for the UV absorption behavior, then it must be verified how equivalent the gasolines originating from different parts of the world are in the respect of these components.

7.4. PUBLICATION EUROSENSORS XXX

The measurements, interpretation and the conclusions of the optical absorbance spectroscopy part of this work were used to write a 4 page abstract paper for the 30st version of the Eurosensors conference, which was held 4-7 september 2016. This 4 page abstract paper is included in the proceedings of the conference. Furthermore an A0 poster was made and presented at the conference. The abstract paper and the A0 poster are included in appendix A.

A

EUROSENSORS ABSTRACT PAPER & POSTER

Available online at www.sciencedirect.com

SciVerse ScienceDirect

Procedia Engineering 00 (2016) 000–000

Procedia Engineering

www.elsevier.com/locate/procedia

30th Eurosensors Conference, EUROSENSORS 2016

Optical Spectroscopy for Biofuel Composition Sensing

L.M. Middelburg[a,*], G. de Graaf[a], M. Ghaderi[a], A. Bossche[a], J. Bastemeijer[a], J.H. Visser[b], R.E. Soltis[b], R.F. Wolffenbuttel[a]

[a] *Delft University of Technology, Mekelweg 4, Delft 2628CD, The Netherlands*
[b] *Ford Motor Company, Village Rd, Dearborn MI, USA*

Abstract

The optical absorption of water-containing bio-fuel is investigated as a parameter to determine the gasoline content of this fuel. Optical measurements reveal that gasoline shows an interesting and useful spectrum with typical absorption behavior in the UV range between 230 and 300 nm. This result indicates that significant information can be obtained to determine the gasoline concentration in bio-fuel by UV absorption spectroscopy. A concept for a low-cost measurement system in the fuel line is presented, by implementing a LVOF in combination with a wide-band light source and detector arrays.

Peer-review under responsibility of the organizing committee of the 30th Eurosensors Conference.

Keywords: Optical spectroscopy; optical absorption; UV-spectroscopy; ternary mixture; bio-fuel; bio-ethanol; LVOF; microspectrometer

1. Motivation

Bio-fuel typically consists of a gasoline/ethanol blend. The ethanol originates from different sources. Production of ethanol from sugar cane typically results in hydrous ethanol, hence causes some water in the resulting bio-fuel blend. Another cause for the presence of water in bio-fuel is the practice of fouling, water is added to increase profit. As a consequence the ternary mixture of ethanol, gasoline and water should be continuously monitored in the fuel line in order for Flex Fuel Vehicles to start smoothly and to run cleanly and efficiently on different compositions of bio-fuel. Currently available sensor systems only measure the permittivity of the fuel [1]. Their performance is not adequate, as operation is based on an assumed constant water concentration, therefore more information is required for a full fuel composition measurement [2].

2. Theory

Based on preliminary measurements the absorption in the UV range between 220 nm and 350 nm is strongly dominated by the gasoline content in the bio-fuel. According to the Beer-Lambert law, the total resulting absorbance is determined by the extinction coefficient ϵ_i, the molar concentration c_i and the optical path length l. If there is no

* L.M. Middelburg. Tel.: +31(0)152787534
E-mail address: l.m.middelburg-1@student.tudelft.nl

Peer-review under responsibility of the organizing committee of the 30th Eurosensors Conference.

interaction between the ethanol and gasoline fraction of the bio-fuel, the resulting absorbance should therefore be the summation of the absorbance of the separate components of the bio-fuel. The separate absorbance of gasoline, water and ethanol should therefore add up. If one of the three components is the dominating factor in the total absorbance, a linear behavior over the different mixing ratios is expected.

3. Measurements UV

3.1. Measurement Setup

Multiple absorption measurements were carried out, in order to identify which parts of the spectra of the three components would be suitable. For these measurements, a Varian Cary 500 Spectrophotometer was used in combination with quartz cuvettes. This device uses a double beam, one for a reference sample and one for the actual measurement. Initial measurements revealed that the best results were obtained when an optical path length of 1 mm is used and when the gasoline/ethanol mixtures were diluted with a suitable solvent. Cyclo-hexane was chosen as the solvent, because of the low absorption over the entire UV-spectrum and the fact that it dissolves the relevant components well. During initial measurements it was already found that D.I. water does not absorb significant light in the UV range, hence does not interfere using this measurement technique.

Table 1: Measurement parameters

Parameter	Value
Average time	0.3 s
Spectral BW	2.000 nm
Measurement range	200-400 nm
Optical Pathlength	1 mm
Cuvettes	Quartz
Solvent	Cyclo-hexane

3.2. Gasoline/Ethanol Mixtures

The absorption of gasoline/ethanol in different ratios was measured. Indolene 50E clear was used, which is a standardized test gasoline free of additives and coloring, in combination with the so-called 200 proof ethanol (>99.98% pure). The dilution ratio of 1/10 is used to optimally use the dynamic range of the spectrophotometer. No dilution is applied when measuring pure ethanol to prevent further loss of spectral information. As can be seen in figure 1 a suitable absorption peak is visible around 265 nm. Despite the dilution and the pathlength of 1 mm, saturation at minimum sensitivity setting results at 70% Indolene concentration and beyond. On the other hand, no saturation is present and the absorption is dominated by gasoline content at 240 nm. To investigate if this gasoline-dependent absorption behavior could be utilized in determining the composition of the initial ternary mixture problem, Indolene 50E was replaced with Unleaded Low Octane gasoline 87RON (Research Octane Number) in a new series of identical measurements and the results are shown in figure 2. The absorption behavior seems to resemble the measurements of Indolene gasoline, the spectral behavior is very similar. This result can be considered as promising in the final application of a future optical extension of the fuel composition sensor system in flex fuel vehicles.

To compare the absorption behavior of the different gasolines in combination with pure ethanol, the absorbance at two different wavelengths in the UV is plotted against gasoline content. The 240 nm wavelength was chosen, because of the local minimum, which has turned out to be typical for different gasolines. Because of the saturation effect at 265 nm, a higher dilution ratio or smaller optical path-length should be used at and around this wavelength. Because of the saturation effect in this setup at 265 nm, the wavelength 290 nm was chosen instead. The result is included in figure 3. It can be concluded from this plot that the relationship between gasoline content and optical absorbance is linear, and the slope between both is dependent on the used wavelength. Since both gasolines have different compositions, this explains the discrepancy at higher gasoline content.

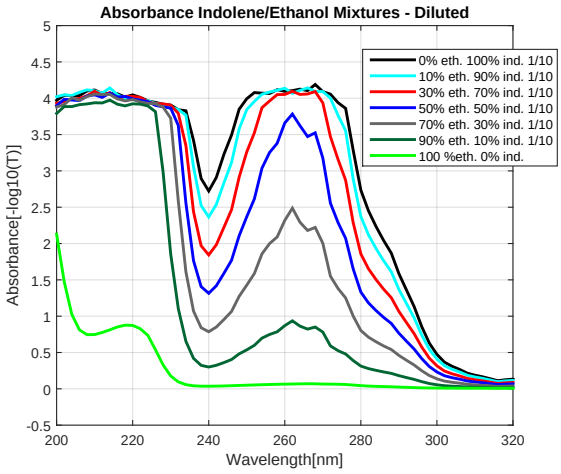

Fig. 1: The measured absorbance of different ethanol/indolene ratio's. The dilution ratio is included in the legend.

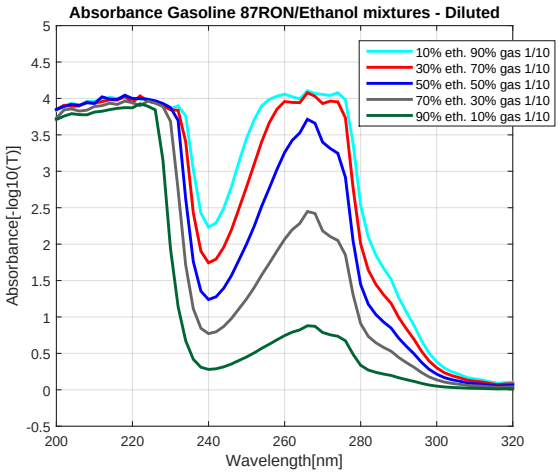

Fig. 2: The measured absorbance of different ethanol/gasoline ratio's. The dilution ratio is included in the legend.

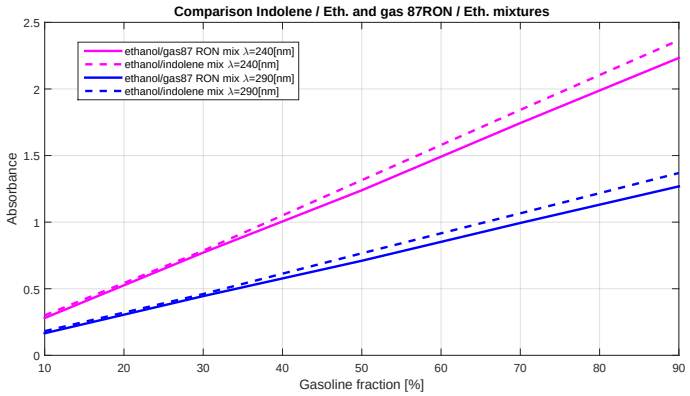

Fig. 3: The absorbance as function of the gasoline fraction. Compared are the 87RON and Indolene mixtures at two different wavelengths.

3.3. Octane content and Summer/Winter grade

During the research, some practical 'off the shelf' fuel blends were available. Again, absorption measurements were carried out to investigate the dependency on octane number and summer/winter blends. The results are included in figures 4 and 5. The effect of the octane content on the absorption behavior is very small, it can also be concluded that the higher volatility winter fuel behaves similarly to the E85 summer version. This result can be considered as promising, since insensitivity for these type of uncertainties is preferred. Note the different dilution ratios that were used to prevent loss of spectral information.

4. Implementation technique

As discussed before, a spectral measurement on three optical channels centered at 240 nm, 265 nm, and 290 nm is sufficient for a complete composition analysis. However, according to the spectral measurements presented in Fig 1 and 2, a spectral resolution of about $\delta_\lambda = 1$ nm is required for such an analysis. Mass fabrication of high resolution fixed filters, considering the process tolerances, is challenging. The use of UV LEDs and UV photodetectors would require high performance optical filters, therefore a Linearly Variable Optical Filter (LVOF) type microspectrometer system is proposed [3]. The LVOF is composed of two reflectors separated by a cavity. The depth of the cavity determines the transmission wavelength. The resolution is determined by both the reflectivity and the cavity depth.

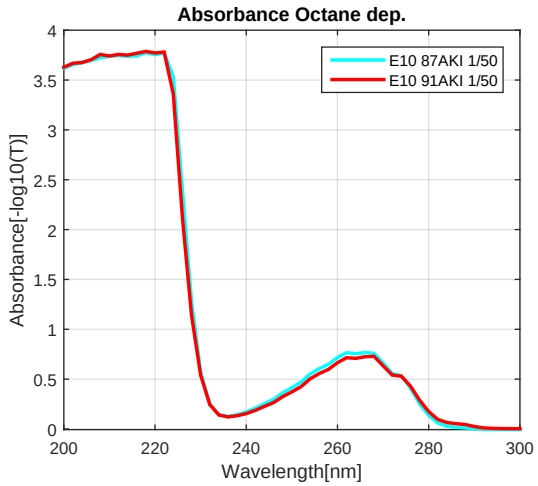

Fig. 4: Two representative American gasolines, low and mid grade octane rating compared. Note the higher dilution ratio.

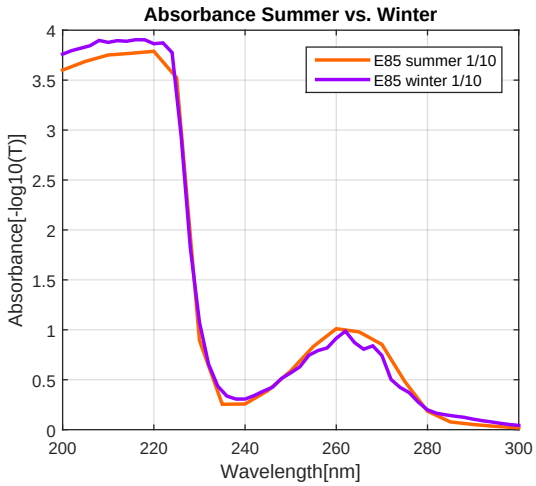

Fig. 5: The summer and winter grade E85 compared. The same dilution as previous gasoline/ethanol mixtures is used.

Figure 6 shows the schematics of the optical sensor design. The structure consists of four main components: 1) a light source, 2) a sample cell, 3) LVOF, and 4) the photo detectors. Advantages of LVOF-microspectrometer designs are the CMOS compatibility and high spectral resolution when operated over a relatively narrow band. Therefore, a sensor system based on multiple-LVOFs centered around the intended spectral channels is promising for this application.

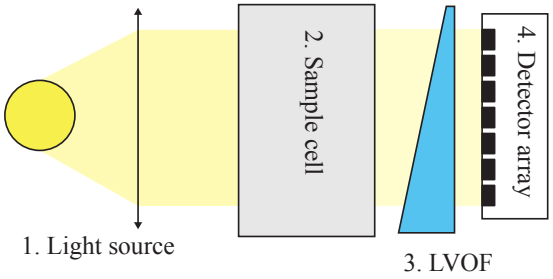

Fig. 6: A schematic overview of the measurement system based on an LVOF.

5. Conclusion

Two different gasolines were used to investigate the effect of gasoline content in bio-fuel on the optical absorption. It was found that there is a reproducible linear absorption behavior between both, but at high gasoline concentrations there is a small discrepancy between both. It was found that the octane content and the summer/winter grade had a negligible influence on the spectral behavior. Some more research in this findings, also considering the chemical composition of gasoline, is required to fully understand the underlying mechanisms. An advanced implementation technique based on a LVOF based spectrometer was proposed.

References

[1] M. Jankovic, D. Hagner (2013): Twin-model method for ethanol detection in flex fuel vehicles, 2013 American Control Conference (ACC) Washington, DC, USA, June 17-19, 2013

[2] G. de Graaf, G. Lacerenca and R.F. Wolffenbuttel (2015): Dielectric Spectroscopy for Measuring the Composition of Gasoline/Water/Ethanol Mixture, Proc. IEEE I2MTC.

[3] A. Emadi, H. Wu, G. de Graaf and R.F. Wolffenbuttel (2012): Design and implementation of a sub-nm resolution microspectrometer based on a Linear-Variable Optical Filter, Opt. Express, pages 489-507

Optical Spectroscopy for Bio-fuel Composition Sensing

L.M. Middelburg[@*] G. de Graaf[*] M. Ghaderi[*] A. Bossche[*] J. Bastemeijer[*]
J.H. Visser[†] R.E. Soltis[†] R.F. Wolffenbuttel[*]

[@]l.m.middelburg-1@student.tudelft.nl, [*]Delft University of Technology, Delft, [†]Ford Motor Company, Dearborn

Introduction

Bio-fuel mixtures typically consist of a gasoline/ethanol blend. The ethanol originates from different sources. Production of ethanol from sugar cane typically results in hydrous ethanol, hence causes water in the resulting bio-fuel blend. The ternary mixture of ethanol, gasoline and water should continuously be monitored to supply important information on the engine control unit of a Flex-Fuel Vehicle. The optical absorption of water-containing bio-fuel mixtures is investigated as a parameter to determine a gasoline content of this fuel, and might be exploited in a measurement system for a new generation of Flex-Fuel sensors.

Figure 1: E85 gas station

Figure 2: Sugar cane crops

Concept

According to the Beer-Lambert law, the resulting absorbance of the bio-fuel mixture is the sum of each of its components, assuming no interaction. $A = \sum_{i=1}^{N} \epsilon_i c_i l$, where ϵ_i is the extinction coefficient, c_i the molar concentration and l the optical path length. Preliminary optical absorption measurements were carried out from 200 nm up to 3300 nm. The most promising results were obtained in the UV range between 220 nm and 350 nm, where the absorption is strongly dominated by gasoline. D.I. water is not absorbing in this range and the absorption of ethanol is negligible compared to gasoline. Therefore a linear absorption behavior as function of increasing gasoline content is expected.

Measurements

Indolene 50E clear (standardized test gasoline, premium octane rating) and 87RON gasoline were mixed in different ratio's with ethanol (>99.98% pure) and were diluted in a 1/10 ratio to prevent loss of spectral information. The setup which was used consists of a Varian Cary 500 spectrometer and quartz cuvettes with an optical pathlength of 1 mm.

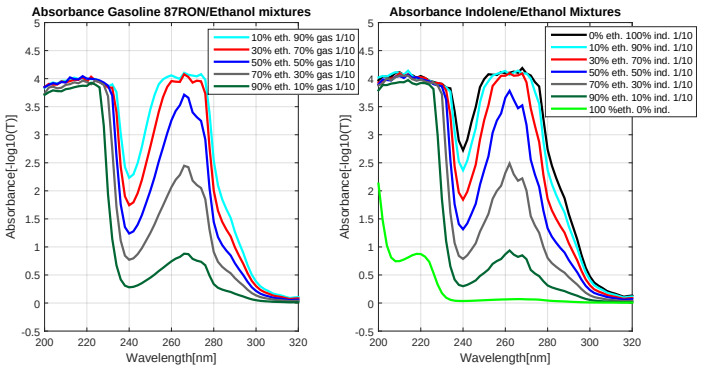

Figure 3: The absorbance behavior for different gasoline/ethanol mixtures

The result for both types gasoline is included in figure 3. Two suitable absorption features are present, at 240 nm and at 265 nm, whereas the rest of the UV spectrum is flat at no significant absorption. The absorption behavior of 87RON mixtures resembles the one with Indolene 50E gasoline. This can be considered as positive since the octane rating of both fuels differ strongly, 87RON vs. 98RON, and an insensitivity for this variable is advantageous in the final application. The optical absorbance as function of gasoline content is plotted to investigate the relation between both.

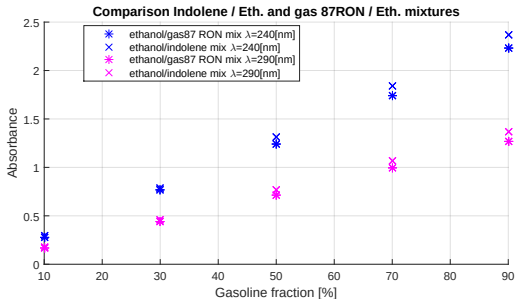

Figure 4: The absorbance as function of gasoline content at two different wavelengths: $\lambda = 240nm$ and $\lambda = 290nm$ for the Indolene and 87RON mixtures

It follows from figure 4, that the relationship between gasoline content and optical absorbance is linear, and the slope between both varies depending on the used wavelength. In other words, the optical absorbance has different sensitivities to gasoline content, depending on the used wavelength. A saturation effect occurred in the absorbance measurements for a gasoline fraction of 70% and beyond at and around a wavelength of 265 nm. Therefore, the wavelength 290 nm was chosen instead, to plot the optical absorbance as function of the gasoline fraction.

Implementation Method

A spectral measurement on three optical channels centered at 240 nm, 265 nm, and 290 nm could be utilized as a gasoline estimator. A Linearly Variable Optical Filter (LVOF) type micro-spectrometer is proposed. The LVOF is composed of two reflectors separated by a cavity, which depth determines the transmission wavelength. The resolution is determined by both the reflectivity and the cavity depth. The detector array can be implemented using integrated UV enhanced photo-diodes. Advantages of LVOF-microspectrometer designs are the CMOS compatibility, robustness and high spectral resolution when operated over a relatively narrow band. Therefore, a sensor system based on multiple-LVOFs centered around the intended spectral channels is promising for this application.

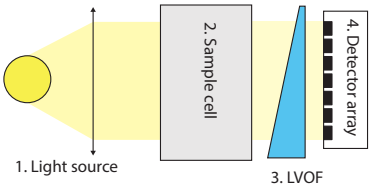

Figure 5: Schematic overview of the system using LVOF

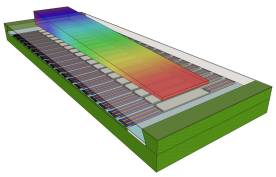

Figure 6: The LVOF on top of a detector array

Conclusion

Two different gasolines were used to investigate the effect of gasoline content in bio-fuel on the optical absorption. It was found that there is a reproducible linear absorption behavior between both. Furthermore, the octane content and the summer/winter grade had a negligible influence on the spectral behavior. An implementation technique based on a LVOF based spectrometer was proposed. A LVOF-microspectrometer system in the range 320-350 nm has already been designed for a different application. [A. Emadi, *Linear-Variable Optical Filters for microspectrometer application*, 2010]

Acknowledgement

This work is funded by the Ford Poling Award. It has been carried out in collaboration with the Research and Advanced Engineering Department from Ford Motor Company, Dearborn, US.

B

MATLAB CODE

B.1. MEDIUM APPROXIMATION

B.1.1. THE FUNCTION MAXWELL-GARNETT

```
%Maxwell Garnett

% INPUTS:
%   eps_base: dielectric constant of base material;
%   eps_incl: dielectric constant of inclusion material;
%   vol_incl: volume portion of inclusion material;
% OUTPUT:
%   eps_mean: effective dielectric constant of the mixture.

function [eps_mean] = MaxwellGarnettFormula(eps_base, eps_incl, vol_incl)

small_number_cutoff = 1e-6;

if vol_incl < 0 || vol_incl > 1
    disp(['WARNING: volume portion of inclusion material is out of range!']);
end
factor_up = 2*(1-vol_incl)*eps_base+(1+2*vol_incl)*eps_incl;
factor_down = (2+vol_incl)*eps_base+(1-vol_incl)*eps_incl;
if abs(factor_down) < small_number_cutoff
    disp(['WARNING: the effective medium is singular!']);
    eps_mean = 0;
else
    eps_mean = eps_base*factor_up/factor_down;
end
```

B.1.2. CODE TO GENERATE COMPARISON PLOTS

```
%Validity check linear model according to Maxwell Garnett
% Author: Luke Middelburg
% Date: 18-11-15
% Mixture: Ethanol (Base)/Gasoline(inclusion) (i.e. E85)

% input arguments
e_base = 24.3;    %permittivity ethanol
e_incl = 2;       %permittivity gasoline

y = linspace(0, 0.5, 11); %inclusion fraction
```

```
e_mean_mg = size(11); %mean according to maxwell garnett
e_mean_lin = size(11); %mean according to linear model
e_mean_error = size(11); %error in percentage from maxwell garnett


for c = 1:11

    e_mean_mg(c) = MaxwellGarnett(e_base, e_incl, y(c));
    e_mean_lin(c)= (y(c)*e_incl) + ((1-y(c))*e_base);

end

e_mean_error=(e_mean_lin-e_mean_mg)./(e_mean_mg)*100;

figure(1)
plot(y, e_mean_error)
xlabel('Inclusion fraction')
ylabel('Error [%]')
title('Percentual error Lin.model w.r.t. Maxwell-Garnett')


figure(2)
plot(y, e_mean_mg)

hold on
grid on

plot(y, e_mean_lin)

xlabel('Inclusion fraction')
ylabel('Epsilon mean')
title('Epsilon as function of inclusion (gasoline) fraction in ethanol')
legend('Maxwell-Garnett', 'Linear 1st order approx.')
```

B.2. CODE TO READ OUT THE IMPEDANCE ANALYSER

```
% Author: Johan Vogel
% Edited by: Luke Middelburg
% Script to sweep and read out data from Agilent 4294A Impedance Analyzer
% based upon the generic Visa code http://www.mathworks.com/matlabcentral
% fileexchange/28887-capturing-a-waveform-from-an-agilent-oscilloscope-
%over-a-standard-visa-interface
% for more machine commands, have a look in the 4294A Programming Manual

% Make sure to have installed and configured Keysight Connection Expert
% before running this code.
%% Interface configuration and instrument connection

visaObj = visa('agilent','TCPIP0::192.168.2.10::5025::SOCKET');% Insert the
%right IP adress of the machine
visaObj.InputBufferSize = 100000;
visaObj.Timeout = 5;% This should be long enough to transfer all measurement
%data. 5 seconds was enough for 201 sweep samples
visaObj.ByteOrder = 'littleEndian';
fopen(visaObj);

fprintf(visaObj,'TRGS BUS');%Trigger via LAN

%%
```

```
% Trigger
fprintf(visaObj,'*TRG');
pause(25) % Pause during sweep time

% Get frequency vector freqs
outp=query(visaObj,'OUTPSWPRM?');
freqs=str2num(outp);

% Get measured data
outp=query(visaObj,'OUTPDATA?');
bla=str2num(outp);
Imp=bla(1:2:end)+i*bla(2:2:end);

G = real(Imp)./(abs(Imp).^2);
Cp = (-imag(Imp))./((abs(Imp).^2)*2*pi.*freqs);

save(['E85G15W0_' datestr(now,'yyyy-mm-dd HHMMSS') '.mat'], 'Cp', 'G', 'freqs', 'Imp');

 %% Delete objects and clear them.
fclose(visaObj);
delete(visaObj);
clear visaObj;
```

C

S11 - DIELECTRIC RELAXTION

This appendix is referred to by the dielectric relaxation section from chapter 2. Below the measured S11 parameter is shown as function of frequency, which ranges from 200 MHz up to 14 GHz. The influence of water is clearly visible.

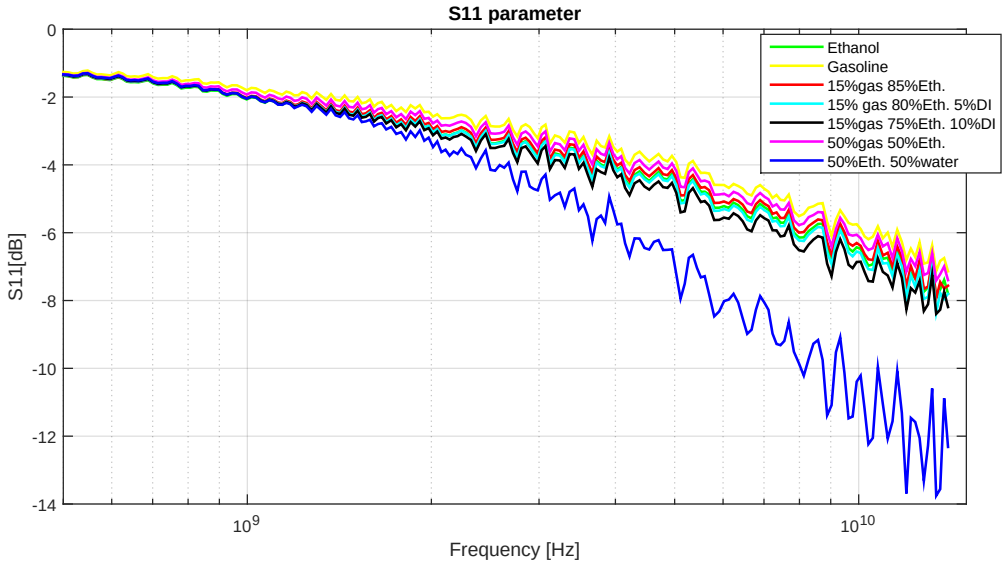

Figure C.1: The measurement results of the measurements with the impedance analyzer at Process and Energy Department

D

Accuracy in Cp - G calculation

To get an idea of the accuracy of the impedance analyzer used for these measurements, the accuracy was calculated according to the datasheet of Agilent 4294A. The total error is dependent on D, also called the dissipation factor. This factor is defined as:

$$DF = tan(\delta) = \frac{ReZ}{|ImZ|} \tag{D.1}$$

Assume now that we calculate the accuracy of this conductivity measurement at a frequency f=102.9kHz for the mixture self-mixed E85. The obtained dissipation factor: DF=0.145. This implies the first calculation method of figure D.1.

The calculation of E is dependent on multiple settings and quantities during the measurement, like the oscillator level, the measurement bandwidth, the DC-bias range, the applied frequency and the magnitude of the measured impedance. To get a idea about the calculation, the figures D.2 and D.3 are included for completeness.

The eventually calculated E is equal to:

$$E = 0.83 + (\frac{5.103 m\Omega}{22.07 k\Omega} + 25 nS \cdot 22.07 k\Omega) \cdot 100\% = 0.885[\%] \tag{D.2}$$

Following formula 1 in figure D.1:

$$G \pm 0.885 \cdot \frac{\sqrt{1+0.145^2}}{0.145} = 6.16[\%] \tag{D.3}$$

For the parallel capacitance, the following value is obtained:

$$Cp \pm 0.885 \cdot \sqrt{1+0.145^2} = 0.894[\%] \tag{D.4}$$

G accuracy	
at D_x >0.1	$\pm E \times \frac{\sqrt{1+D_x^2}}{D_x}$ [%]
at $D_x \leq 0.1$	$\pm E/D_x$ [%]

Figure D.1: Accuracy in measured G, source: Data sheet Agilent 4294A

Equation 3. Impedance Measurement Accuracy [%] at 3.5-mm Port of the Agilent 42941A

$$E = E_p' + \left(\frac{Z_s'}{|Z_x|} + Y_o' \cdot |Z_x| \right) \times 100$$

Where,

$E_P' = E_{PBW} + E_{POSC} + E_P$ [%]
$Y_O' = K_{BW} \times Ky_{OSC} \times (Y_{ODC} + Y_O)$ [S]
$Z_S' = K_{BW} \times Kz_{OSC} \times Z_S$ [Ω]

Figure D.2: source: Data sheet Agilent 4294A

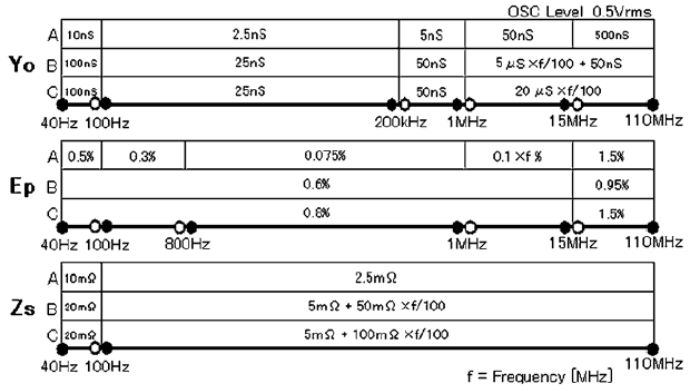

A = 4294A front panel 4 terminal pair port (no extension).
B = 7-mm one port (with 42942A).
C = Probe 3.5-mm port (with 42941A).
For accuracy at probe tip, add the following error factors (typical):
Yo: + 2πf×0.1 μS
Zs: + 20mΩ

Figure D.3: source: Data sheet Agilent 4294A

BIBLIOGRAPHY

[1] *Picture continental flex-fuel sensor,* http://paceperformance.com (), accessed: 08-2016.

[2] *The clemson university vehicular electronics laboratory,* http://www.cvel.clemson.edu (), accessed: 08-2016.

[3] *Application note: Basics of measuring the dielectric properties of materials,* http://literature.cdn.keysight.com/litweb/pdf/5989-2589EN.pdf?id=670519 (2016), accessed: 20-07-2016.

[4] P. B. Ishai, M. S. Talary, A. Caduff, E. Levy, and Y. Feldman, *Electrode polarization in dielectric measurements: a review,* Measurement Science and Technology **24** (2013).

[5] H. Schwan, *Electrode polarization impedance and measurements in biological materials,* Annals New York Academy of Sciences (1968).

[6] Comsol, *Finding the impedance of a coaxial cable,* (2015), (Rev: 2015-02-26).

[7] F. Wolffenbuttel, *Coaxial probe for gasoline mixture measurements,* Internship report (2016).

[8] J. S.-M. M.S. Rocha, *A simple impedance method for determining ethanol and regular gasoline mixtures mass contents,* Fuel 84 , 447 (2005).

[9] *Absorption spectroscopy information benzene,* http://www.chem.uiuc.edu/organic/Arenes/Chapter205/sec5-14/5-14.htm (1999), accessed: 07-2016.

[10] K. h. Ahn, A. G. Stefanopoulou, and M. Jankovic, *Afr-based fuel ethanol content estimation in flex-fuel engines tolerant to maf sensor drifts,* IEEE Transactions on Control Systems Technology **21**, 590 (2013).

[11] J. J. Batteh and E. W. Curtis, *Modeling transient fuel effects with alternative fuels,* in *SAE Technical Paper* (SAE International, 2005).

[12] F. M. M. Theunissen, *Percent ethanol estimation on sensorless multi-fuel systems; advantages and limitations,* in *SAE Technical Paper* (SAE International, 2003).

[13] G. Lacerenza, *A feasebility study of a sensor system to detect the amount of water and ethanol in petrol,* MSc. Thesis (2013).

[14] K. E.L., *Applied combustion,* (2007).

[15] *Anp - agência nacional do petróleo, gás natural e biocombustíveis,* http://www.anp.gov.br/ (2016), accessed: 09-2015.

[16] M. Balat and H. Balat, *Recent trends in global production and utilization of bio-ethanol fuel,* Applied Energy **86**, 2273 (2009).

[17] A. Demirbas, *Political, economic and environmental impacts of biofuels: A review,* Applied Energy **86, Supplement 1**, S108 (2009), bio-fuels in Asia.

[18] *International safety guide for inland navigation tank-barges and terminals,* http://www.isgintt.org/files/documents/Chapter_03en_isgintt_062010.pdf (2010), accessed: 08-2016.

[19] *U.s. energy information administration,* http://www.eia.gov (2013), accessed: 08-2016.

[20] S. J. Friedmann, R. Upadhye, and F.-M. Kong, *Prospects for underground coal gasification in carbon-constrained world,* Energy Procedia **1**, 4551 (2009).

[21] *Figure of dielectric relaxation of water,* http://www1.lsbu.ac.uk/ (2016), accessed: 20-07-2016.

[22] J. T. I. M. Y. Onimisi, *Comparative analysis of dielectric constant and loss factor of pure butan-1-ol and ethanol,* American Journal of Condensed Matter Physics **5** (2015).

[23] R. Karthik, N. H. Nagarajan, B. Raja, and P. Damodharan, *Measurement of Thermal Conductivity of Fluids Using 3 Method in a Suspended Micro Wire,* Journal of Engineering Thermophysics **21**, 60 (2012).

[24] M. J. Vellekoop, *A smart lamb-wave sensor system for the determination of fluid properties,* Ph.D. thesis, Delft University of Technology (1994).

[25] *Values for speed of sound,* https://engineeringtoolbox.com (2016), accessed: 02-2016.

[26] G. de Graaf, G. Lacerenza, R. Wolffenbuttel, and J. Visser, *Dielectric spectroscopy for measuring the composition of gasoline/water/ethanol mixtures,* Instrumentation and Measurement Technology Conference,IEEE Conference Publications , 154 (2015).

[27] R. Ruppin, *Validity range of the maxwell-garnett theory,* physica status solidi (b) **87**, 619 (1978).

[28] D. Gottlieb and V. Halpern, *The electrical conductivity of very thin metal films,* Journal of Physics F: Metal Physics **6**, 2333 (1976).

[29] D. Kirk, *Conductivity of gasoline-ethanol-water mixtures,* Fuel 62 , 1512 (1983).

[30] A. Emadi, *Linear-Variable Optical Filters for microspectrometer applications,* Ph.D. thesis, Delft University of Technology (2010).

[31] S. Ito, *Analysis of aromatic hydrocarbons in gasoline and naphtha,* (2013).

[32] *Absorption spectroscopy information aromatic compounds,* https://www2.chemistry.msu.edu/faculty/reusch/virttxtjml/spectrpy/uv-vis/spectrum.htm (2013), accessed: 07-2016.

[33] W. Dabelstein, A. Reglitzky, A. Schütze, and K. Reders, *Automotive fuels,* in *Ullmann's Encyclopedia of Industrial Chemistry* (Wiley-VCH Verlag GmbH and Co. KGaA, 2000) Chap. 3.

[34] P. S. Kumar, *Spectroscopy of organic compounds,* (2006).

[35] *Taoyuan electron (hk) limited,* http://www.ledwv.com/uv (2016), accessed: 05-2016.

[36] A. Emadi, H. Wu, G. de Graaf, and R. Wolffenbuttel, *Design and implementation of a sub-nm resolution microspectrometer based on a linear-variable optical filter,* Opt. Express **20**, 489 (2012).